Northumbria Research Link

Characterisation and Optimisation of the Semiconductor Optical Amplifier for Ultra-High Speed Performance

Ahmed Abd El Aziz Shalaby

A thesis submitted in partial fulfilment of the requirements of the University of Northumbria at Newcastle for the degree of Doctor of Philosophy

Research undertaken in the School of Computing, Engineering and Information Sciences

December 2011

ABSTRACT

This research is in the area of high speed telecommunication systems where all-optical technologies are being introduced to meet the ever increasing demand for bandwidth by replacing the costly electro-optical conversion modules. In such systems, all-optical routers are the key technologies capable of supporting networks with high capacity/bandwidth as well as offering lower power consumption. One of the fundamental building blocks in all-optical routers/networks is the semiconductor optical amplifier (SOA), which is used in for clock extraction, wavelength conversion, all-optical gates and optical processing. The SOAs are perfect for optical amplification and optical switching at a very high speed. This is due to their small size, a low switching energy, non-linear characteristics and the seamless integration with other optical devices. Therefore, characterisation of the SOA operational functionalities and optimisation of its performance for amplification and switching are essential and challenging. Existing models on SOA gain dynamics do not address the impact of optical propagating wavelength, the combined input parameters and their adaptation for optimised amplification and switching operations. The SOA operation is limited at high data rates > 2.5 Gb/s to a greater extent by the gain recovery time. A number of schemes have been proposed to overcome this limitation; however no work has been reported on the SOA for improving the gain uniformity. This research aims to characterise the boundaries conditions and optimise the SOA performance for

amplification and switching. The research also proposes alternative techniques to maximise the SOA gain uniformity at ultra-high speed data rates theoretically and practically. An SOA model is been developed and used throughout the research for theoretical simulations. Results show that the optimum conditions required to achieve the maximum output gain for best amplification performance depends on the SOA peak gain wavelength. It is also shown that the optimum phase shift of 180° for switching can be induced at lower input power level when the SOA biasing current is at its maximum limit. A gain standard deviation equation is introduced to measure the SOA gain uniformity. New wavelength diversity technique is proposed to achieve an average improvement of 7.82 dB in the SOA gain standard deviation at rates from 10 to 160 Gb/s. Other novel techniques that improved the gain uniformity employing triangular and sawtooth bias currents, as replacements for the uniform biasing, have been proposed. However, these current patterns were not able to improve the SOA gain uniformity at data rates beyond 40 Gb/s. For that reason, an optimised biasing for SOA (OBS) pattern is introduced to maximise the gain uniformity at any input data rates. This OBS pattern was practically generated and compared to the uniform biased SOA at different data rates and with different input bit sequences. All executed experiments showed better output uniformities employing the proposed OBS pattern with an average improvement of 19%.

ACKNOWLEDGEMENTS

My thanks are wholly devoted to ALLAH for this opportunity, his blessings, and helping me all the way to conclude this work.

First and foremost, I am honoured that my work has been supervised by Dr. Wai Pang Ng. I am greatly indebted to him for his patience, inspiring guidance, valuable advices, endless support for work and life and all the time he has given me. This work and publications could not been achieved without his discussions, suggestions and many revisions. I also would like to thank my second supervisor Prof. Zabih Ghassemlooy who was always supportive and provided me with fruitful discussions and extensive guidance. I would also like to thank Prof. Moustafa Hussien and Dr. Razali Ngah for accepting to join the supervision team.

I wish to express my gratitude to Northumbria University and especially for the School of Computing, Engineering and Information Sciences for the studentship in throughout my PhD. I would like to thank my colleagues, Hoa, Wisit, Ming Feng, Popoola, Sujan, Rupak, Arash and Thavamaran. I also enjoyed lots of joys and fun with all OCRG group colleagues and my best friends Kirill, Shoib, Kalam Hamza and Basak.

Words can't express the thanks I owe to my wife for her endless encouragements, countless support and love. I'm grateful for the sacrifice my wife and son did to me. To my beloved parents, my brother Mohamed, sisters Dina and Rasha and my nephews my utmost thanks for without whom, never could have happened. I

would never forget the support of all these years from my father-in-law, my brothers-in-law Amr and Hesham and my sisters-in-law Samar, Shorian and Salma.

I finally dedicate this work to the most important people whom I lost during my PhD, my nephew Youssef and my mother-in-law Moushira.

DECLARATION

I declare that the work contained in this thesis has not been submitted for any other award and that it is all my own work. I also confirm that this work fully acknowledges opinions, ideas and contributions from the work of others.

Name: Ahmed Abd El Aziz Shalaby

Signature:

Date:

TABLE OF CONTENTS

Chapter 1: Introduction

Chapter 2: Semiconductor Optical Amplifier

Chapter 3: SOA Characteristics and Segmentation Model

Chapter 4: Optimisation of Key SOA Parameters for Amplification Function

Chapter 5: Optimisation of Key SOA Parameters for Switching Function

Chapter 6: SOA Gain Uniformity Improvement Employing Wavelength Diversity Technique for High Speed Optical Routers

Chapter 7: SOA Gain Uniformity Improvement Employing Classical Non-Uniform Biasing Technique for High Speed Optical Routers

Chapter 8: Optimised Biasing for SOA (OBS)

Chapter 9: Experimental Implementation of Optimised Biasing for SOA (OBS) Pattern

Chapter 10: Conclusions and Future Work

GLOSSARY OF ACRONYMS

ASE   Amplified Spontaneous Emission

AT   Agilent Technologies

BERT   Bit Error Rate Tester

BRM   Bit Rate Multiplier

CIP   Centre of Integrated Photonics

CP   Control pulse

CW   Continuous Wave

EDFA   Erbium Doped Fibre Amplifier

FP-SOA   Fabry-Perot Semiconductor Optical Amplifier

FWHM   Full-Width-Half-Maximum

FWM   Four-Wave-Mixing

ITU   International Telecommunication Union

MLC   Multi Laser Controller

MQW   Multi-Quantum-Well

MZI   Mach-Zehnder Interferometer

OBS	Optimised Biasing for SOA
OCRG	Optical Communication Research Group
O-E-O	Optical-Electrical-Optical
OTDM	Optical Time Division Multiplexing
PBS	Polarisation Beam Splitter
PC	Polarisation Controller
PM	Polarisation Maintaining
PPM-HP	Pulse Position Modulation Header Processing
PSL	Pico-second pulsed fibre Laser
RF	Radio Frequency
SMF	Single Mode Fibre
SMZ	Symmetric Mach-Zehnder
SOA	Semiconductor Optical Amplifier
SOA-MZI	Semiconductor Optical Amplifier based Mach-Zehnder Interferometer
SPM	Self-Phase Modulation
SW	Switching Window

TE	Transverse Electric
TM	Transverse Magnetic
TOAD	Terahertz Optical Asymmetric Demultiplexer
TW-SOA	Travelling-Wave Semiconductor Optical Amplifier
UNI	Ultra-fast Non-linear Interferometer
WDM	Wavelength Division Multiplexing
WDT	Wavelength Diversity Technique
XPM	Cross-Phase Modulation
XGM	Cross-Gain Modulation

GLOSSARY OF SYMBOLS

A Surface and defect recombination coefficient

a_1 Differential gain parameter

a_2 Gain constant

a_3 Gain constant

a_4 Gain peak shift coefficient

B Radiative recombination coefficient

C Auger recombination coefficient

C_1 Acceleration constant of the triangular biasing signal

C_2 Deceleration constant of the triangular biasing signal

dN/dt Carrier density rate of change within the SOA active region

dn/dt Refractive index shift coefficient

f Input light frequency

G Total SOA gain achieved by propagating optical wave

G_1 Total SOA gain achieved by the 1st propagating pulse

G_{av} Average SOA gain achieved by all propagating pulses

G_m	Maximum SOA gain value of the n_pth pulse that intersects with all pulses gains within the input packet applied to the SOA
G_{ss}	Total SOA gain at steady state
G_y	Total SOA gain achieved by each propagating pulse
g	Material gain coefficient
g_1	Material gain coefficient at the departure of the 1st optical pulse from the SOA
g_{ss}	Material gain coefficient at steady state
g_T	Net gain coefficient
g_{Tss}	Net gain coefficient at steady state
H	SOA height (thickness)
h	Plank's constant
I	SOA bias current
I_{av}	Average non-uniform bias current
I_{max}	Maximum non-uniform bias current
I_{min}	Minimum non-uniform bias current
i	Current pulse number to enter the SOA

j	Following pulse number to enter the SOA
k	Instantaneous pulse number to enter the SOA
L	SOA length
l	SOA segment length
m_1	Acceleration slope of the triangular or the sawtooth shape biasing current
m_2	Deceleration slope of the triangular shape biasing current
N	Carrier density
N_o	Carrier density at transparency point
N_1	Carrier density at the departure of the 1st optical pulse from the SOA
N_i	Initial carrier density
N_{ss}	Carrier density at steady state
n_{eq}	Equivalent refractive index
n_p	Number of successive pulses applied to the SOA
P_{av}	Average output power over the SOA length (or the segment length)
P_{av1}	Average power of the 1st propagating optical pulse
P_{in}	Input signal power

P_{out1}	Power at output port 1 of SMZ
P_{out2}	Power at output port 2 of SMZ
P_p	Input pulse peak power
P_{poav}	Average output pulses peak powers from the SOA
q	Electron charge
SW	Width of the SMZ switching window
T	Non-uniform (triangular or sawtooth) cycle duration
T_{delay}	Time difference between applying both control pulses to the SMZ
t	Time
t_{bias}	Time taken for the SOA gain to reach steady state due to biasing
t_{int}	Propagation time of the optical pulse through the SOA length
t_p	Optical packet time duration
t_r	SOA gain recovery time
t_{sep}	Separation time between optical pulses
V	SOA active volume
W	SOA width
x	The point where the following optical pulse enter the SOA

z	Any given location within the SOA active region
α_{LEF}	Linewidth enhancement factor
α_s	Internal waveguide scattering loss
Γ	Confinement factor
Δn	Effective refractive index variation within the SOA active region
$\Delta \phi$	Induced phase shift experienced by propagating optical signal through the SOA active region
$\Delta \varphi$	Phase difference of the input signals between both arms of the SMZ
ε	Gain compression factor
λ	Input signal wavelength
λ_o	Peak gain wavelength at transparency
λ_N	Peak gain wavelength
σ	Gain or output power standard deviation

LIST OF FIGURES

Chapter 1: Introduction

Chapter 2: Semiconductor Optical Amplifier

Chapter 3: SOA Characteristics and Segmentation Model

Chapter 4: Optimisation of Key SOA Parameters for Amplification Function

Chapter 5: Optimisation of Key SOA Parameters for Switching Function

Chapter 6: SOA Gain Uniformity Improvement Employing Wavelength Diversity Technique for High Speed Optical Routers

Chapter 7: SOA Gain Uniformity Improvement Employing Classical Non-Uniform Biasing Technique for High Speed Optical Routers

Chapter 8: Optimised Biasing for SOA (OBS)

Chapter 9: Experimental Implementation of Optimised Biasing for SOA (OBS) Pattern

xxix

LIST OF TABLES

xxx

Chapter 1   Introduction

1.1.   Research Fundamentals

As the demand for network capacity is rising due to the rapid increase in the Internet traffic volume, there is a growing need for all-optical based system. The all-optical system should offer much greater bandwidth and higher reliability than the traditional copper cables and the optoelectronic based communication technologies. The speed of the conventional electronic components used in these systems is limited to 40 Gb/s [1, 2] and therefore, imposes a speed and a capacity bottleneck to the networks.

In the beginning, optical fibre network started as a simple connection with no routing capability. The use of wavelength division multiplexing (WDM) and optical time division multiplexing (OTDM) [3-6] increased the overall capacity of the point-

to-point optical fibre transmission systems. The development of second-generation high speed systems such as the synchronous optical network and the synchronous digital hierarchy offered supplementary switching and routing capabilities to the network [7-9]. Optical add/drop multiplexers and optical cross-connectors were further introduced to the network in order to offer wavelength routing capabilities [7, 10]. However, in such systems the switching process is still performed in the electrical domain requiring optical-electrical-optical (O-E-O) conversion modules [11, 12]. To meet the network speed and capacity demands and to overcome the bottlenecks of O-E-O conversion, ultra-fast photonic networks that rely on photonic signal processing are required. The next generation optical network is aimed to carry out all the processing in the optical domain, operating at speeds (hundreds of gigabits per second) well beyond the existing electronic devices [13-18]. It is important to note that an all-optical processing technology is not a replacement but is a complementary alternative to the electrical processing particularly at the backbone optical layer where the data rate is extremely high.

Both circuit and packet switching schemes could be adopted in all-optical networks. However, packet switching is more flexible than the circuit switching in dealing with the bursty traffic and having higher throughput and switching speed [19-21]. An all-optical network offers transparency [22], implying that data can be carried at a range of bit rates and protocols and it can also support different higher layers. Figure 1.1 shows a typical packet switching core network. It is composed of optical core routers (nodes) where packets are routed from edge routers that are

2

identified by unique addresses and the fibre links connecting these routers. In optical core networks, packets traverse a number of different nodes before reaching their destination ones.
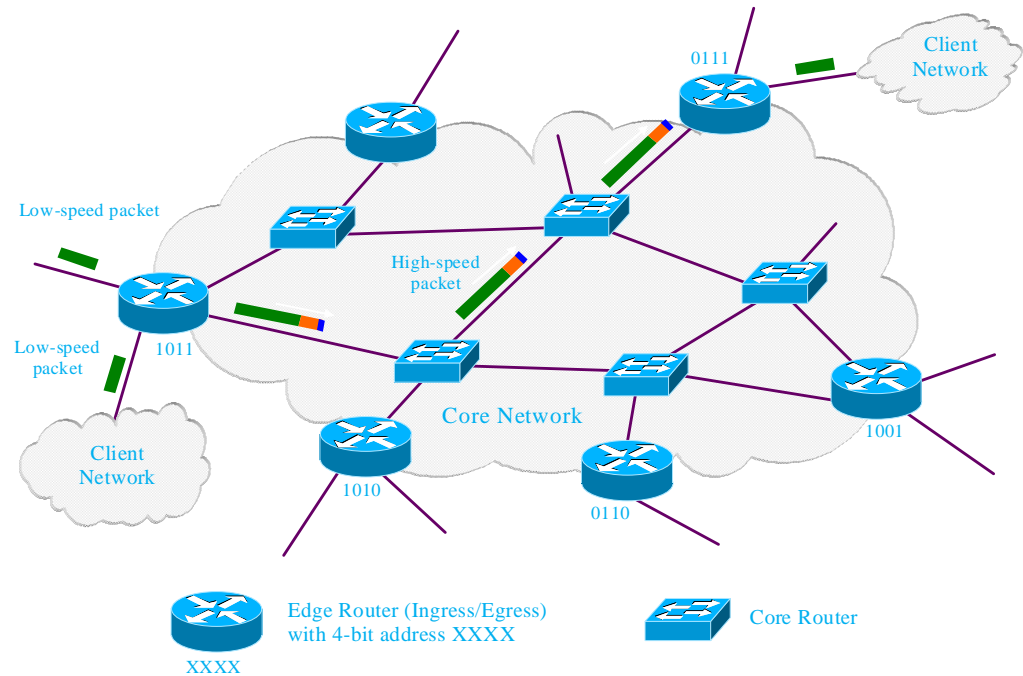
Figure 1.1 A photonic packet switching core network [23]

The transmitted optical packet consists of a clock signal, address bits and the data payload as shown in Fig. 1.2. A typical all-optical core router consists of a clock extraction module, header extraction, header recognition (to compare the header with a routing table) and an optical switching unit (see Fig. 1.3).
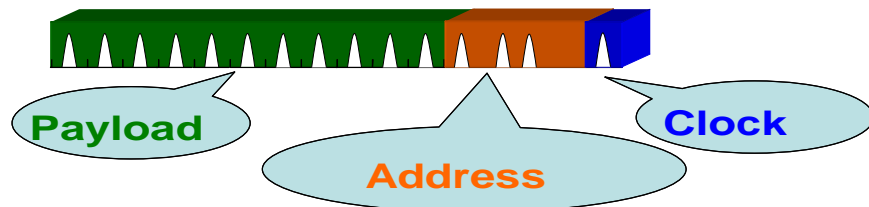
Figure 1.2 A typical format of an optical packet

3

The router architecture is based on the pulse position modulation header processing (PPM-HP) scheme that has been developed in the Optical Communication Research Group (OCRG) at Northumbria University. In this scheme, an N-bit packet header address and a look-up routing table are converted into the PPM format. PPM-HP scheme significantly downsizes the look-up routing table and offers robust packet routing regardless of the packet header length and network dimension as well as improved processing time and reduced system complexity [23].
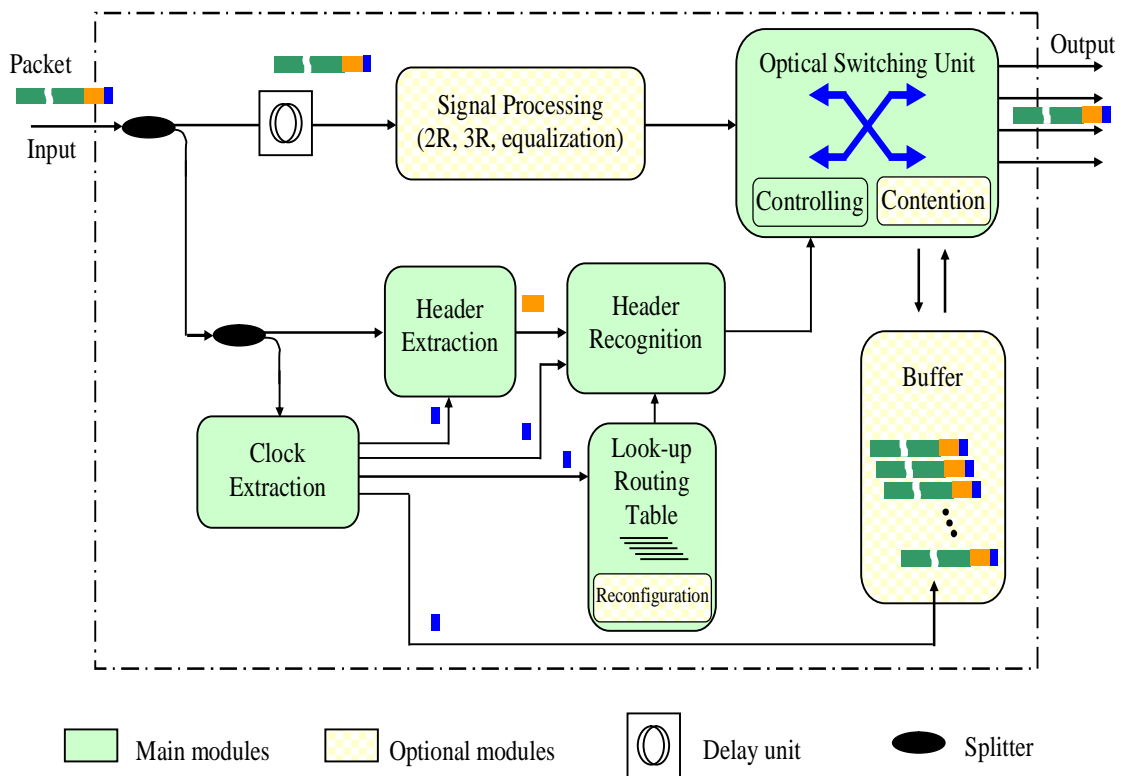
Figure 1.3 Block diagram for an all-optical router [23]

With reference to Fig. 1.3, on arrival of packets first of all the clock signal is extracted for system synchronisation. The header extraction module is used to

4

recover the address or label of the packet and then converts it into an appropriate format for the header recognition module. The function of the header recognition is to process the extracted header and to compare it with the routing table; the matching output signal is then forward to the optical switching unit.

The development of high capacity optical networks increased the demand for new optical devices that are able to perform in almost all all-optical functions. The key processes in all-optical switching are regeneration and wavelength conversion where SOA is the key building block. Among all-optical switches [24], ultra-fast all-optical switches based on the SOA, such as Mach-Zehnder interferometers (MZI) [25-31] are the most promising candidates for the realisation of all-optical switching and processing applications compared to other switches, such as ultra-fast non-linear interferometers (UNIs) [32, 33] and terahertz optical asymmetric demultiplexers (TOADs) [34-36].

The use of SOA-based Mach-Zehnder interferometer (SOA-MZI) schemes will allow the processing of packets 'on-the-fly' in future photonic routers. The SOA-MZI is used in almost all functions inside a photonic router such as, clock extraction circuits, header/payload separation, optical flip-flops, wavelength converters, all-optical gates and switching [37-48]. The performance of SOA, in terms of the gain temporal behaviour, the carrier density and stimulation emission, is affected by several factors including the dimensions of the waveguide and input parameters such as the external bias current and the power and wavelength of the propagating input pulses. Controlling these factors will lead to improving and optimising the SOA amplification and/or switching characteristics as well as the

5

uniformity of the generated output pulses that is necessary to reduce the system power penalty.

A number of models have been proposed to investigate the SOA gain dynamics, which also includes the pump signal propagation [49-53]. However, in these models the direct relationship between the input signal gain and wavelength which would help maximising amplification has not been addressed. Moreover, the fast and the strong non-linear features that characterise SOAs are widely studied in the literature [54-57]. Nevertheless, these features were not adapted to set the optimum conditions for the switching operation.

The SOAs performance is determined, to a great extent, by their gain recovery time characteristics. To that end, for many high speed applications, SOAs must have a fast gain recovery in order to ensure a minimum gain standard deviation for the input pulses and therefore, avoid system power penalties arising from bit pattern dependencies [58-60]. The SOA gain uniformity is also essential when used in high speed optical routers. The gain recovery of SOA is limited by the carrier lifetime, which itself depends on the applied or bias current [61]. Different approaches have been used to speed-up the SOA gain recovery time. This is done by changing the SOA cavity length, by changing the input pulse width or by externally injecting an assist light at the transparency point of the SOA [38, 62-66]. However, no work on directly improving the SOA gain uniformity using its characteristics has been reported in the literature.

Limited investigations have reported applying non-uniform currents to the SOA in literatures. Only narrow impulses [67] and exponential [68] shaped currents were recorded to reduce the SOA switching time. However, these biasing schemes require more applied energy to the SOA device. Nevertheless, the linearity of the output gain experienced by all input pulses has not been addressed by the researchers.

1.2.   Aims and Objectives

All-optical routers are able to support networks with high capacity and with reduced power consumption. In an all-optical router, the building block for most of the modules is the symmetric Mach-Zehnder (SMZ) which is a SOA-based Mach-Zehnder interferometer. The aim of this research is to optimise the performance of the SOA in order to efficiently execute different tasks within the optical router and to overcome some of the SOA limitations observed at high speed data rates. The key objectives are outlined as follows:

1. Designing a position-dependent segmentation model of SOA in order to analyse the propagation of input signals through its active region. The model should execute all the rate, propagation and phase shift equations to investigate the factors affecting the SOA operation.

2. Locating and controlling the boundaries and conditions for the SOA in order to optimise its characteristics so that it could be used to perform different functions such as amplification and switching when used in all-optical routers.

3. Improving the SOA gain uniformity when injected with high speed input data in order to reduce the system power penalties arising from bit pattern dependencies. This task includes proposing novel techniques to minimise the gain standard deviation of the output pulses.

4. Developing an experimental setup to demonstrate improved SOA gain uniformity at high speed using the optimised non-uniform bias current.

1.3.   Original Contributions

This thesis introduces a number of original contributions to the knowledge that are summarised as follows:

- Proposing a segmentation model of the SOA based on the numerical and mathematical equations. The model is used to analyse the impact of the input parameters and propagating signals on the SOA carrier density and its gain response to further understand the SOA operation [A3].

- Optimisation of conditions required for the SOA to maximise the output gain for amplification. The direct effects of the input pulse power, the bias current and the input signal wavelength on the SOA are investigated for the optimum amplification [A5, A7].

- Optimisation of SOA non-linear characteristics when used in optical switching. The boundaries and conditions necessary for the input parameters to achieve the 180° induced phase shift are identified and managed for switching function in SOA-based optical switches. These

investigations are essential in order to select the optimum control pulse needed for non-linear operation of SOAs [A5, A7].

- Proposed a new wavelength diversity technique to improve the gain uniformity of the SOA at high data rates. A gain standard deviation equation is introduced in order to measure the SOA gain uniformity [A9, A12].

- Proposed a novel technique, which employs electrical current characteristics, for enhancing the SOA gain uniformity at the high speed under certain conditions. Non-uniform biasing currents are used as alternatives to the uniform biasing current [A6, A11]. The non-uniform current pattern is then optimised to maximise the SOA gain uniformity for any input data rates [A15].

- Demonstration of practical implementation of the optimised non-uniform biasing technique to verify the improvement of the SOA gain uniformity at high input data rates [B1] and with different input bit patterns [B2].

In Fig. 1.4, a research road map is presented summarising the research areas and original contributions of this thesis.
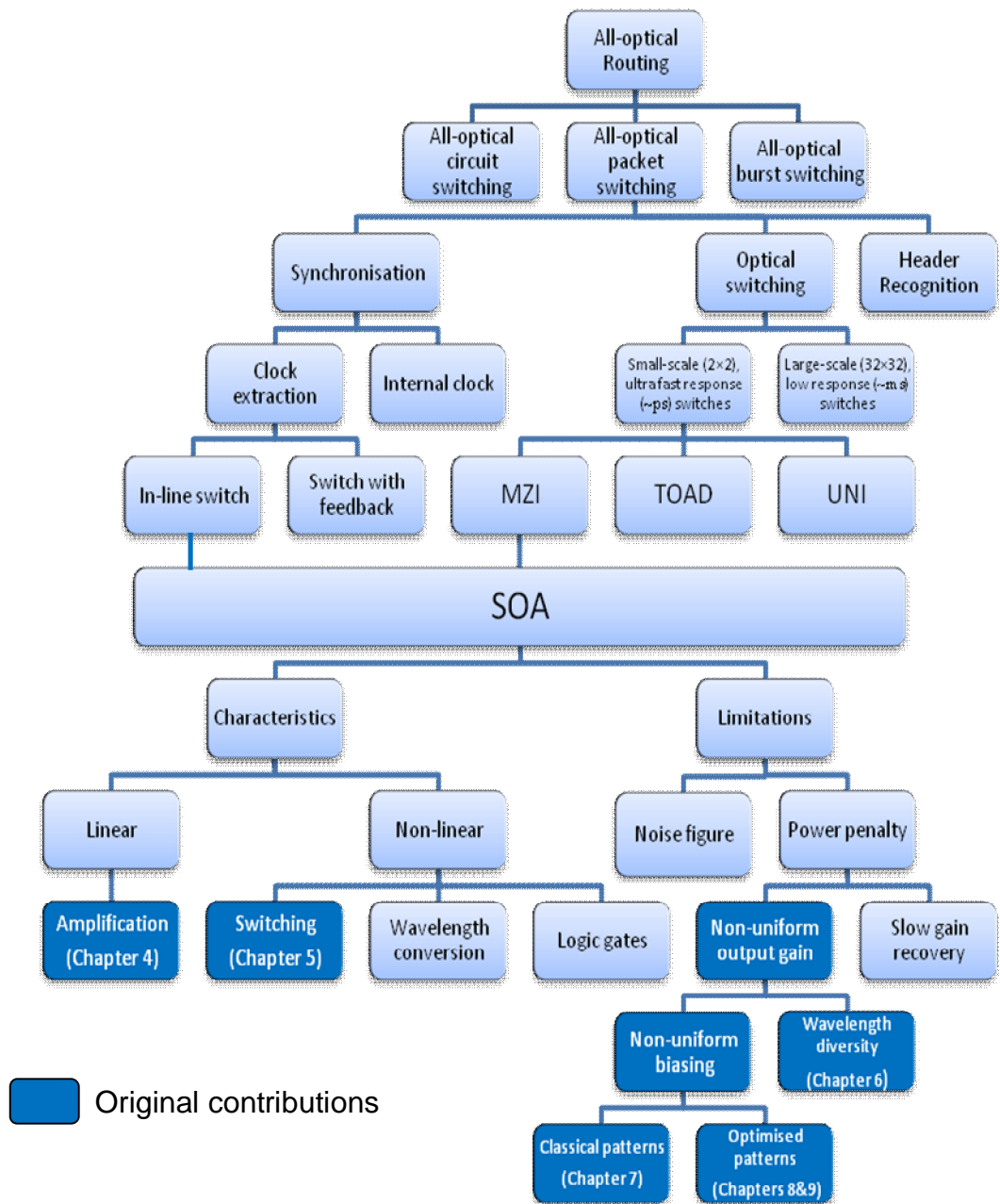
Figure 1.4 Research road map

1.4.   Publications

In this section, a list of the published and accepted papers generated from the work carried out through the thesis is presented.

1.4.1. Conference papers

[A1]   Chiang, M. F., Ghassemlooy, Z., Ng, W. P., Le Minh, H., and Abd El Aziz, A.: '*An ultrafast 1 x M all-optical WDM packet-switched router based on the PPM header address*', ICEE 2008, Paper No. 2631, Tehran, Iran, 13-15 May 2008.

[A2]   Chiang, M. F., Ghassemlooy, Z., Ng, W. P., Le Minh, H., and Abd El Aziz, A.: '*Multiple-hop routing in ultra-fast all-optical packet switching network using multiple PPM routing tables*', proceeding of IEEE International Conference on Communications 2008 (ICC 2008), ISBN: 978-1-4244-2075-9, pp. 5231-5325, Beijing, China, May. 2008.

[A3]   Abd El Aziz, A., Ng, W. P., Ghassemlooy, Z., Aly, M. H., and Chaing, M. F., '*Optimisation of the key SOA parameters for amplification and switching*', The 9th annual Postgraduate Symposium on the convergence of Telecommunications , Networking & Broadcasting (PGNET 2008), ISBN 978-1-902560-19-9, Liverpool, UK, pp 107-111, June (2008).

[A4]   Chiang, M. F., Ghassemlooy, Z., Ng, W. P., Le Minh, H., and Abd El Aziz, A.: '*1 x M Packet-switched router based on the PPM header address for all-optical WDM networks*', XIII Congreso Internacional de Telecomunicaciones SENACITEL 2008, paper no. T38, Valdivia, Chile, November 2008.

[A5]   Abd El Aziz, A., Ng, W. P., Ghassemlooy, Z., Aly, M. H., Ngah, R. and Chaing, M. F.: '*Characterization of the semiconductor optical amplifier for amplification and photonic switching employing the segmentation model*', *International Conference on Transparent Optical Networks "Mediterranean Winter"* 2008 (ICTON-MW'08), ISBN 978-1-4244-3485-5, Marrakech, Morocco, pp Fr1A.1 (1-6), 11-13 December (2008). **Invited paper**.

[A6]   Abd El Aziz, A., Ng, W. P., Ghassemlooy, Z., Aly, M. H., Ngah, R. and Chaing, M. F.: '*The effect of the input energy on the SOA gain with non-uniform biasing*', The 14th European Conference on Networks and Optical Communications (NOC/OC&I 2009), ISBN 978-84-692-2943-9, Valladolid, Spain, pp 307-315, June 2009.

[A7]   A. A. El Aziz, W. P. Ng, Z. Ghassemlooy, M. H. Aly, R. Ngah, and M. F. Chiang, '*Impact of signal wavelength on the semiconductor optical amplifier gain uniformity for high speed optical routers employing the segmentation model*', presented at Information Sciences Signal Processing and their Applications (ISSPA), 2010 10th International Conference on, pp. 259-262, 13-15 May 2010.

[A8]   Bahrami, A., Kanesan, T., Ng, W. P., Ghassemlooy, Z., Abd El Aziz, A., and Rajabhandari, S.: '*Performance evaluation of radio-over-fibre (RoF) system using Mach-Zehnder Modulator (MZM) and on-off keying (OOK) modulation schemes*', The 11th annual Postgraduate Symposium on the convergence

of Telecommunications , Networking & Broadcasting (PGNET 2010): Liverpool, UK, 2010.

[A9]   Abd El Aziz, A., Ng, W. P., Ghassemlooy, Z., Aly, M., and Ngah, R., '*Employing wavelength diversity to improve SOA gain uniformity*', The 15th European Conference on Networks and Optical Communications (NOC 2010) ,ISBN 978-972-9341-93-9, pp. 301-306, Faro-Algarve, Portugal, 8-10 June 2010.

[A10]   Ahmed, A., Elkomy, A. A., Aly, M. H., Ng, W P., Ghassemlooy, Z., and Abd El Aziz, A.: '*Performance of digital optical communication link: effect of in-line EDFA parameters',* Proceeding of the 7th Symposium on Communication Systems, Networks and Digital Signal Processing 2010 (CSNDSP 2010), ISBN: 978-1-86135-370-2, pp. 766-770, Newcastle upon Tyne, UK, July 2010.

[A11]   Abd El Aziz, A., Ng, W. P., Ghassemlooy, Z., Aly, M. H., Ngah, R.: '*SOA gain uniformity improvement employing a non-uniform biasing technique for ultra-high speed optical routers*', Proceeding of the 7th Symposium on Communication Systems, Networks and Digital Signal Processing 2010 (CSNDSP 2010), ISBN: 978-1-86135-370-2, pp. 702-707, Newcastle upon Tyne, UK, July 2010

[A12]   Abd El Aziz, A., Ng, W. P., Ghassemlooy, Z., Aly, M., and Ngah, R., '*Employing Multiple Wavelengths for an Input Packet to Achieve Uniform SOA Gain for High Speed Optical Applications*', The 16th European

Conference on Networks and Optical Communications (NOC 2011) ,ISBN 978-1-61284-753-5, pp. 99-102, Newcastle upon Tyne, UK, 20 22 July 2011.

1.4.2. Journal papers

[A13] Chiang, M. F., Ghassemlooy, Z., Ng, W. P., Le Minh, H., and El Aziz, A. A.: '*Simulation of an all-optical 1x2 SMZ switch with a high contrast ratio*', The Mediterranean Journal of Electronics and Communications, 6 (2). pp. 58-64, 2010.

[A14] Chiang, M. F., Ghassemlooy, Z., Ng, W. P., Le Minh, H., and El Aziz, A. A.: '*1xM Packet-switched router based on the PPM header address for all-optical WDM networks*', The Mediterranean Journal of Electronics and Communications, 6 (3), pp.78-85, 2010.

[A15] Ng, W. P., Abd El Aziz, A., Ghassemlooy, Z., Aly, M., and Ngah, R., '*Optimised Non-uniform Biasing Technique for High Speed Optical Router to Achieve Uniform SOA Gain*', Special Issue IET Communications Journal, 2011. **Accepted**.

1.4.3. Papers in progress

[B1] Abd El Aziz, A., Ng, W. P. and Ghassemlooy, Z., '*Experimental Demonstration of Optimised Non-uniform Biasing Technique to Improve SOA Output Power Uniformity at High Speed Data Rates*', IEEE Photonics Technology Letters, 2011.

[B2]   Ng, W. P., Abd El Aziz, A. and Ghassemlooy, Z., '*SOA Output Power Uniformity Improvement with Experimental Optimised Non-uniform Biasing for Different Input Bit Patterns*', *Lightwave Technology, Journal of,* 2011.

1.5.   Chapter Outline

This research first studies the fundamental characteristics and types of SOA devices. The structure and theory of operation for both the SOA and SMZ devices are also explained in Chapter 2.

Chapter 3 presents the entire mathematical analysis used in this work and the proposed segmentation model of the SOA. The impacts of input signals on the segmentation model are simulated employing all the rate, propagation and phase shift equations.

In Chapter 4, key parameters of the SOA are optimised for maximum amplification. The chapter locates and controls the factors affecting the SOA amplification operation. On the other hand, Chapter 5 depicts the boundary conditions and requirements for the SOA optimal switching operation. The key optimisations for switching are obtained by controlling the input parameters to achieve the desired phase shift.

Chapter 6 proposes a novel wavelength diversity technique to the SOA in order to avoid the power system penalty by improving the gain uniformity at the high speed.

In Chapter 7, a novel technique is proposed to improve the SOA gain uniformity. Periodic non-uniform biasing current signals are used as an alternative to the more established uniform biasing current. The non-uniform biasing current pattern is optimised in Chapter 8 to maximise the gain uniformity at high speed and to overcome all limitations observed in Chapter 7. The chapter also proposes a non-uniform biasing equation to optimise the gain flatness of the input data at any speed.

In Chapter 9, a practical work is demonstrated by employing the optimised non-uniform biasing current introduced in Chapter 8 in order to confirm the SOA gain uniformity improvement. Finally, Chapter 10 concludes this thesis by summarising all the research findings and proposals while Chapter 11 outlines the future research work.

Chapter 2   Semiconductor Optical Amplifier

2.1.   Introduction

In modern photonic networks, optical amplifiers are not only used as a general gain unit but they also have many functional applications [7, 18, 41, 45, 46]. Optical amplifiers can be categorised into two classes: Optical fibre amplifiers such as erbium doped fibre amplifiers EDFAs [69, 70] and waveguide amplifiers such as SOAs [71, 72]. EDFAs are mainly used for in-line optical signal amplification because of their wide optical amplification bandwidth, simplicity, a high output saturation gain, low polarisation insensitivity, a low coupling loss and a low noise figure [7, 9, 69, 70]. On the other hand, SOAs are used in many functional applications including all-optical switching, regeneration and optical logic signals

due to their small size, a low switching energy, high stability, fast and strong non-linear characteristics, and the potential of integration with other electronic and optical devices [7, 18, 71, 72].

The SOA is also considered a key component for cascaded optical fibre systems and optical gating [73-75]. Optical gates are needed in most all-optical functions such as the wavelength conversion, the add-drop wavelength and time multiplexing, the clock recovery and the simple bit pattern recognition [44, 76].

Due to the lower cost and no requirement for optical isolators as often used in different types of amplifiers such as EDFAs [77], SOAs are furthermore used as in-line amplifiers for bi-directional transmission in local and metropolitan systems and networks. For that reason, it is important to recognise SOA characteristics and its functionality.

2.2. Semiconductor Optical Amplifier

2.2.1. SOA structure

Semiconductor optical amplifier is an optoelectronic device composed of an optical waveguide. An input light signal injected into a SOA from the input facet side through the active region will experience gain (amplification) under certain conditions. The gain is achieved by applying an external electrical current to the SOA [71]. The SOA is coated with an input and output facets as depicted in the schematic diagram in Fig. 2.1. The SOA input and output facets result in gain ripples due to their reflective characteristics [71].
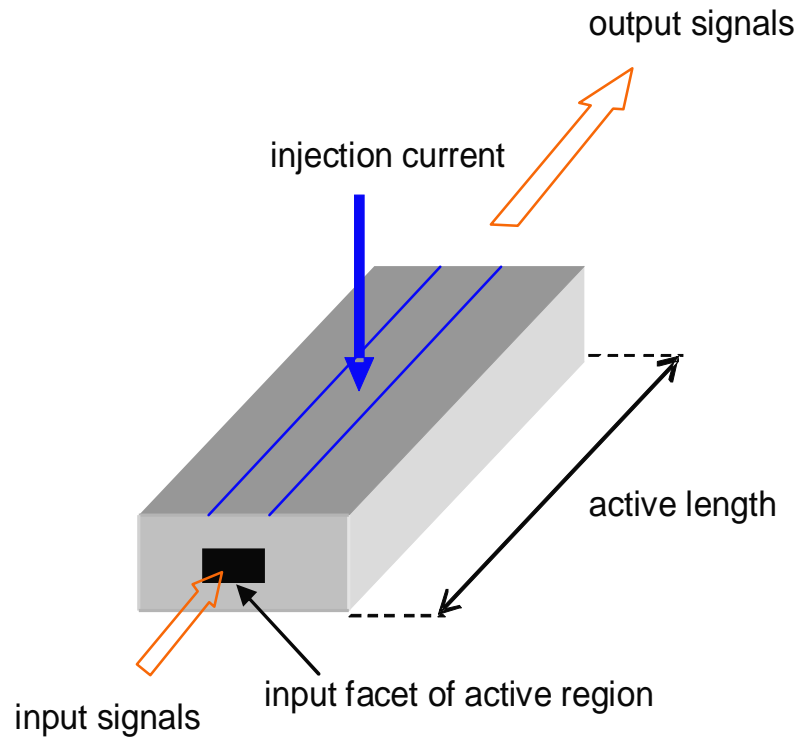
Figure 2.1 Schematic diagram of the SOA

2.2.2. SOA types

There are two main types of SOAs: the Fabry-Perot SOA (FP-SOA) and the travelling-wave SOA (TW-SOA) as shown in Fig. 2.2. In case of FP-SOA, the injected optical signal undergoes several reflections from the end facet [71, 78, 79]. On the other hand, in TW-SOA the injected signal undergoes a single pass due to the very low level of reflectivity on the end facet. TW-SOA offers several advantages over FP-SOA including a wider bandwidth, improved gain saturation and lower noise characteristic. Moreover, the impacts of the bias current, temperature and signal polarisation fluctuations are more effective in the FP-SOA

type than the TW-SOA [71, 80]. However, FP-SOA operates below a threshold level and offer significant amplifications at low applied currents.
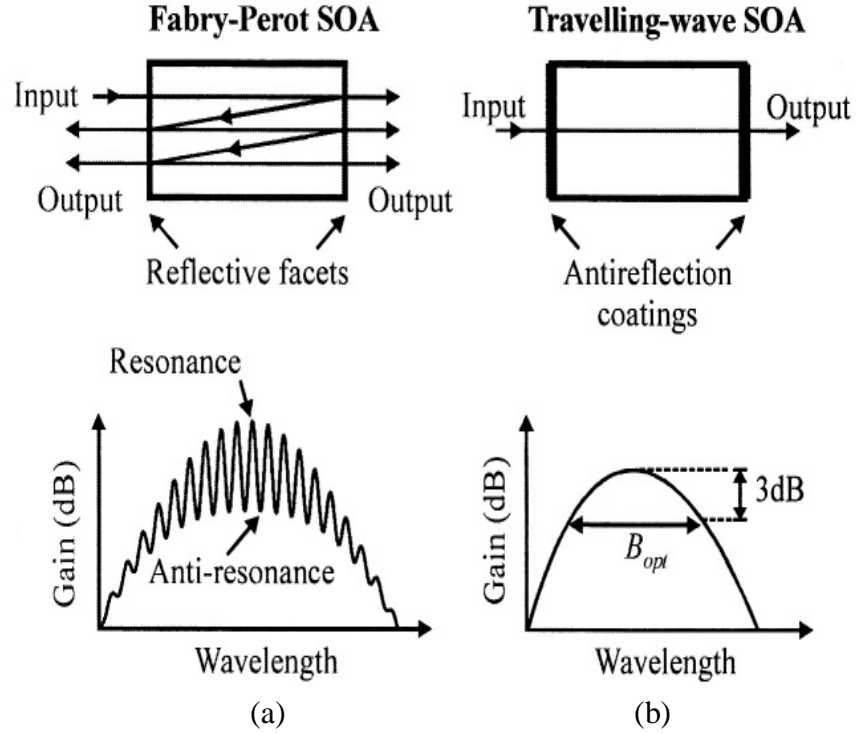
Figure 2.2 SOA types; (a) FP-SOA with ripples on the gain spectrum and (b) TW-SOA with a smooth gain spectrum [71]

The gain spectrum of the FP-SOA exhibits ripples caused by the reflections at the end facets (see Fig. 2.2 (a)), thus making the device strongly frequency dependent. For this reason, FP-SOAs are replaced by TW-SOAs in almost all practical applications [81, 82]. This research has used the TW-SOA.

2.2.3. Amplification principles

Electrons acquire higher energy when the SOA is biased with a direct current. Therefore, applying more bias current will result in a larger number of excited electrons in the conduction band. Hence, the conduction and valence bands

(energy levels) containing electrons and holes, respectively are formed [39]. The formation of these energy levels results in three different processes that occur within the active region of the SOA as shown in Fig. 2.3:
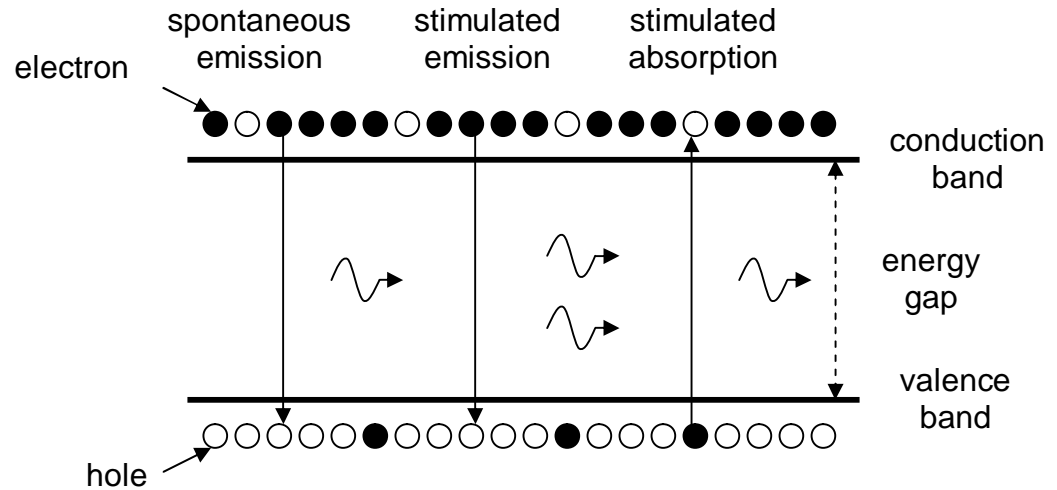
Figure 2.3 Three processes that along the active region of the SOA

1. **Spontaneous emission:** this is the process where an excited electron from the conduction band drops to the valence band releasing a photon or generating heat in the active region. This process is considered as a loss or noise because the generated photon is radiated with different phase and direction.

2. **Stimulated absorption:** this is the process by which an electron in the valence band absorbs enough energy from an incident photon to overcome the energy gap and move to the conduction band. As a result, power is lost from the input light signal and also considered as noise.

3. **Stimulated emission:** this process occurs when an incoming optical beam enters the active region of the SOA waveguide via the input facet. The input photons interact with a number of excited electrons from the conduction band releasing stimulated photons with the same phase, frequency and direction (i.e. amplification takes place). More identical photons are released by this interaction, thus amplifying the input beam [23, 39] (see Fig. 2.4).
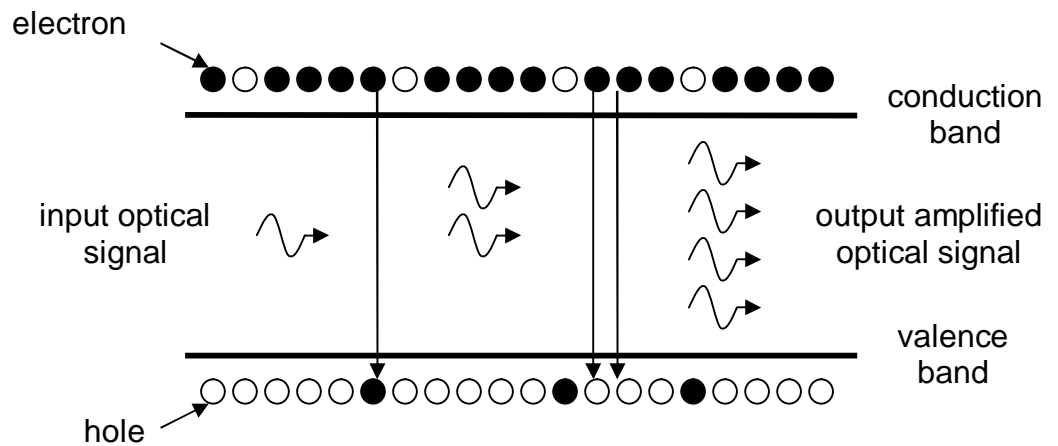
Figure 2.4 SOA amplifications due to stimulation emission process

The reduction of excited electrons (i.e. the carrier density) in the conduction band will lead to a drop in the SOA gain. This gain depletion is proportional to the carrier population density and will furthermore increase the active refractive index. The reason for such increase is the dependence of the non-linear refractive index on the SOA carrier density [83, 84].

The carrier non-equilibrium is governed mainly by the spectral hole burning effect [85-87]. The distribution recovers to the equilibrium state by the carrier-carrier scattering process. Instantaneous mechanisms such as the two-photon absorption [88-90] and the optical Kerr effects [91-93] will then influence on the SOA response. After few picoseconds, a quasi-equilibrium distribution will take place due to the carrier temperature relaxation process and then the carrier density will be recovered [94].

2.2.4. Types of SOA material structure

Bulk and multi-quantum-well (MQW) SOAs are the two most commonly used types of material structure to fabricate the SOA active region. The type of material structure used will determine the SOA gain spectrum and operational characteristics.

The bulk SOA active region is fabricated using a direct band-gap material while the active region of a MQW-SOA is fabricated by an indirect material. Generally, the direct band-gap structure is more likely to be used due to the higher probability of electrons conversion into photons [71].

The MQW-SOAs material structure type have the advantage of providing higher saturation power, higher gain, wider bandwidth and lower noise figure compared to bulk SOAs. On the other hand, a bulk SOA is preferred for applications requiring strong cross phase modulation because of its larger phase-to-amplitude coupling factor and larger optical confinement factor. As a result, offering stronger non-linear effect. In this research, the SOA used is of the bulk material structure.

23

2.3.   Fundamental SOA Characteristics

Semiconductor optical amplifier is an optical gain device that can be used for several different optical applications. The desired properties of the SOA depend on the function of the application. This section introduces the fundamental characteristics of the SOA.

2.3.1.   Signal gain

There are two types of signal gain for SOAs: the fibre-to-fibre gain, where the input and output coupling losses are considerate. The other gain is the intrinsic gain, which is the ratio between the signal output and input power at the output and input facets, respectively. The SOA gain depends on its type, material structure and operational parameters. In this thesis, the SOA model used is the bulk TW-SOA as mentioned earlier in the previous sections. The SOA operational parameters are discussed in details in the next chapter.

2.3.2.   Saturation gain

One of the key factors affecting the SOA gain is the input signal power. The depletion of carriers in the conduction band (i.e. carrier density) is higher for higher input signal power. As a result lower gain is achieved by the input signal. An important parameter is the saturation output power, which is output signal power when the amplifier gain is halved (i.e. -3 dB). For SOA amplification applications, the saturation gain can result in a significant signal distortion, while it can be useful

for other functions such as switching. The SOA operation for amplification and switching functions are further discussed in Chapters 4 and 5.

2.3.3. SOA polarisation sensitivity

The SOA structure, the type and the active region material are factors defining the input signal polarisation condition. Due to the dependence of the SOA gain on the signal polarisation, it is more complicated for some applications to employ this feature such as cascaded SOAs applications. However, other applications such as SMZs rely on the SOA polarisation sensitivity for achieving the efficient switching function. The SMZ theory of operation will be discussed and explained later in this chapter. There are two main polarisation orthogonal modes for the SOA waveguide: the transverse electric (TE) and the transverse magnetic (TM) modes. Therefore, the polarisation sensitivity of the SOA can be defined as the magnitude of the difference between the TE and TM mode gains [71].

2.3.4. SOA gain recovery time

When an input signal enters the SOA, depletion in the carrier density, which corresponds to the input signal power, will takes place. As a result, the SOA gain saturates and recovers back within few hundred picoseconds (see Section 2.2.3) [95]. In high speed optical applications, the input bit streams are applied to the SOA prior to full recovery of the SOA gain. Therefore, the input signals will experience different gains thus resulting in system power penalty [58]. In this thesis, new techniques are proposed in Chapters 6, 7 and 8 to overcome the addressed problem.

If input pulses with wide durations are applied to the SOA, then the amplifier gain will react relatively quickly to changes in the input signal power, which can cause signal distortion. In this research, short pulses are used as the input signal is outlined in the next Chapter.

2.3.5. SOA non-linearities

Although the non-linear features of the SOA can cause problems, such as frequency chirping, these features are useful in applications such as the wavelength conversion and switching widely used in high speed photonic networks. There are three major non-linear effects based on SOA;

1. **Cross-gain modulation (XGM):** this takes place when a strong signal at a given wavelength λ_1 is applied to saturate the carrier density of SOA. This saturation results in modulation of the weak continuous wave (CW) input signal at a different wavelength λ_2 applied to the SOA. The XGM causes an inversion of the input signal shape and acts as a wavelength converter as displayed in Fig. 2.5 [96-98].
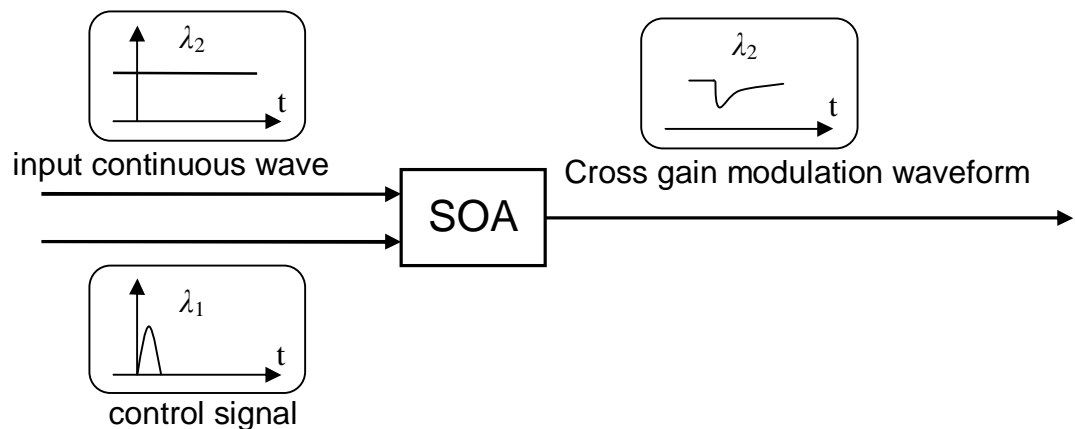
Figure 2.5 Cross-gain modulation in wavelength conversion

26

2. **Self-phase modulation (SPM) and cross-phase modulation (XPM):** the depletion of carrier density due to the propagation of an input signal pulse through the active region of the SOA results in changes of the effective refractive index. The leading edge of the propagating pulse achieves a different induced phase shift compared to the lagging edge. This behaviour is known as SPM that affects the input pulse shape. This non-linear characteristic of the SOA can be used in several applications including the dispersion compensation [99, 100].

When two or more input signals are applied to the SOA, XPM will takes place between the signals [101]. A number of applications have been developed based on XPM including the wavelength conversion and optical switches, which depend on phase changes [102-104]. SMZ is a good example for an optical switch that utilises XPM as explained in the following section.

3. **Four-wave mixing (FWM):** this is the process where two input signals with the same polarisation at different wavelengths are applied to the SOA, resulting in a new signal at a different frequency ($\lambda_o+\Omega$) due to gain modulation, see Fig. 2.6. The two input signals are the strong control signal and the input signal at wavelengths of λ_o and ($\lambda_o-\Omega$), respectively. The generated signal is similar to the input signal however, the spectrum is inverted (i.e. opposite phase), and thus the conjugate signal.
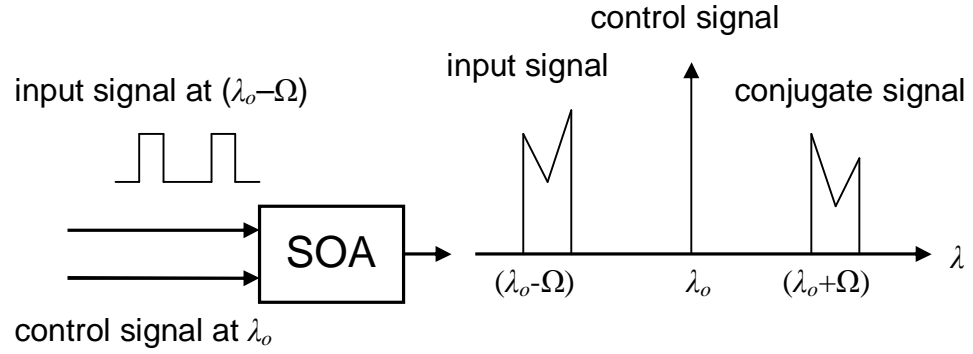
Figure 2.6 Four-wave mixing

Since more than one input signals are required in FWM, the generated signal may be turned on and off by switching one of the input signals on and off. A number of applications such as all-optical wavelength converters [105-107], and all-optical logic gates [45, 108] have been developed based on the FWM. Moreover, FWM allows multi-channel operation and provides phase conjugation, which is an efficient method to overcome the dispersion problem in optical fibre communications [109]. However, there are some drawbacks to this technique such as the polarisation sensitivity, the wavelength dependency of SOA and lower conversion efficiencies [71].

2.4. Main SOA Applications

2.4.1. SOA-based switches

There are several optical switches that are used in all-optical networks. One of the most promising switches among those is the SMZ due to its compact size, thermal stability, low power operation and their short and square switching window.

28

Considering various MZI configurations, the SMZ structure provides the highest flexibility and shortest switching window [31, 110]. As displayed in Fig. 2.7, the SMZ structure consists of two identical SOAs, polarisation beam splitters (PBSs), two polarisation controllers (PCs) and four 3 dB couplers.

Switching operation is performed with the aid of two high power control pulses (CP1) and (CP2). These control pulses create a switching window in order to switch the input signal from one port to another. The switching time duration is the time difference between applying both control pulses to the two identical SOAs (T_{delay}).
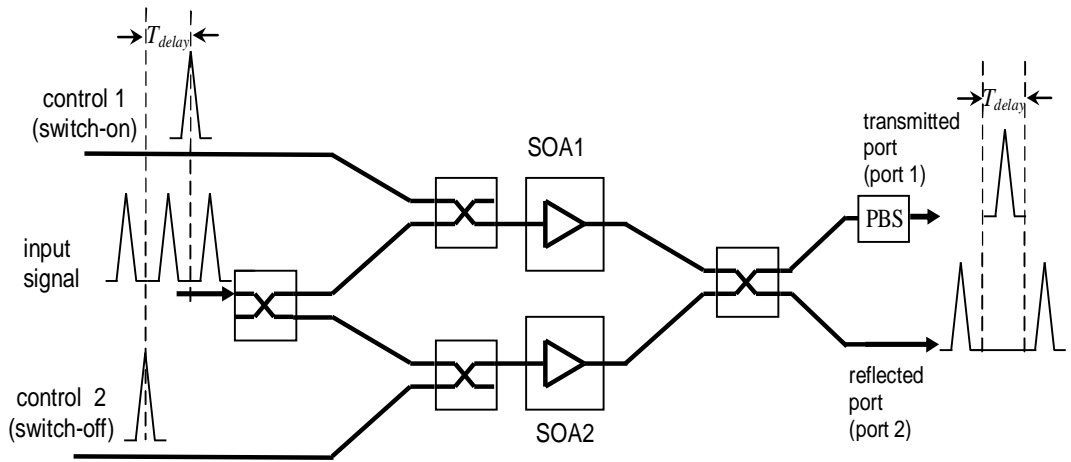
Figure 2.7 SMZ structure for switching operation

Before applying any control pulse to the SOA, both arms of the SMZ are in the balanced state and the input signal will exit the SMZ via port 2. The switching window starts by applying CP1 to SOA1, which will result in variations in SOA gain characteristics and therefore will change the balanced state of the SMZ. As a

29

result, the output signal is switched from port 2 to port 1. To switch off the switching window, CP2 is then applied to SOA2 delayed by the switching time duration T_{delay} from the entrance of CP1. Consequently, the SMZ balances again and results in the emerging of the input signal from port 2. In order to differentiate between the CPs and input signals at the SMZ output ports, CPs are applied at orthogonal polarisation to the data pulses by using two PCs. At the output ports, PBS is used to the separation of signals.

The power at both output ports of the SMZ are given as [111], respectively:

$$P_{out1} = \frac{1}{8} \cdot P_{in} \left[G_1 + G_2 - 2 \cdot \cos(\Delta\varphi) \cdot \sqrt{G_1 G_2} \right], \tag{2.1}$$

$$P_{out2} = \frac{1}{8} \cdot P_{in} \left[G_1 + G_2 + 2 \cdot \cos(\Delta\varphi) \cdot \sqrt{G_1 G_2} \right], \tag{2.2}$$

where P_{in} is the power of the input signal, G_1 and G_2 are the gains of the upper and lower SOAs and are described in the following chapter. $\Delta\varphi$ is the phase difference of the input signals between the upper and lower arms of the SMZ given by [111]:

$$\Delta\varphi = -0.5 \cdot \alpha_{LEF} \cdot \ln(G_1 / G_2), \tag{2.3}$$

where α_{LEF} is the linewidth enhancement factor.

The width of the switching window (*SW*) profile is given by [111]:

$$SW = \frac{1}{4} \left[G_1 + G_2 - 2 \cdot \cos(\Delta\varphi) \cdot \sqrt{G_1 \cdot G_2} \right]. \tag{2.4}$$

2.4.2. SOA wavelength converters

One of the most important functions required for increasing the optical networks flexibility and capacity is all-optical wavelength conversion [112, 113]. An all-optical wavelength converter is not only used to support high speed bit rates, it is a key solution for the wavelength blockage in optical cross-connects in WDM networks and contention problems in all-optical routers [114-116]. Contention occurs when two packets arrive simultaneously to a routing node at the same wavelength and compete for the same output port.

The optoelectronic wavelength converter consisting of a detector followed by a laser that re-transmits the incoming signal on a new wavelength results in large power consumption and introduces additional complexity [117]. An all-optical wavelength converter is a device that transfers information from one wavelength to another without entering the electrical domain. The non-linear characteristics are major advantages for the SOA to perform as an all-optical wavelength converter employing XGM, XPM and FWM (see Section 2.3.5).

In XGM, an input signal is used to modulate the SOA gain. A CW signal at the desired output wavelength λ_c enters the SOA to carry the same information as the intensity modulated input signal at λ_s. As shown in Figs. 2.8 (a) and (b), both input and CW signals either propagate through the SOA in the same or the opposite direction, respectively. In the case of both signals propagating in the same direction (i.e. co-propagating), an optical filter is used to separate the converted

signal from the input signal. On the other hand, if both signals propagate in the opposite direction (counter-propagating), there is no need for an optical filter.

(a)

(b)
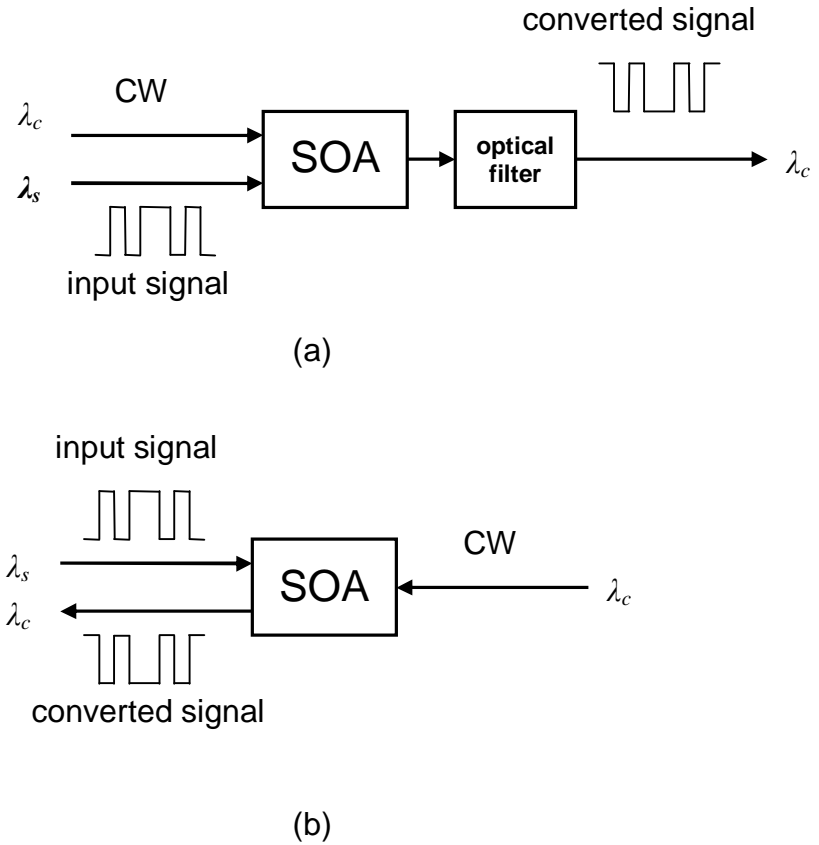
Figure 2.8 XGM wavelength conversions for (a) co-propagating and (b) counter-propagating input signals

The advantages of using XGM wavelength conversion devices are their simplicity, a high conversion efficiency, polarisation independence, and insensitivity to the input data wavelength [96, 117, 118]. However, these devices result in degradation of the extinction ratio. To overcome this problem the SOA converter can be used in the XPM mode.

The XPM scheme relies on the dependency of the refractive index on the carrier density in the active region of SOA. An incoming signal that depletes the carrier density will modulate the refractive index and therefore, result in the phase modulation of a CW signal coupled into the converter [117, 119, 120]. A good example for XPM wavelength converters is the MZI converter. The MZI configuration can be symmetric or asymmetric as shown in Figs. 2.9 (a) and (b), respectively.

(a)

(b)
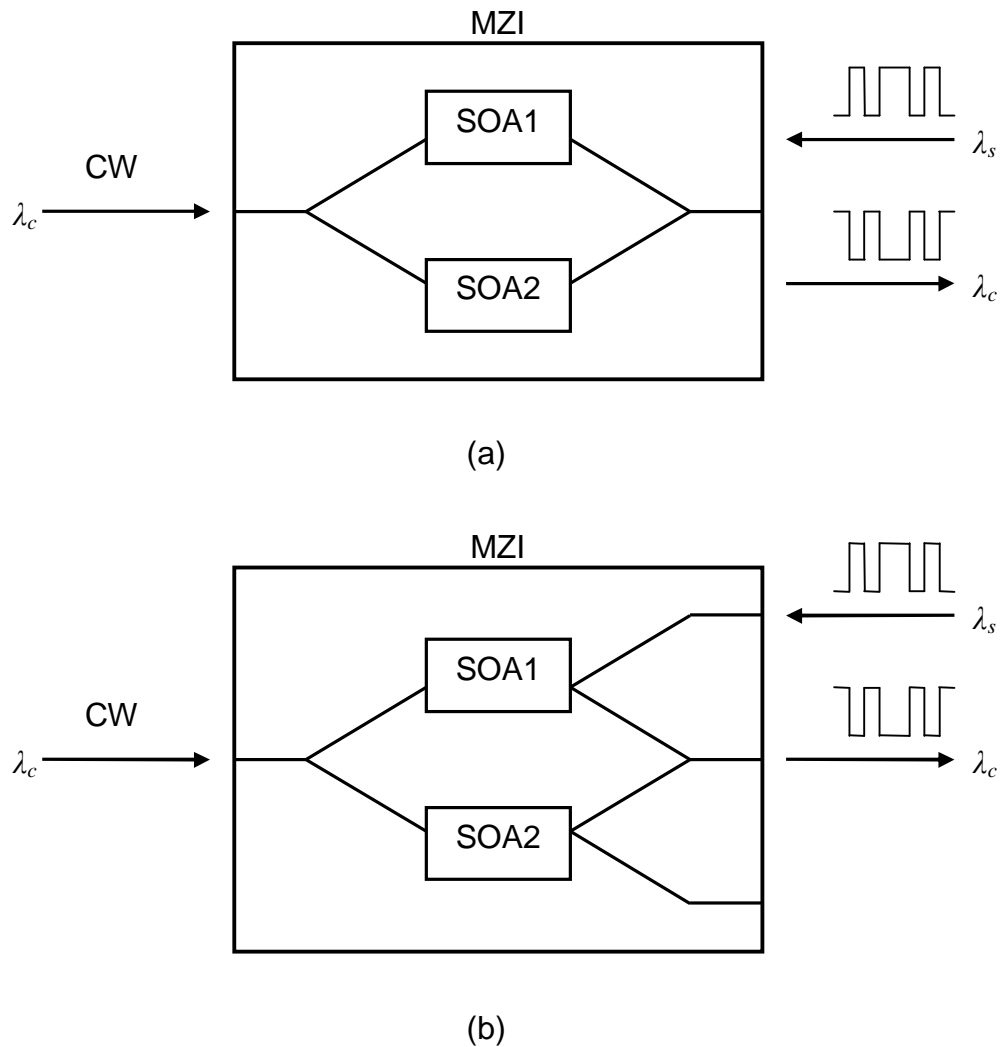
Figure 2.9 XPM wavelength conversions for (a) symmetric and (b) asymmetric MZI configurations

Interferometric devices such as MZIs utilising SOA non-linear characteristics offer excellent performance in wavelength conversion applications. They have the advantage of polarisation and wavelength independency, a low chirp, a non-inverting output, a partial regeneration of the input, and a high extinction ratio. On the other hand, restrictions on the amplitude modulation formats that could be used as well as a complex control biasing mechanism are the drawbacks of this device [117].

The SOA can also use FWM for wavelength conversion where CW and modulated input signals applied to the active region generate a new conjugate signal, which is an opposite phase to the input signal. An optical filter is used to select the conjugate signal (i.e. wavelength converted signal). The main disadvantages of FWM are their polarisation sensitivity and the frequency shift dependent conversion efficiency [121].

2.4.3. SOA dispersion compensation

In long haul communication link channel induced dispersion, in particular the chromatic dispersion limits the transmission data rates and/or the link span at higher data rates. As discussed in the Section 2.3.5, XPM and FWM schemes have been employed for effective dispersion compensation [122, 123].

2.4.4. SOA gates

For majority of all-optical functions in optical networks, there is a need for simple gates that can be controlled optically, as shown in Fig. 2.10. A gate used to

modulate a CW signal (or an input signal) can act as a wavelength converter, or part of an optical regenerator as shown in Figs. 2.10 (a), (b) and (c), respectively [76]. Whereas gating of an optical input signal can be used for time demultiplexing [124, 125].
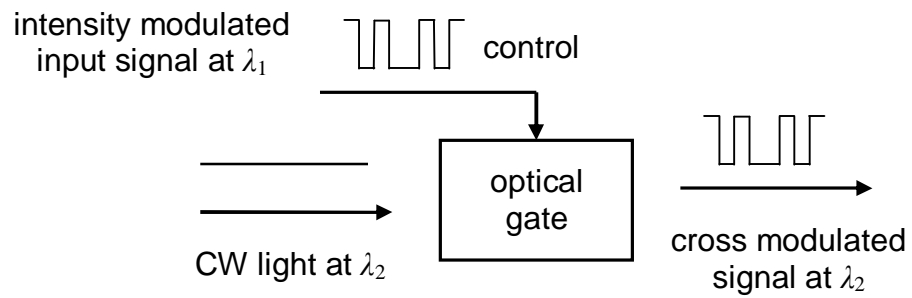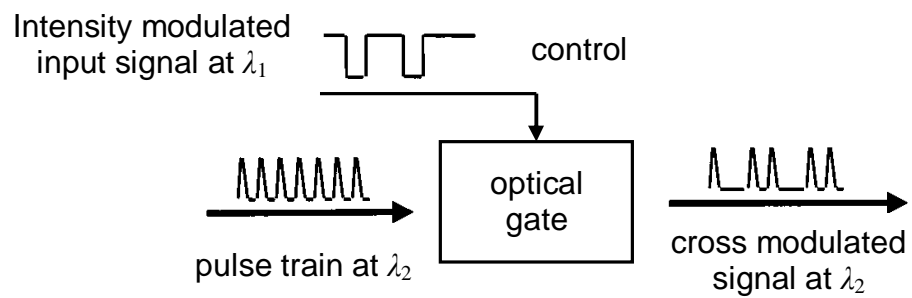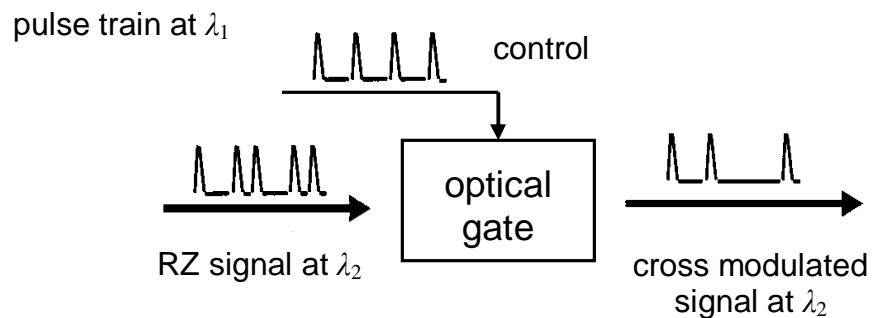
Figure 2. 10 Schematic of optically controlled gate used for: (a) wavelength conversion by gating of CW light, (b) regeneration and wavelength conversion by gating of clock pulses and (c) demultiplexing sampling by gating of optical signal using clock pulses.

Optical elements that can perform simple logic operations such as AND, XOR or NOR [76] are also useful for routing functions. Many different gate configurations can be constructed, the simplest of which consists of a single device as shown in Fig. 2.10 [126]. SOA gate arrays can also be used to construct all-optical packet switching nodes to direct the arriving optical packet to the desired output port. The gate array can be fully integrated with input and output waveguides and couplers [127].

2.5.   Summary

Realisation of signal processing in the optical domain overcomes the speed bottleneck imposed by the electronic components in very high speed optical networks. In such networks, one of the key components employed in amplification, wavelength conversion, switching and routing of optical signals is the SOA. This chapter focused on the SOA and its structure. The chapter outlined the SOA operation principle and different processes that occur during propagation of an input signal through the waveguide. The SOA structure and types were introduced. The chapter emphasised the fundamental SOA characteristics including the non-linear effects such as the XGM, XPM and FWM. In this chapter, the main applications that depend on the SOA such as switching and wavelength conversion were also highlighted.

In the following chapter, a segmentation model of the SOA is proposed utilising all the mathematical equations in order to study the factors affecting the SOA performance and to realise its boundaries and limitations.

Chapter 3   SOA Characteristics and Segmentation Model

3.1.   Introduction

This chapter presents the entire mathematical analysis used in this work and the proposed segmentation model of the SOA. A full mathematical analysis of the gain and the change of the carrier density of the SOA due to the propagation of input signals are presented in terms of the rate, propagation and phase shift equations based on the Wang's work [128]. In this chapter, a segmentation model of the SOA is proposed to further understand the factors affecting the SOA operation. The chapter also investigates the effect of an input pulse and a CW probe signals on the SOA gain responses.

3.2. Theoretical Model

In order to analyse the input parameters effect on the SOA gain and phase characteristics, a numerical model is developed. The model is based on the position-dependent rate and optical propagation equations for the carrier density and gain in the co-propagating direction for the injected input signals. Therefore, the model accounts for a non-uniform carrier distribution. The complete rate equations for the SOA are iteratively calculated in small segments with 1st and 3rd order gain coefficients [128-130].

3.2.1. Rate equations

When light is injected into the SOA, the carrier and photon densities within its active region will be altered. These changes can be described using the rate equations. The gain medium of the amplifier is described by material gain coefficient g (per unit length), which is dependent on the carrier density N and is given by [128, 129, 131]:

$$g = a_1(N - N_o),$$
(3.1)

where a_1 is the differential gain parameter and N_o is the carrier density at transparency point. The net gain coefficient is defined by:

$$g_T = \Gamma \cdot g - \alpha_s,$$
(3.2)

where Γ is the confinement factor which is the ratio of the light intensity within the active region to the sum of light intensity [71] and α_s is the internal waveguide

scattering loss. Assuming a constant carrier density at any given location z within any segment in the active region of the SOA, the total gain experienced by an optical wave can be calculated according to [131]:

$$G = e^{g_T \cdot z},$$ (3.3)

Therefore, the average output power P_{av} over the length of the SOA L can be expressed by:

$$P_{av} = \frac{1}{L} \int_0^L P_{in} \cdot G \ dz,$$ (3.4)

where P_{in} is the input signal power. Equation (3.4) can be rewritten as [129]:

$$P_{av} = P_{in} \frac{e^{(g_T \cdot L)} - 1}{g_T \cdot L}$$ (3.5)

The rate of change of the carrier density within the active region of the device is given by [53]:

$$\frac{dN}{dt} = \frac{I}{q \cdot V} - (A \cdot N + B \cdot N^2 + C \cdot N^3) - \frac{\Gamma \cdot g \cdot P_{av} \cdot L}{V \cdot h \cdot f},$$ (3.6)

where I is the SOA bias current, q is the electron charge and V is the active volume of the SOA. A is the surface and defect recombination coefficient while B and C are the radiative and Auger recombination coefficients, respectively. h is the Plank's constant and f is the input light frequency. The active volume is determined by $V = L \times W \times H$ where, W and H are the width and the thickness of the active region, respectively.

39

The cubic equation is the best fit to the real gain coefficient g, with the Lorentzian and the quadratic failing to replicate the gain at shorter wavelengths [132]. The material gain coefficient depends on both the carrier density N and the input signal wavelength λ and can be rewritten as [128]:

$$g = \frac{a_1(N - N_O) - a_2(\lambda - \lambda_N)^2 + a_3(\lambda - \lambda_N)^3}{1 + \varepsilon \cdot P_{av}}, \tag{3.7}$$

where a_2 and a_3 are empirically determined constants that are chosen to fit an experimentally measured SOA gain curve [132] to characterise the width and asymmetry of the gain profile, respectively. λ_N is the peak gain wavelength and ε is the gain compression factor. The peak gain wavelength is give by:

$$\lambda_N = \lambda_o - a_4(N - N_O), \tag{3.8}$$

where λ_o is the peak gain wavelength at transparency and a_4 denotes the empirical constant that shows the shift of the gain peak.

3.2.2. Propagation equation

The SOA is assumed to have negligible reflectivity at the end facets, so the reflected waves are omitted. The propagation of the input signal in the forward light direction along the length of the SOA is presented by the propagation equation and is given by [128]:

$$\frac{dP_{in}}{dz} = (\Gamma \cdot g - \alpha_s)P_{in}. \tag{3.9}$$

3.2.3. Phase shift equations

Changes in the carrier density take place with the propagation of the input signal pulse through the SOA, hence affecting its propagation coefficient (via the non-linear refractive index variations in the SOA active region). Because of the finite carrier lifetime, the leading edge of the input pulse experiences a different phase shift relative to the lagging edge. This process is (SPM) as highlighted in Chapter 2 [71, 128]. Let Δn represent the effective refractive index variation within the active region [128]:

$$\Delta n = \Gamma \frac{dn}{dN}(N - N_{ss}),$$ (3.10)

where dn/dN is the refractive index shift coefficient and N_{ss} is the carrier density at steady state (i.e. with no input signal launched to the biased SOA). The total phase shift experienced by the propagating input signal is [128]:

$$\Delta\phi = \int_{0}^{L} \frac{2\pi}{\lambda} \Delta n \cdot dz.$$ (3.11)

3.3. Segmentation Model

In order to understand the factors affecting the SOA gain and the emerging output signals, a segmentation model of the SOA is introduced where the SOA is divided into fifty equal segments of length $l = L/50$ each. The model helps in identifying the small changes that occur within the short length of each segment. Fifty segments were chosen for a sufficient accurate investigation on the change in the carrier

density and the signal gain along the SOA that match high speed input data rates up to 160 Gb/s.

3.3.1. Model characteristics

The above equations are adopted in order to fit the proposed segmentation model using Matlab[TM]. This model presents a bulk homogeneously broadened travelling-wave type SOA. The SOA segmentation model is illustrated in Fig. 3.1, showing the reduction of N due to the input pulse propagation through all segments. The carrier density is assumed to be constant within each segment. However, the carrier density and the signal power changes from segment-to-segment depending on the input power and the carrier density of the previous segment.
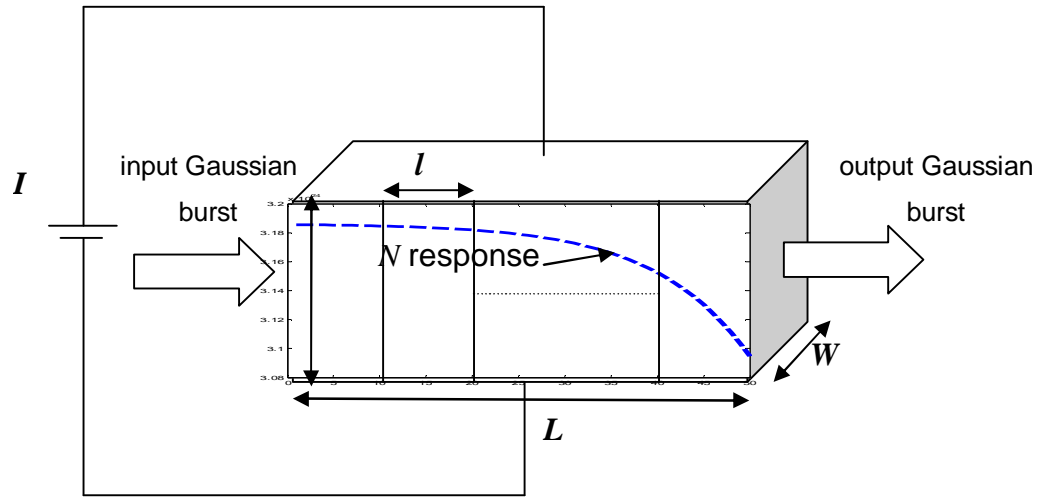
Figure 3.1 SOA active waveguide segmentation model

To calculate the segment total gain and its carrier density, the SOA length L is replaced with l in all the equations given in Section (3.2). The physical SOA parameters that are used for the rest of the study are given in Table 3-1. The SOA

input parameters, if not changed within the rest of the study, are λ = 1550 nm, I = 150 mA and input pulse peak power P_p = 1 mW. These parameters are used in theoretical and practical systems [71, 128].

Table 3-1 Physical parameters of the SOA

Parameter	Value
Carrier density at transparency (N_0)	1.4×10^{24} /m^3
Wavelength at transparency (λ_0)	1605 nm
Initial carrier density (N_i)	3×10^{24} /m^3
Internal waveguide scattering loss (α_s)	40×10^2 /m
Differential gain (a_1)	2.78×10^{-20} m^2
Gain constant (a_2)	7.4×10^{18} /m^3
Gain constant (a_3)	3.155×10^{25} /m^4
Gain peak shift coefficient (a_4)	3×10^{-32} m^4
SOA Length (L)	500 µm
SOA width (W)	3 µm
SOA height (H)	80 nm
Confinement factor (Γ)	0.3
Surface and defect recombination coefficient (A)	3.6×10^8 /s
Radiative recombination coefficient (B)	5.6×10^{-16} m^3 /s
Auger recombination coefficient (C)	3×10^{-41} m^6 /s
Gain compression factor (ε)	0.2 /W
Equivalent refractive index (n_{eq})	3.5
Differential of equivalent refractive index with respect to carrier density (dn/dN)	-1.2×10^{-26} /m^3

There are two kinds of transparency wavelengths: the material transparency wavelength (where the material gain is zero) and the device transparency wavelength (where the fibre to fibre gain is zero). Due to the coupling and waveguide loss, the device transparency wavelength is longer than the material transparency wavelength. The region between both wavelengths is called the transparency region [128]. The study focuses on the impacts of the material transparent light on the performance of SOA.

3.3.2. Input pulses characteristics

In this study, input pulses to the SOA model are single mode with narrow linewidths. The input optical pulse is Gaussian shaped with a full-width-half-maximum (FWHM) of 1.167 ps and peak power P_p of 1 mW as shown in Fig. 3.2. In the following chapters, the pulse power is the peak power of the Gaussian pulse. All the signal power is coupled directly into the SOA. The reason for chosen a pulse with a width of > 1 ps is that at shorter pulses (i.e. widths < 1 ps) intraband relaxation processes are not sufficiently fast to instantaneously replenish the depleted carriers due to amplification in the energy range corresponding to the pulse spectrum (spectral hole burning). If the average energy of the hole is lower than that of the initial state, the result is a rise in the average carrier temperature. The carrier-heating component becomes non-negligible as the pulse width approaches 1 ps [89].
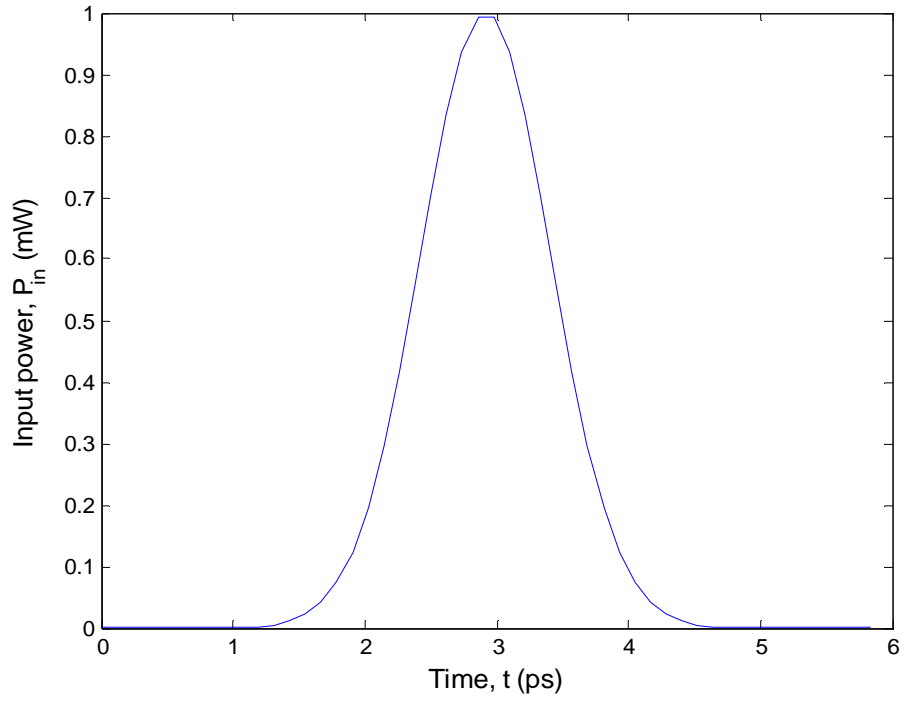
Figure 3.2 Input optical Gaussian pulse profile adopted in the SOA model

3.4.   SOA Gain Response

All the figures illustrated in this section are achieved using the SOA segmentation model. The normalised gain response of the SOA using the physical parameters in Table 3-1 with no input signal launched into the SOA can be shown in Fig. 3.3. The rapid increase in the gain reaching a steady state value within t_{bias} ~1 ns is due to the SOA biasing. A large quantity of electrons in the valence band will gain enough energy to overcome the energy gap, which increases N in the conduction band and hence the SOA total gain.

45
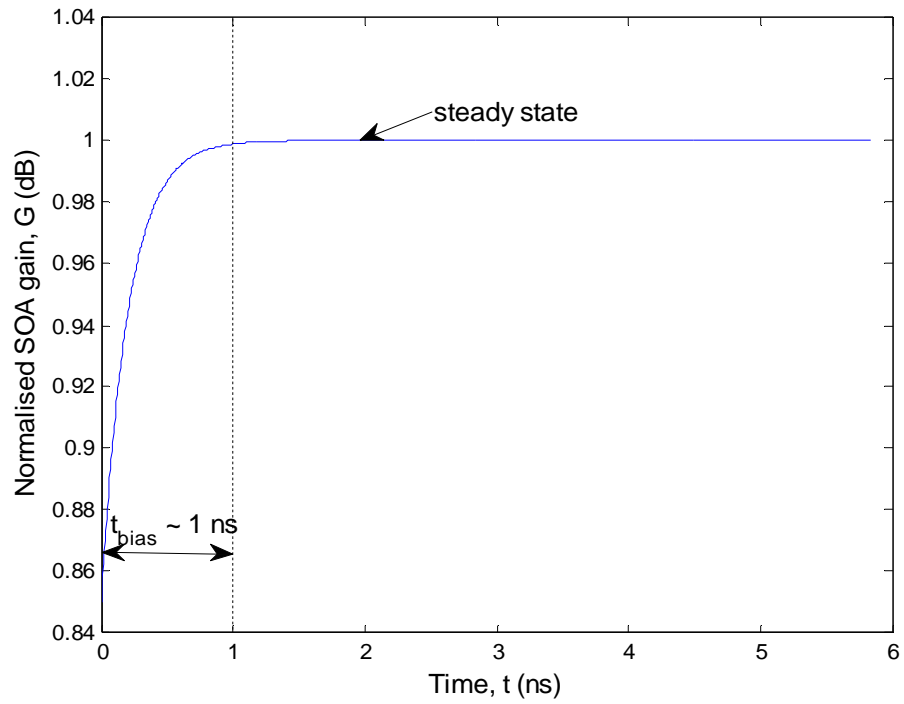
Figure 3.3 The normalised gain response of the SOA with no input signal

From Fig. 3.4, one can observe the sudden drop in the SOA gain when the input pulse shown in Fig. 3.2 enters the SOA at time $t \sim 3$ ns. This depletion in the gain is because of the sudden decrease in the carrier density that occurs during the pulse propagation along the SOA lasting 5.83 ps as explained in Chapter 2. This depletion is the signal output gain and it depends on the power and wavelength of the input signal, which will be discussed in details in the next chapter. Following the input pulse exit from the active region, the gain is recovered back to its steady state value (see Section 2.2.2) within a recovery time of $t_r \sim 670$ ps.
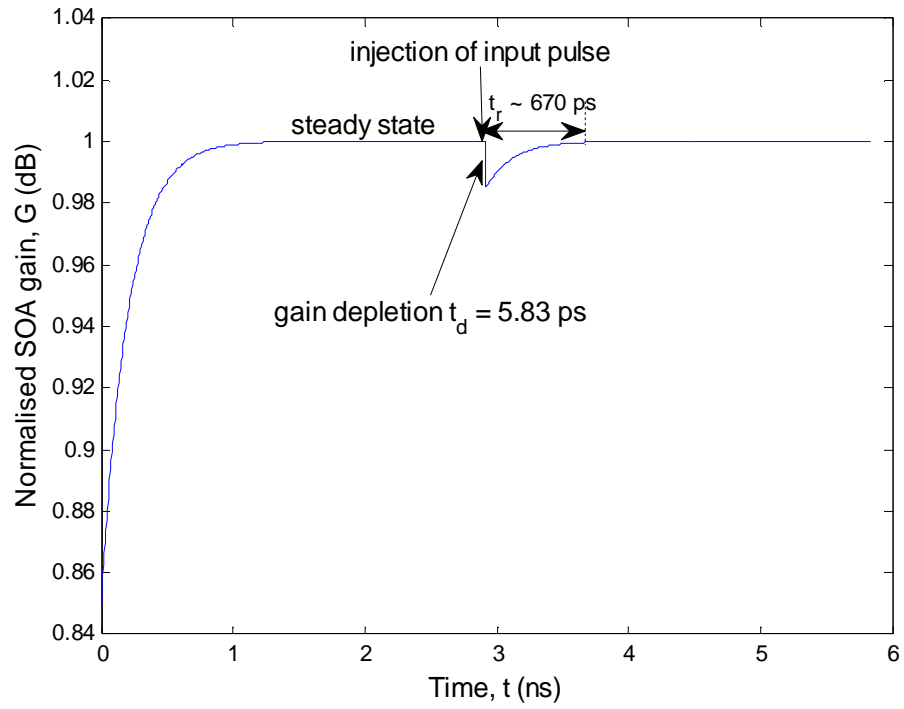
Figure 3.4 The normalised SOA gain response due to an input Gaussian pulse

In order to further understand the SOA gain response to the injection of input signals, a CW probe signal is applied to the SOA model. The CW signal causes a continuous depletion in the SOA gain until reaching a stable saturated gain level as seen in Fig. 3.5. The reason for such a response is the continuous stimulation emission process. The carrier density, and hence the gain, continues to decrease until excited electrons in the conduction band are no longer available.
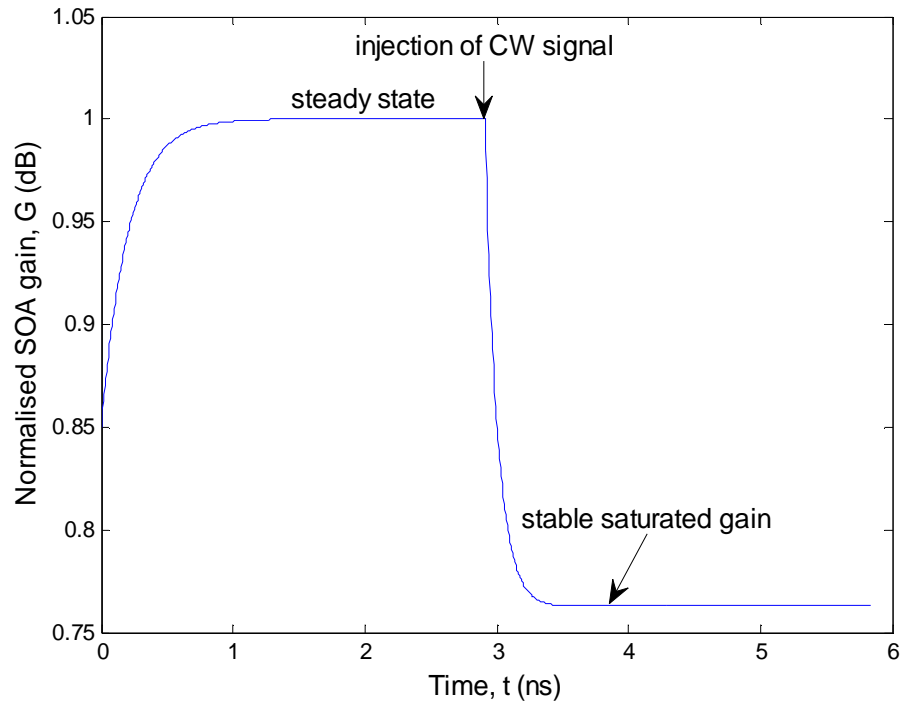
Figure 3.5 The normalised gain response of the SOA due to an input continuous wave probe signal

3.5.   Summary

This chapter has presented the mathematical model that describes the SOA features utilising the complete rate, propagation and phase equations necessary for the SOA operation. The segmentation model proposed was also introduced. The chapter depicted the characteristics of both the model and the launched optical input signal that are used for the rest of the thesis. The model of 10 μm segments showed an accurate and efficient understanding of the SOA gain response. Therefore, the following chapter uses the proposed model to optimise the SOA performance to achieve amplification function.

Chapter 4 Optimisation of Key SOA Parameters for Amplification Function

4.1.   Introduction

The important role that SOA plays in almost all functions within an all-optical router was presented in Chapter 1. This chapter focuses on the SOA performance as an amplifier. For maximum amplification, locating and controlling the peak gain is indispensable. The chapter proposes a direct temporal analysis of the impact of the input signal wavelength and applied bias current on the carrier density and the SOA gain in order to optimise the amplification process. In addition, the dependence of the SOA carrier density on the SOA length is also analysed.

In order for the SOA to perform as an amplifier, the input signal should not be affected by the SOA non-linear response due to the gain saturation. The amplification can only be achieved if the SOA gain does not reach its stable saturation level that is shown in Fig. 3.5 when applying an input signal pulse. For more accurate and efficient analysis, all results obtained in this chapter are based on the 3rd order gain coefficient equation (3.7) using the proposed segmentation model described in the previous chapter.

4.2.   Input Signal Wavelength Investigation

The wavelength of the input pulse has a direct impact on the SOA gain as it can be seen from the 3rd order gain coefficient equation (3.7). The depletion of the SOA gain that occurs due to the injection of input pulse is directly related to the input power. Therefore, in order to understand these effects, the SOA gain as a function of the peak power P_p of the input Gaussian signal described in the previous chapter for a range of wavelengths in the C-band (1530 to 1565 nm) is illustrated in Fig. 4.1. As expected, the SOA gain reduces with increasing the input pulse power at all wavelengths. This gain reduction is because a signal with higher power level will interact with a larger number of excited electrons in the conduction band, thus resulting in higher depletion of the carrier density and the SOA gain. From the figure, it is observed that at lower wavelengths, lower gains are achieved. Note that at specific power values the gain is higher for lower wavelengths compared to the higher wavelengths. Intersections take place at 1.5, 6, 10 and 18 mW.
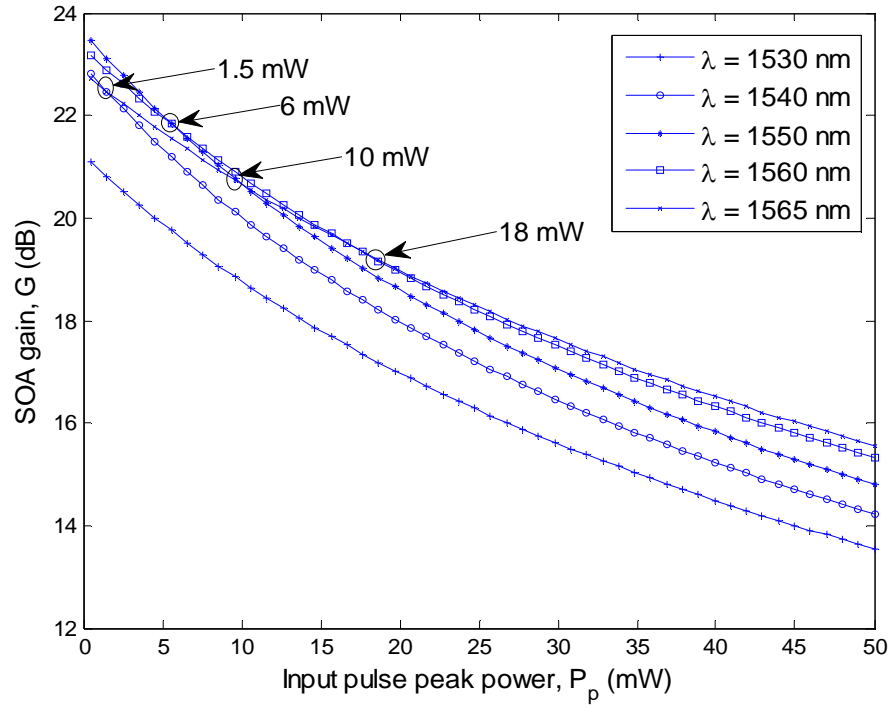
Figure 4.1 The SOA gain as a function of the input peak power when operated in the C-band

The reason for such response is best explained in Fig. 4.2. The figure displays the SOA gain against the input signal wavelength for a range of input peak power measured at the intersection points in Fig. 4.1. In Fig. 4.2, the relationship between the gain and bandwidth of the optical amplifier is shown. For the amplifier, at any input power, the gain has a peak value within its bandwidth at a wavelength λ_N and decays at both ends from this particular wavelength as defined in (3.8). These peak gains are observed around 1550-1560 nm. At P_p of 1.5 mW the gain is ~ 22.5 dB for 1540 and 1565 nm wavelengths (dashed line) which explains the intersection observed in Fig. 4.1. Similarly, at 6, 10 and 18 mW the gains are ~ 21.7, ~ 20.7 and ~ 19.3 dB at wavelengths 1550 and 1560 nm, 1550 and 1565 nm, and 1560 and 1565 nm, respectively.

51
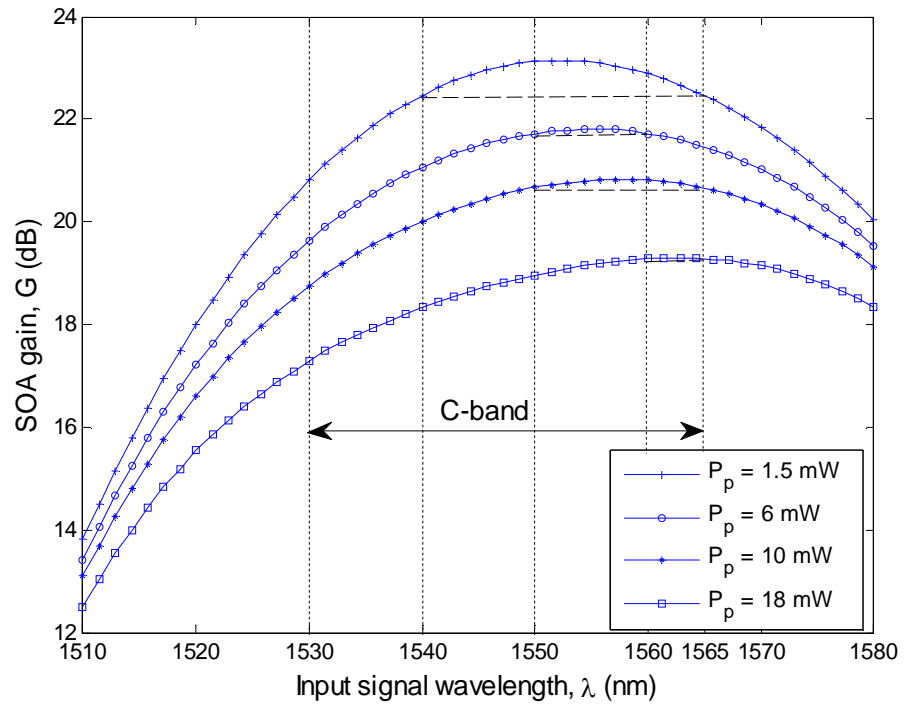
Figure 4.2 The SOA gain response against the input signal wavelength for a range of input peak power values

4.3.   Applied Bias Current Investigation

The applied current that is used for biasing the SOA has also a direct impact on the SOA carrier density and gain. At higher bias current, the number of electrons overcoming the energy gap increases (i.e. carrier density increases), thus leading to increased SOA total gain, as shown in Fig. 4.3. The intersections observed on the plot are due to the variation of λ_N at different bias current values.
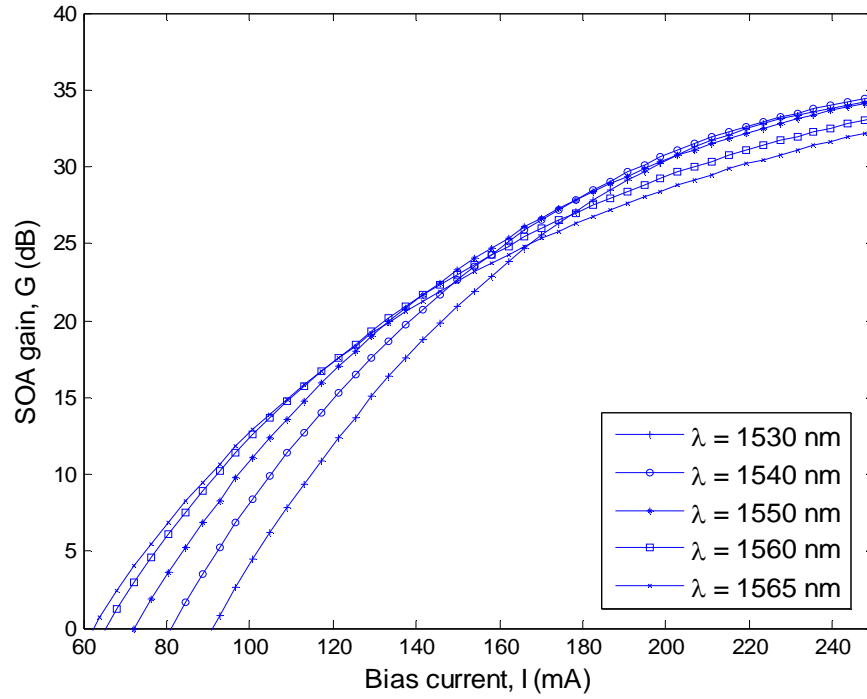
Figure 4.3 The SOA gain versus the bias current for a range of C-band wavelengths

Figure 4.4 depicts both the input peak power and the applied bias current as functions of λ_N that will help to further understand the input factors affecting this wavelength and hence optimum amplification. As Figs. 4.4 (a) and (b) show, λ_N is increased at higher input powers and at lower biasing currents, respectively. When the SOA is injected by higher bias current, higher number of electrons are excited in conduction band (i.e. carrier density) and hence, the SOA gain achieve higher values. As a result, λ_N shifts to lower values.
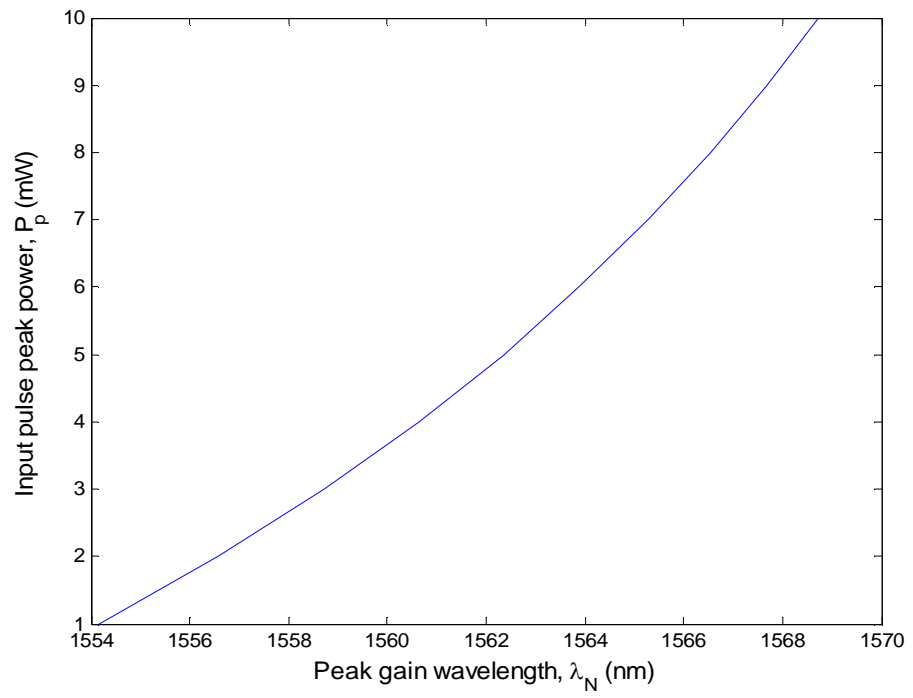
(a)
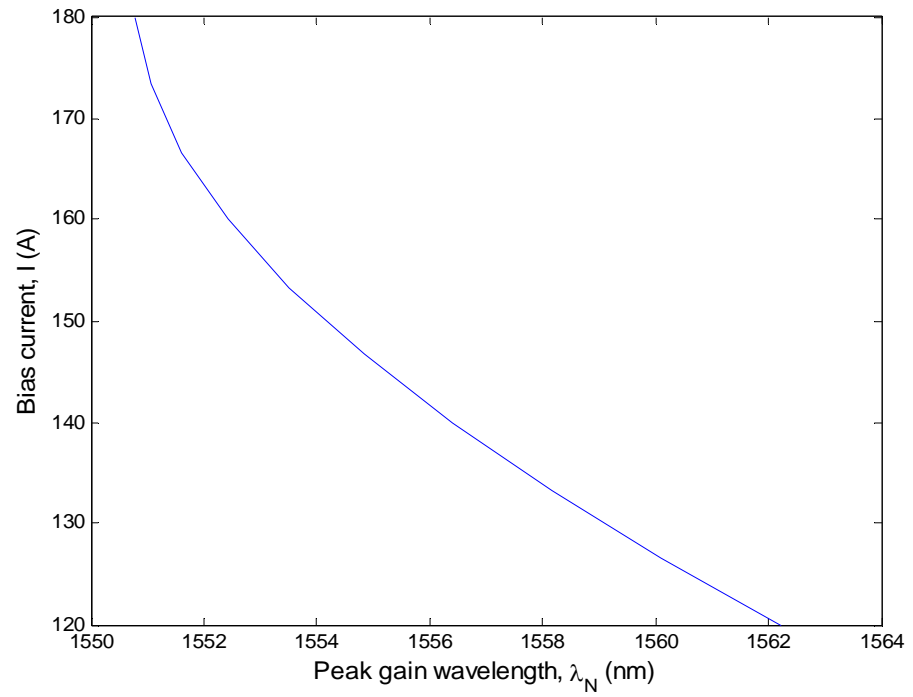
(b)

Figure 4.4 (a) The input peak power and (b) the bias current as functions of the peak gain wavelength

More specifically, this response is outlined in Fig. 4.5. The SOA gain reduces with increasing the input pulse power and this response appears at all bias current values. On the other hand, higher biasing current values result in higher SOA gain achievement (see Fig. 4.3). The highest gain achieved is 31.1 dB with a 2% drop from the steady state value at highest bias current and a peak power of 200 mA and 0.5 mW, respectively. For lower values of bias currents, the gain profile is almost flat. For example injecting the same 0.5 mW input at 100 mA current, 10.85 dB gain is achieved with just 0.2% drop from steady state. These results correspond to the number of electrons available for amplification in the conduction band for each case.
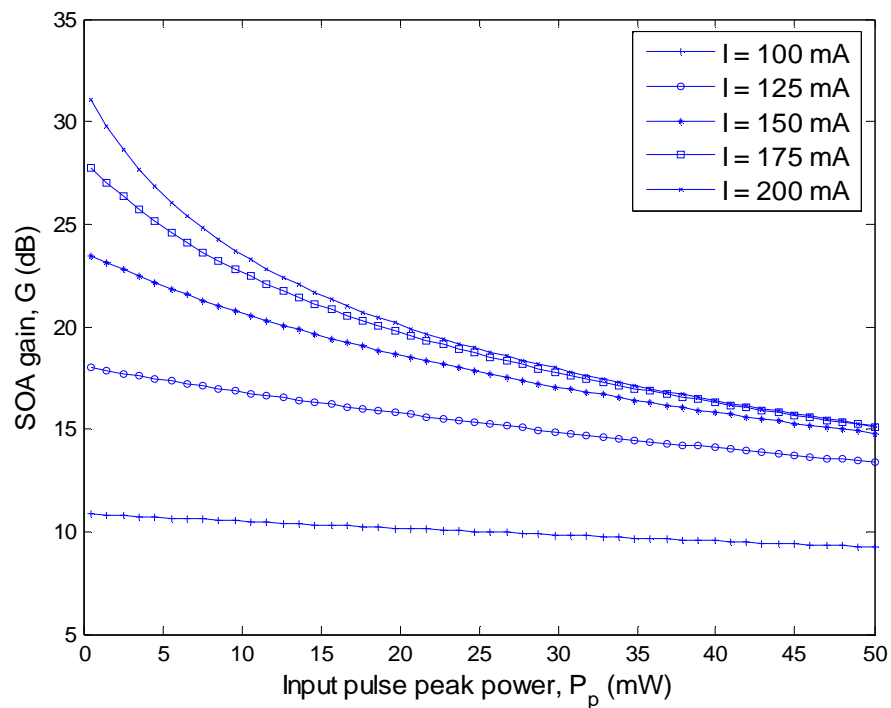
Figure 4.5 The SOA gain versus input pulse peak power for a range of bias currents at a wavelength of 1550 nm

4.4. SOA Length Investigation

The length of the SOA is an important physical parameter that affects the total gain. The dependence of the gain on the SOA length is plotted in Fig. 4.6 (left axis) for a range of input pulse peak power values. For short length (< 200 µm) SOAs, where the depletion of N is negligible, the gain is the same for all values of P_p. On the other hand, for longer length (< 700 µm) SOAs the gain is increasing, peaking at L of ~400 µm beyond which the gain drops. Figure 4.6 confirms that the gain is higher for lower values of P_p.
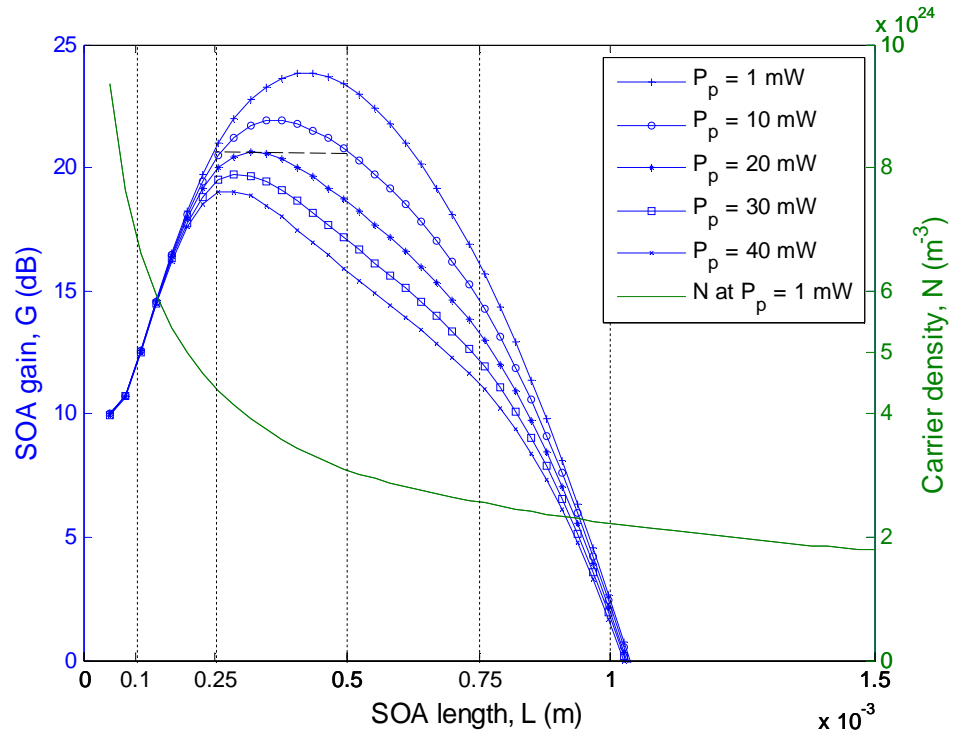
Figure 4.6 The SOA gain and carrier density responses as a function of the SOA length for a range of input power levels

For longer length (700 µm – 1mm) SOAs, maintaining a stable applied bias current, the number of electrons per unit length is smaller because of the lower current density. Therefore, in order to achieve high gain at longer length SOAs the applied bias current needs to be increased in order to maintain the number of electrons per unit length, see inset of Fig. 4.6 (right axis) [133-135].

Figure 4.7 displays the effect of the bias current on the SOA gain for a range of SOA lengths. Although the SOA gain has higher values when biased with more current, for shorter length SOAs (100 µm and 250 µm) the rate of increase of gain is lower than longer length SOAs.
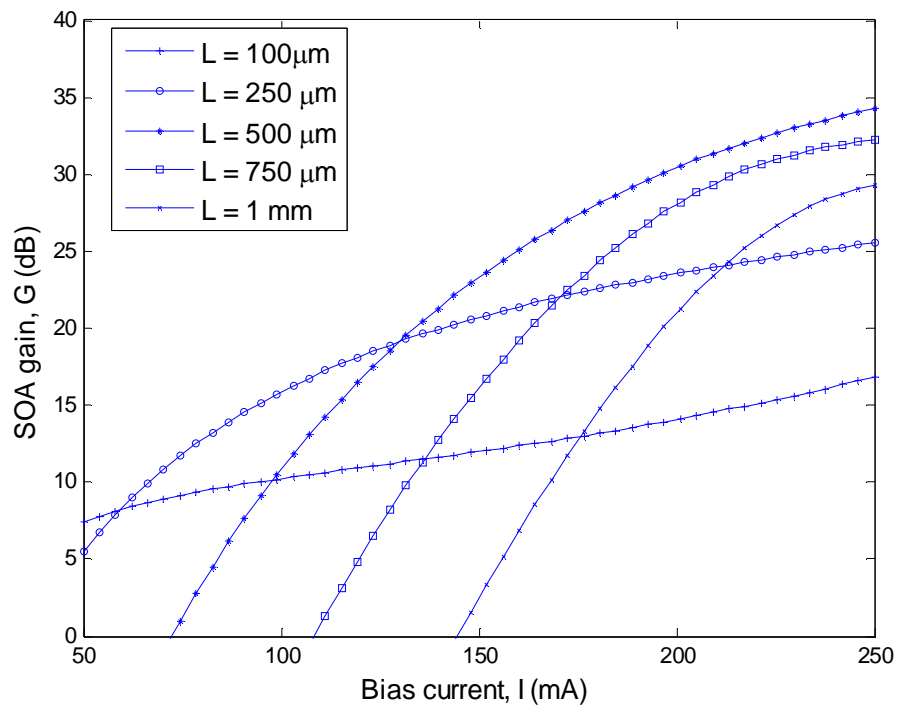
Figure 4.7 The SOA gain corresponding to the bias current at different SOA lengths

4.5. Summary

This chapter introduced the use of the SOA to perform as an amplifier. Results obtained using the proposed segmentation model showed the optimum conditions required to achieve a maximum output gain for amplification function. The chapter depicted the direct effects of the input pulse power, the bias current and the input signal wavelength within the C-band on the carrier density and gain of the SOA to optimise the performance as an amplifier. The SOA gain dependence on the length of the SOA is also investigated.

It was shown that the maximum gain of the SOA can be achieved for low power input signals propagating close to the peak gain wavelength. High biasing currents are required in order to ensure higher amplifications. However, in fabricating the SOA, there is an optimum length that is dependent on its parameters. In this investigation this optimum SOA length was 400 µm $<L<$ 500 µm.

The following chapter modifies these input parameters in order to set the boundaries for the SOA to efficiently perform as a switch. The chapter introduces the essential conditions required for optimised switching function.

Chapter 5   Optimisation of Key SOA Parameters for Switching Function

5.1.   Introduction

Semiconductor optical amplifier is considered the key element in all-optical switching processes for their fast and strong non-linear characteristics, small size and low switching energy (see Chapter 1). This chapter investigates the input boundaries and requirement conditions to the SOA in order to achieve optimum switching operation. The key optimisations for switching are obtained by controlling the power and wavelength of the input signal and the SOA biasing current to achieve the desired phase shift. The chapter also studied the impact of the SOA length on the carrier density and the induced phase shift.

On the contrary to amplification, in order to use the XPM characteristics of SOA for switching function, the signal should experience a phase shift of 180° for the complete deconstructive interference [136]. Therefore, in this chapter, the phase shift calculation employing equations (3.10) and (3.11) represented in Section 3.2.3 is crucial for setting the boundaries for the SOA switching function. The phase shift could be induced by the input signal or by the aid of a CP injected to the active region of the SOA.

Similarly to the previous chapter, the cubic equation (3.7) is used in the proposed segmentation model as the material gain coefficient g to generate the results obtained in this chapter.

5.2. Input Signal Wavelength Investigation

The phase shift experienced by the input signal, is directly proportional to the depletion of N as defined in (3.10) and (3.11), as a result of changes in the refractive index Δn. Figure 5.1 shows the phase shift as a function of the Gaussian input pulse peak power for a range of wavelengths in the C-band. Intersections between 1550 nm and 1560 nm that attain 100° phase shift and between 1550 nm and 1565 nm that accomplish 149° phase shift are shown at 19 and 39 mW, respectively in the figure.
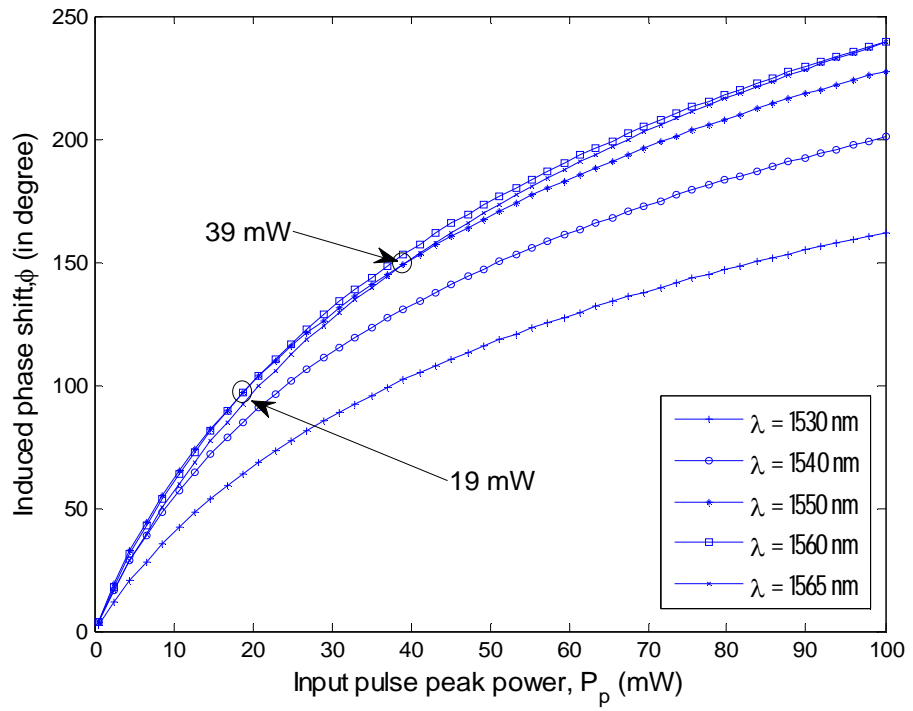
Figure 5.1 The induced phase shift experienced by the input signal against the input pulse peak power for a range of wavelengths

The reason for such intersections is the variation of λ_N at different input peak powers. These intersections are more obvious in Fig. 5.2 (dashed lines), which depicted the induced phase shift corresponding to the input signal wavelength at the intersections of the input power values.
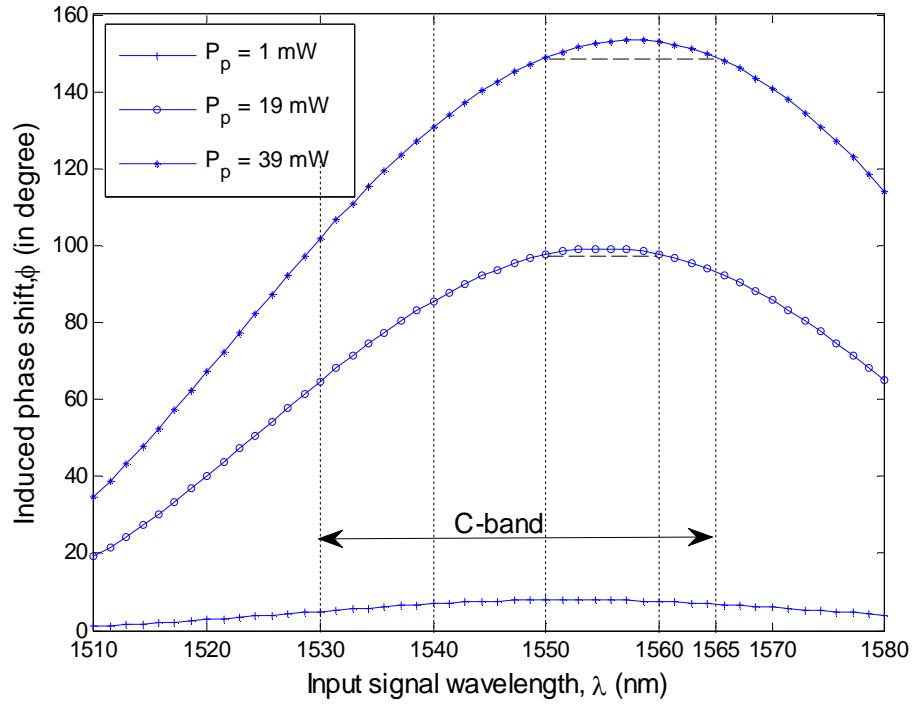
Figure 5.2 The induced phase shift of the input signal versus the input signal wavelength for a range of input pulse powers

5.3. Applied Bias Current Investigation

In order to understand the impact of the bias current on the induced phase shift of the input signal, Fig. 5.3 is plotted. It illustrates the induced phase shift of the input signal achieved at a range of input pulse power at different biasing current values. From Fig. 5.3, it can be seen that at higher bias current values, the input signal propagating along the SOA induces more phase shift. Higher biasing results in higher SOA gain. From the third term in (3.6), which presents the depletion of the carrier density, one can observe that higher gain (i.e. g) results in more N depletion. Therefore, the phase shift increases accordingly.
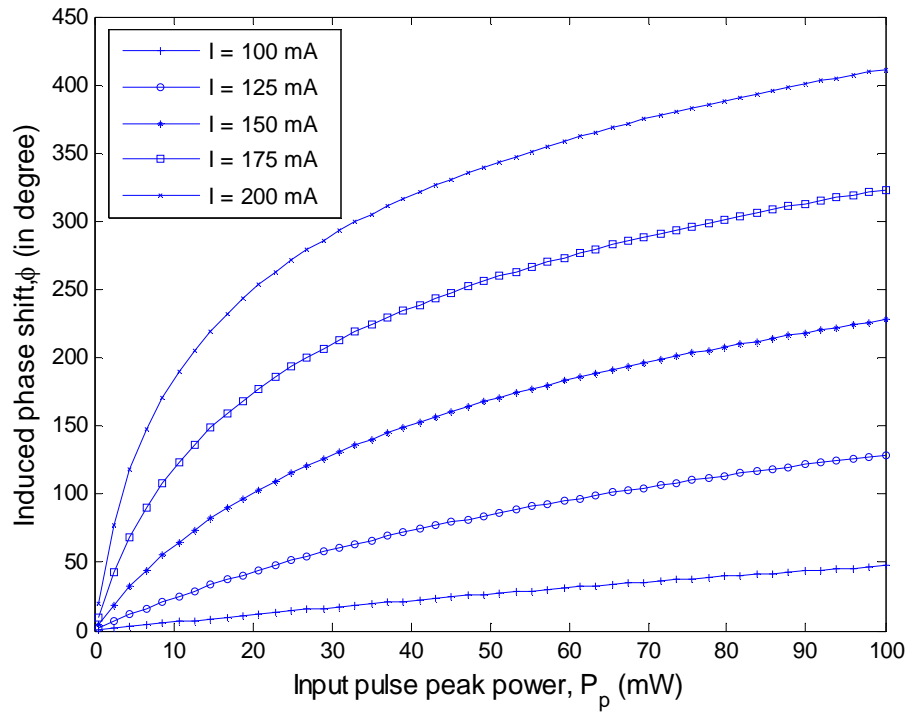
Figure 5.3 The induced phase shift of the input signal achieved against the input pulse power for a range of biasing current values

5.4. SOA Length Investigation

It is also important to report the dependence of the phase shift of the input signal on the SOA length. It is known from Chapter 4 that lower gains are achieved at short (< 200 μm) and long (> 700 μm) SOA lengths. It was also shown in the previous figure that higher input power induces more phase shift, which explains the response of Fig. 5.4. The figure presents the induced phase shift corresponding to the input pulse power at different SOA lengths. As expected the maximum achieved phase shift is at 500 μm.
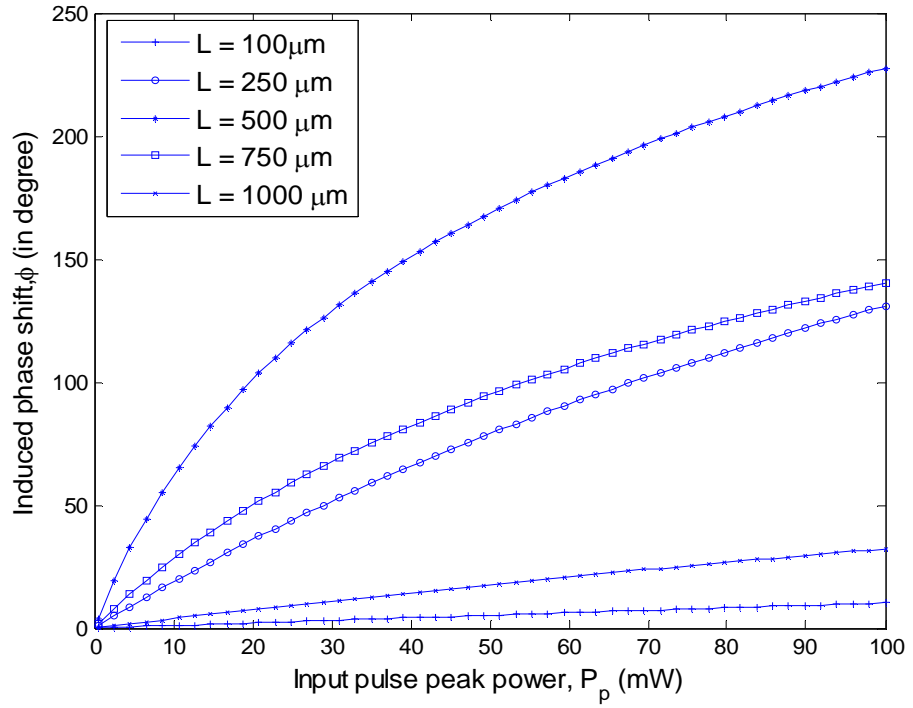
Figure 5.4 The induced phase shift of the input signal achieved as a function of the input pulse powers for a range of SOA lengths

Figure 5.5 depicts the combined effects of L and the bias current on the induced phase shift. The figure shows a symmetrical profile with peaks (i.e. peak gain) occurring at longer SOA length and increasing with the bias current. The bias current values in Fig. 5.5 are chosen to show the same phase shift induced at different SOA lengths (dashed lines).
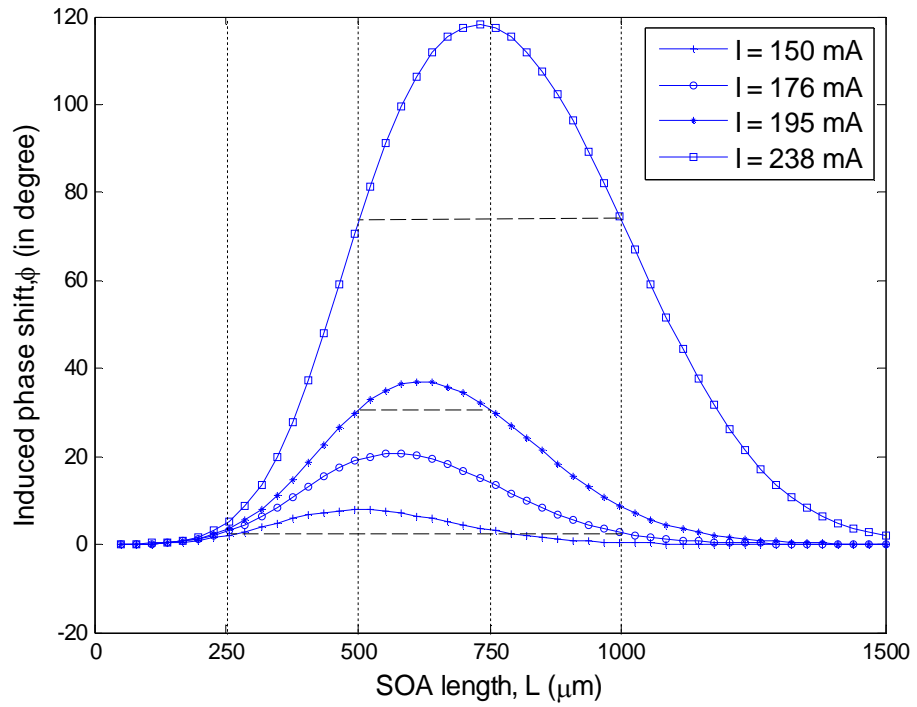
Figure 5.5 The input signal induced phase shift against the SOA length for different biasing values

5.5.   Input Power Required for Switching Application

This section sets the boundaries in which the SOA can be used as a switch. The input power in the form of Gaussian signal or CP is required to achieve 180º phase shift. In this section, the input power required to reach the desired phase shift is studied at different operation conditions regarding the biasing current, SOA length and the input signal wavelength. Figures 5.6 and 5.7 illustrate the input power required to obtain 180º phase shift for the SOA to be used in switching for a range of bias current values at different wavelengths and L, respectively.
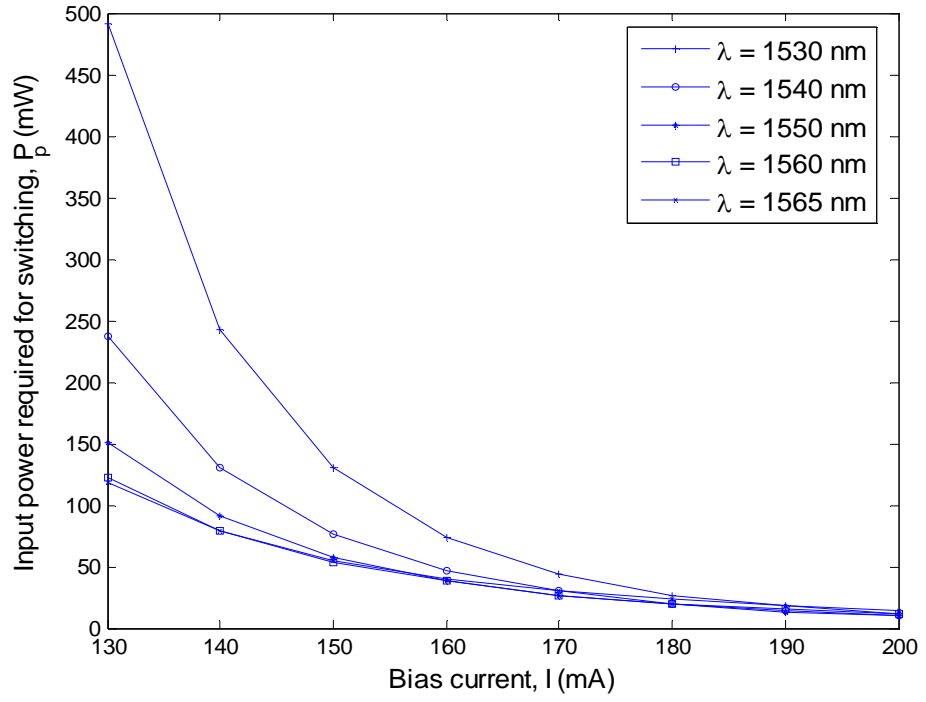
Figure 5.6 The input power required for switching as a function of the biasing current at different wavelengths

Due to the larger phase shift induced at higher bias currents, less input power is required for achieving the 180° phase shift as shown in Fig. 5.6. At 200 mA biasing, the input power required for switching is almost the same, regardless of the wavelength of the input pulse.

As seen in Fig. 5.7, in case of 150 mA, since SOA length of 500 μm achieves the highest phase shift, it requires the least input power needed of 58 mW for switching function. The 750 μm and the 250 μm require the same input power of 170 mW, while the 100 μm needs more than 2.5 W for achieving 180° phase shift, respectively.
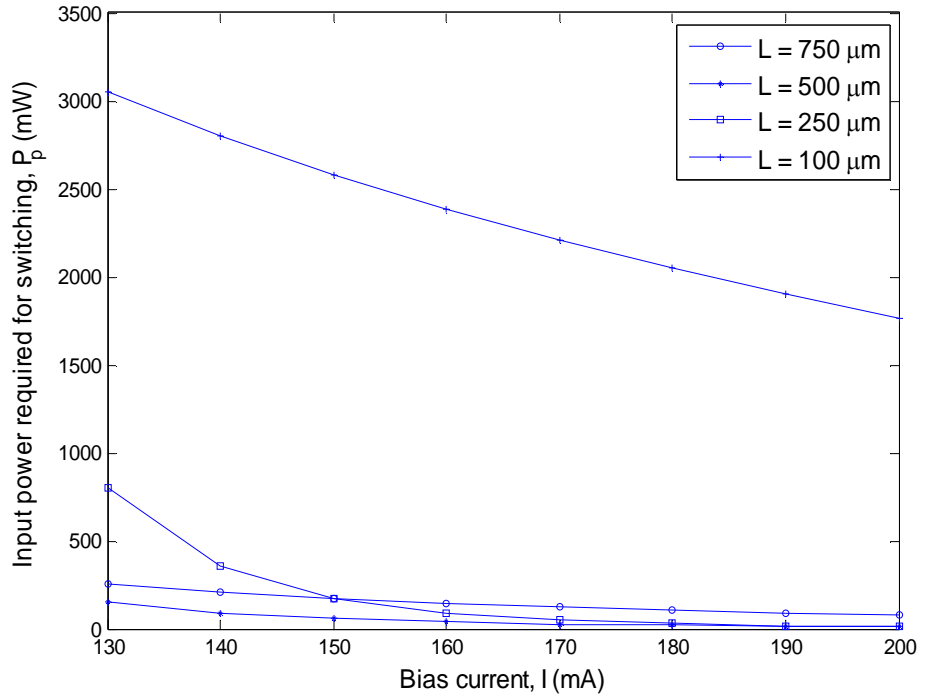
Figure 5.7 The input power required for switching versus the bias current for different SOA lengths

5.6. Summary

In this chapter, the advantages of the SOA non-linear characteristics are optimised for optical switching operation. The chapter presented the boundary conditions required for the input parameters in order to achieve the 180° induced phase shift required for switching function in an SOA-based optical switch. The impact of the SOA length as well as the input parameters regarding the power and wavelength of the Gaussian pulse and the applied biasing current to the SOA are investigated to choose the required control pulse needed for the non-linear response of the SOA.

The achieved results showed that more phase shift is induced in case of higher bias currents applied to the SOA and therefore, less input power is required for achieving the 180⁰ desired phase shift. Results also show that the power of the input pulses is not significant at high bias current values. In this investigation, this power required for switching is almost the same, regardless of the wavelength of the input pulse at bias currents > 200 mA (for the parameters used in Table 3-1).

In high speed optical applications, rapid SOA gain recovery is necessary in order to ensure the minimum gain standard deviation and thus leading to reduction in the system power penalties. The following chapter focuses on the dependence of the SOA gain on the wavelength characteristics of the input signal. The chapter proposes a wavelength diversity technique to enhance the gain uniformity of SOA at high speed data rates.

Chapter 6   SOA Gain Uniformity Improvement Employing Wavelength Diversity Technique for High Speed Optical Routers

6.1.   Introduction

The gain recovery time defines, to a great extent, the performance of SOAs of any types. At low data rates that are slower than the SOA gain recovery time, the input pulse is amplified by an unsaturated gain (i.e. the SOA gain is at steady state level). On the contrary, at high data rates that are faster than the SOA gain recovery time, the input pulses are amplified by a lower gain (i.e. saturated gain) which results in different gain reductions to the output pulses. Such response leads to serious of pulse distortion which is known as patterning effect [59, 137-

139] and results in system power penalties. Therefore, in order to reduce these power penalties at high speed optical routers, fast SOA gain recovery is required to maximise the output gain uniformity.

This chapter proposes a wavelength diversity technique (WDT) to achieve SOA gain uniformity for high speed optical applications. This method can be used to noticeably increase the system capacity by simultaneously transmitting many independent channels at different wavelengths [140-142]. The enormous capacity of the WDM systems is achieved by having a very narrow channel spacing of 0.4 nm (50 GHz) or less. In principle, the capacity of a single mode fibre (SMF) is >30 Tb/s [9, 143], therefore a large number of wavelengths could be used provided the channel spacing is kept to a minimum. However, in a practical system, the minimum channel spacing is limited by the inter-channel crosstalk and by the amplifier gain response [9, 143]. Basically, WDM systems are often classified as coarse or dense systems, depending on their channel spacing (typically, channel spacing of > 5 nm and <1 nm for coarse and dense WDM systems, respectively) [9]. In most commercially available WDM systems channel spacing is 100 GHz (0.8 nm) at 1552 nm [9, 144]. Recently, the International Telecommunication Union (ITU) has specified narrower channel spacing of 25 and 50 GHz for future WDM systems [7, 145].

The chapter investigates the wavelength impact of an input packet of Gaussian pulses on the SOA gain profile. The output gain standard deviation of the packet using a single wavelength is compared to the WDT. The comparison demonstrates the improvement of the SOA gain uniformity employing the WDT at data rates up

to 160 Gb/s. The limitations of the proposed technique regarding the applied bias current are also studied at all input data rates.

6.2.   Impact of Signal Wavelength on SOA Gain Uniformity

The dependence of the SOA gain on the input pulse wavelength was presented and explained in Section 4.2. However, in order to understand the effect of wavelength on the SOA gain uniformity, a number of successive pulses are required to propagate along the SOA active region. Therefore, a packet of identical Gaussian pulses, described in Chapter 3 is applied to the SOA at 1550 nm. The packet consists of 10 pulses of 1 mW peak power each and they are separated by 100 ps (10 Gb/s) for a packet duration t_p of 1 ns.

The gain response of the SOA when the packet is launched into the active region is displayed in Fig. 6.1. When the first pulse in the packet enters the SOA at $t \sim 3$ ns, sudden gain depletion occurs due to the interaction of the input pulse with the excited electrons in the conduction band. Due to the slow recovery of the SOA gain, following the exodus of the first pulse, the next pulse enters the SOA prior to full gain recovery. A further gain depletion is introduced because of the second pulse. This process continues until the last pulse exits the SOA.

In order for all pulses to accomplish the same gain, the gain depletion due to all pulses should reach the same level. It is apparent from Fig. 6.1 that the gain reduction reaches different levels from one pulse to another (i.e. the gain depletion envelope is not uniform). Figure 6.1 also shows that by applying a packet with more pulses, the variation of gain depletion is negligible. Therefore, there is no

71

significant difference when injecting more than 10 pulses in the current investigation.
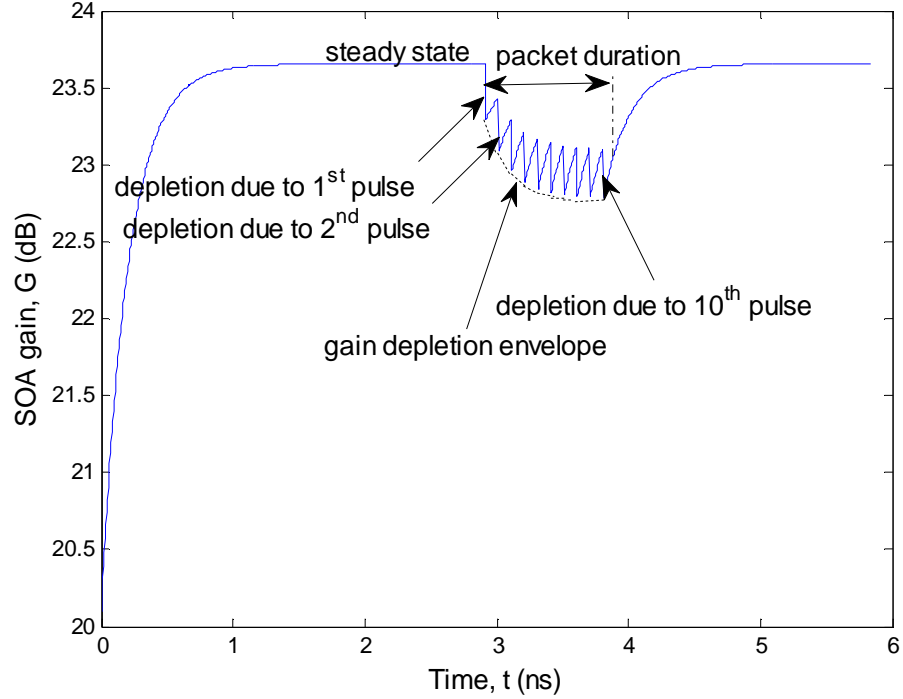
Figure 6.1 SOA gain response to a packet of Gaussian pulses

In this chapter, we have adopted a bit pattern of all '1's in the simulation. This is because the all '1's bit pattern will give the least recovery time for the SOA, thus resulting in the worst case scenario for SOA gain uniformity. This scenario will therefore show the significance of the improvement achieved by the WDT in the following sections.

In order to measure the gain uniformity of the output pulses, the gain standard deviation is introduced, which is given by:

$$\sigma = 10 \log \left(\sqrt{\frac{1}{n_p} \sum_{y=1}^{n_p} \left(G_y - G_{av} \right)^2} \right), \quad (6.1)$$

where n_p is the number of successive input pulses within the packet applied to the SOA, G_y is the gain achieved by each input pulse and G_{av} is the average gain of all the pulses.
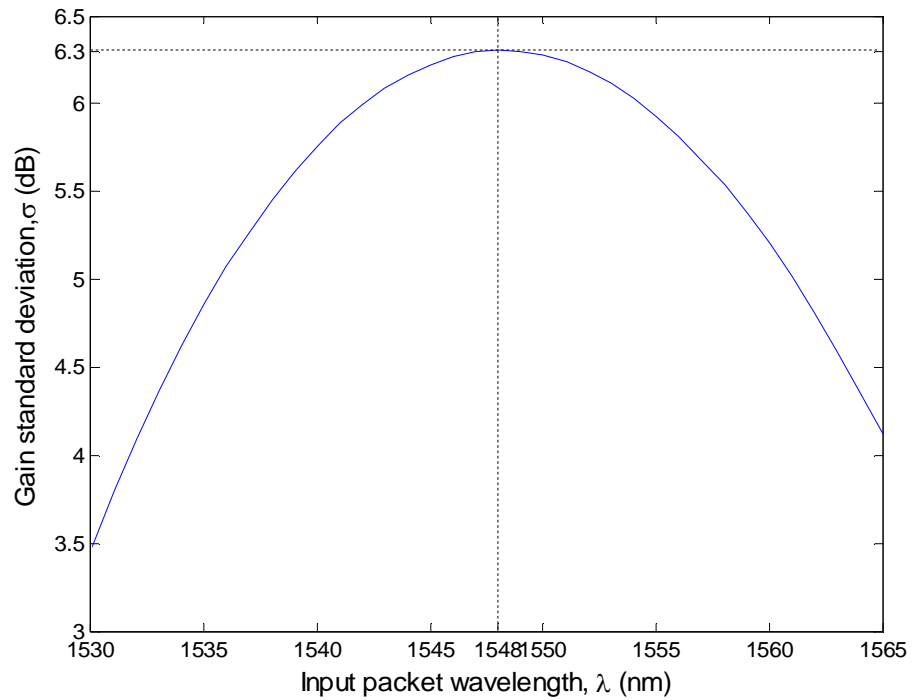
Figure 6.2 Gain standard deviation responses to input packet wavelength within C-band range

Therefore, to identify the dependence of the SOA gain uniformity on the input wavelength, the gain standard deviation is calculated and plotted against the C-band wavelength range in Fig. 6.2. As depicted earlier in Figs. 4.1 and 4.2, the peak gain value is achieved at a wavelength λ_N. On the other hand, at a wavelength of 1530 nm the gain is minimum compared to the C-band

wavelengths. Correspondingly, maximum value of σ is 6.3 dB (i.e. least gain uniformity) is at λ_N. The σ is proportional to the output gain, thus explaining the highest and lowest gain uniformities at 1530 nm and 1548 nm wavelengths, respectively as shown in Fig. 6.2.

6.3.   Wavelength Diversity Technique at 10 Gb/s

Different wavelengths result in different gain responses as presented in the previous section. Therefore, a wavelength diversity technique (WDT) is proposed where each Gaussian pulse is assigned a different wavelength to attain the same output gain. In this section, the input packet to the SOA consists of 10 pulses at a rate of 10 Gb/s.

In order to determine suitable wavelengths for WDT, there is a need to investigate the SOA gain response of all pulses within the packet to the C-band wavelength range (see Fig. 6.3). From Fig. 6.3, it is clear that different pulses can achieve the same gain at different wavelengths and hence, uniform output gain. As shown in Fig. 6.3, the maximum gain value that intersects with all pulses is G_m = 22.85 dB (dashed line) which is the peak gain value of the 10th pulse which appears at a wavelength of 1552.9 nm. The dotted lines in Fig. 6.3 show the wavelengths that achieve the same G_m for the proposed technique and these wavelengths for pulses 1 to 9 are 1542.1, 1544.3, 1546.4, 1547.9, 1549.3, 1550, 1550.7, 1551.4 and 1552.1 nm, respectively.
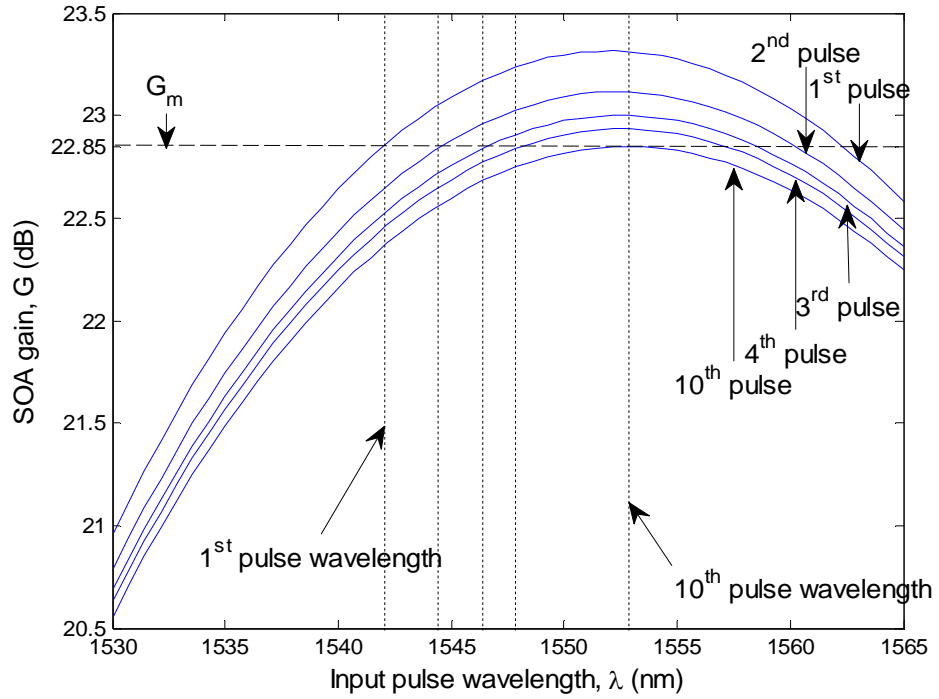
Figure 6.3 SOA gain response of all pulses within the packet to the C-band wavelength range at 10 Gb/s

Comparing the SOA gain uniformity using a single wavelength and the WDT, a significant improvement of 6 dB of the gain standard deviation is achieved using the packet with the proposed technique. The wavelength of the 1st pulse in the WDT packet (i.e. 1542.1 nm) is used as the single wavelength for the other packet. This wavelength is chosen in order to maintain the same impact of the 1st pulse of both packets on the SOA gain.

The SOA gain responses corresponding to both packets are illustrated in Fig. 6.4 to show the improved output gain uniformity. The envelope of the gain depletion using the WDT (circled in Fig. 6.4) is more uniform compared to using a single wavelength packet.
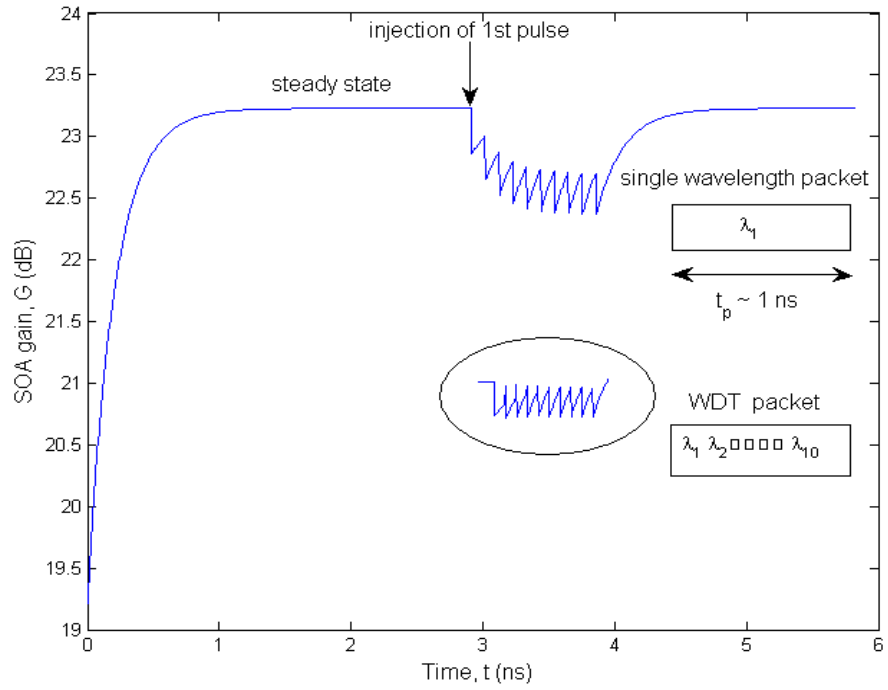
Figure 6.4 Comparison between SOA gain responses to a packet of single wavelength and WDT pulses

Therefore, to measure the ability of the proposed technique to enhance the SOA gain uniformity at higher data rates, the following section repeats the same comparison between both packets at 20, 40, 80 and 160 Gb/s.

6.4. WDT at Higher Data Rates

The same 10 Gaussian pulses with different time separations (i.e. 50, 25, 12.5 and 6.25 ps) are launched to the SOA. The change in the input pulses rate has a direct impact on the SOA total gain and therefore, the gain uniformity. In order to understand this impact, the SOA gain responses to the 10 pulses packet of 1550

nm wavelength are plotted in Fig. 6.5 at 20, 40, 80 and 160 Gb/s. In Fig. 6.5, the

packets at all data rates enter the SOA at the same time.
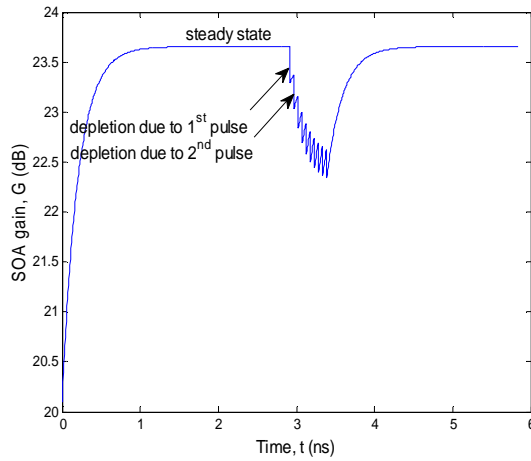
(a)
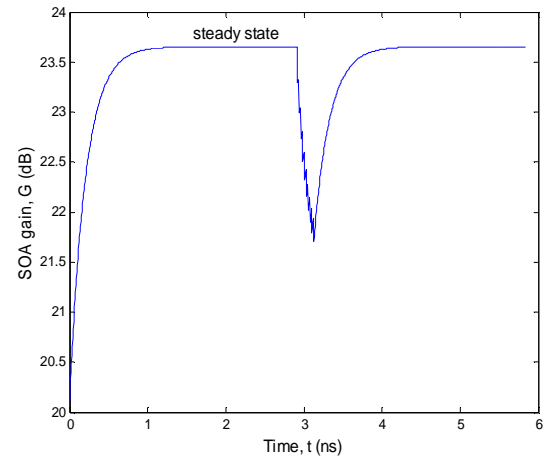
(b)
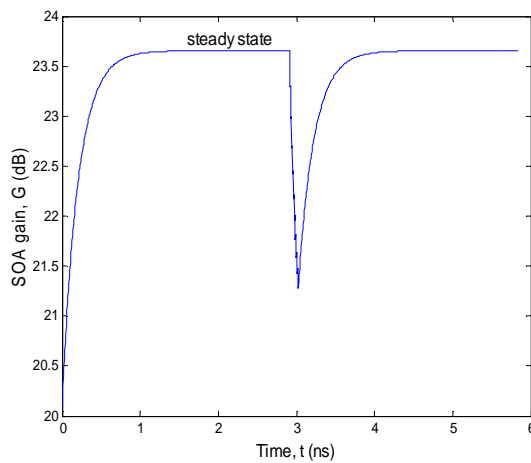
(c)
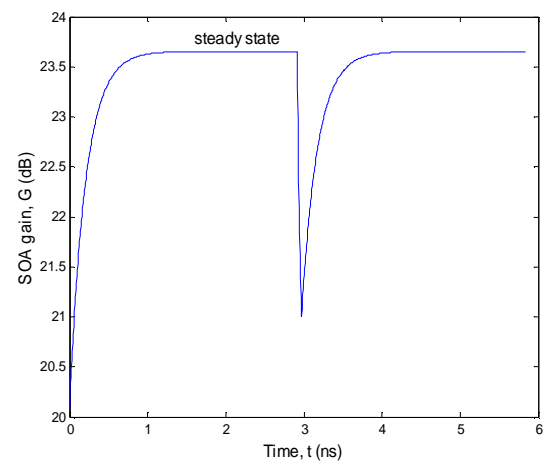
(d)

Figure 6.5 SOA gain responses to a packet of 10 Gaussian pulses at (a) 20 Gb/s, (b) 40 Gb/s, (c) 80 Gb/s and (d) 160 Gb/s

For all data rates, the depletion in the SOA gains due to the propagation of the 1st

pulse of the input packet are similar, however, the time available for the gain to

recover after the departure of the 1st pulse from the SOA is halved in each case. Therefore, the 2nd input pulse enters the SOA at a lower gain level (compared to lower data rate), and results in further gain depletion (i.e. less gain is achieved). This response is more obvious in Fig. 6.6 which displays a comparison between all given data rates for the SOA gain profiles of the packet 2nd pulse corresponding to the C-band wavelength range. As expected, the 2nd pulse of the input packet at higher input data rates achieve less gain at any wavelength and result in a larger gain difference with the 1st pulse. That explains the less uniform envelope of SOA gain depletion achieved at higher input data rates as it can be seen in Fig. 6.5. The input pulses at 160 Gb/s shows the least uniform envelope in Fig. 6.5 (d).
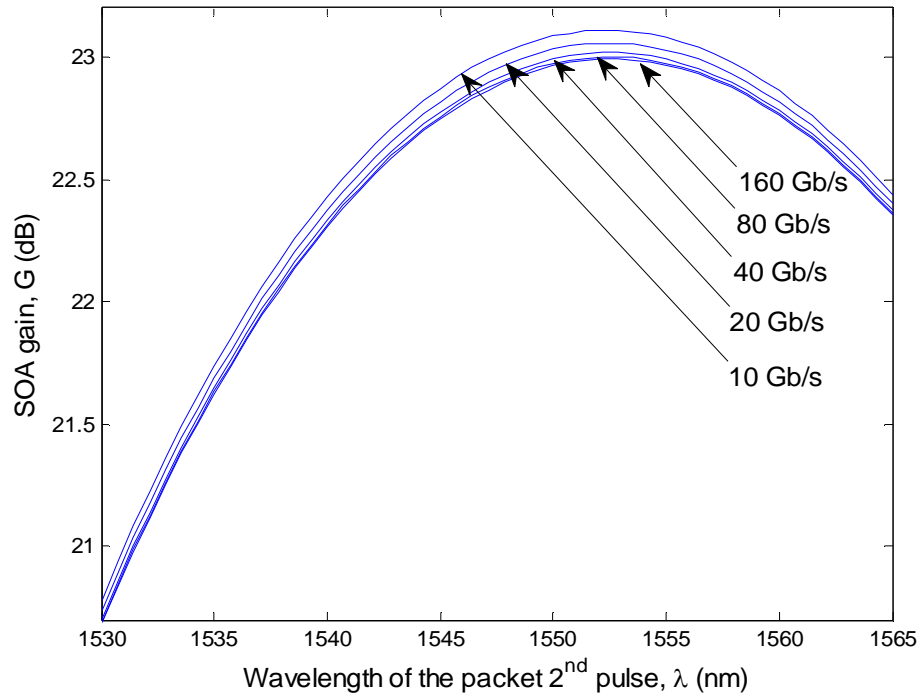
Figure 6.6 Comparison between all input data rates for the SOA gain profiles of the packet 2nd pulse corresponding to the C-band wavelength range

78

For low data rate applications, where the time separation between successive pulses > 670 ps (i.e. SOA gain full recovery time), the gain depletion envelope is flat. The reason for such response is that the 2nd input pulse enters the SOA after the full recovery of gain following the departure of the 1st pulse. In such case, there is no need to apply the WDT to improve the SOA gain uniformity.

The gain standard deviations for the packets at all data rates are measured for a single wavelength and compared to the WDT in order to distinguish the improvement of the SOA gain uniformity. This gain standard deviation comparison between both techniques is illustrated in Fig. 6.7.
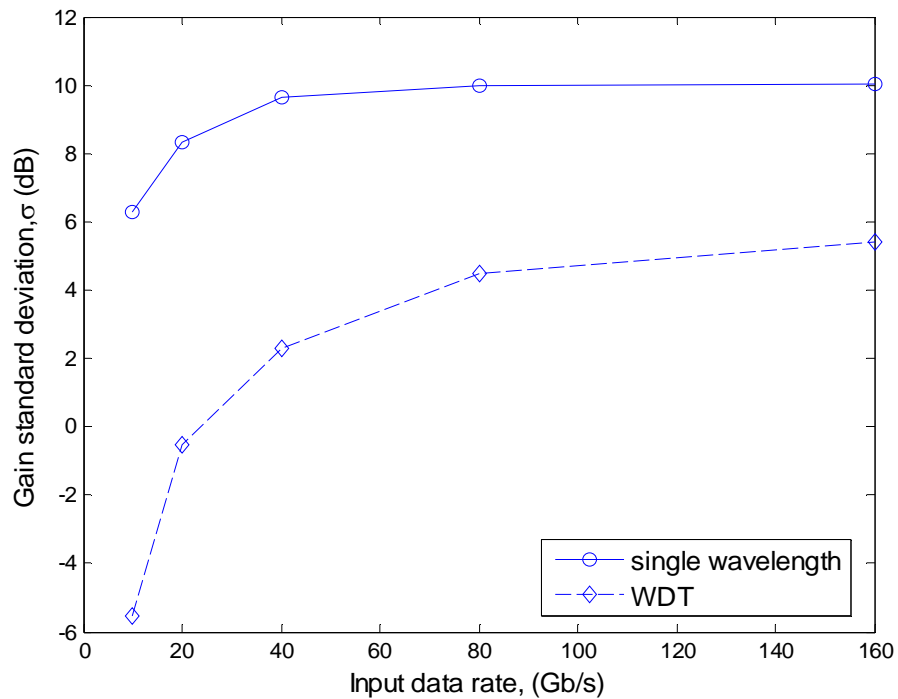
Figure 6.7 Comparison between the gain standard deviation of a packet using a single wavelength and WDT at all data rates

As plotted and explained earlier in Figs. 6.5 and 6.6, the SOA has a better gain uniformity (i.e. σ is lower) at lower data rates which is more noticeable in Fig. 6.7. The figure shows that σ increases at higher data rates for both curves. This response is valid due to applying the same number of pulses at all data rates. Applying more pulses at higher rates will be discussed later in this section. It is clear from Fig. 6.7 that the wavelength diversity technique results in lower σ values at any input data rate. The proposed technique shows enhanced SOA gain uniformity regardless of the input data rate.
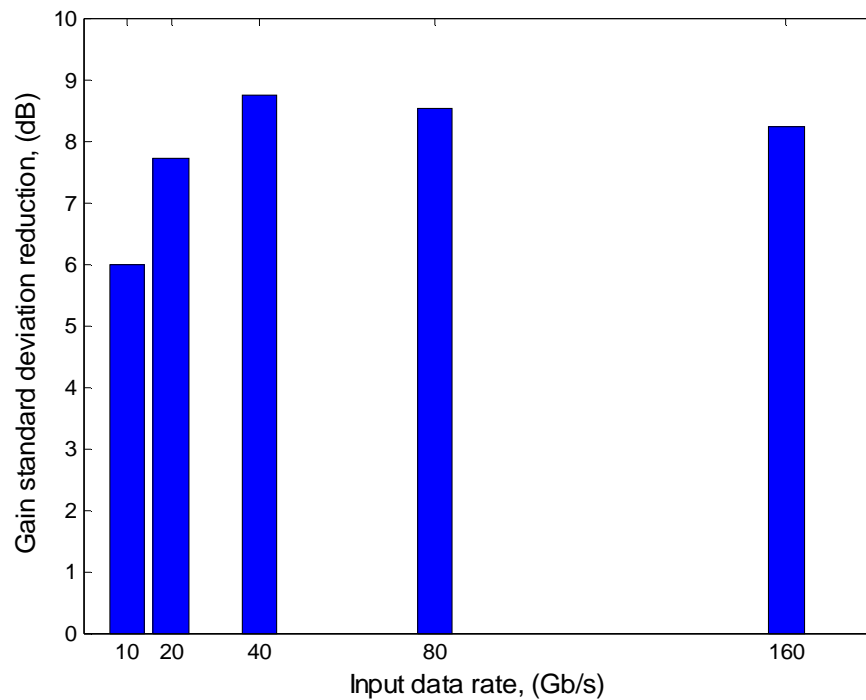
Figure 6.8 Gain standard deviation reduction when using WDT instead of a single wavelength at all data rates

The advantage of using the WDT over a single wavelength can be seen in Fig. 6.8. The figure depicts a bar chart of the gain standard deviation reduction when

the single wavelength is replaced by WDT at all rates. Results obtained show gain standard deviation reductions of 6, 7.7, 8.7, 8.5 and 8.2 dB at 10, 20, 40, 80 and 160 Gb/s, respectively. In case of using the proposed wavelength diversity technique, the average σ improvement is 7.82 dB at data rates investigated in this chapter. At higher rates > 20 Gb/s, more enhancement in the SOA gain uniformity is achieved (> 8 dB) and the fluctuation of σ reduction is less perturbed. The reason for the small differences in σ reduction at higher rates is that time spacing between input pulses is shorter and hence, smaller gain differences.

The wavelengths of the 10 pulses within the WDT packet at all data rates are presented in Table 6-1. On the other hand, the only wavelength used for the other packet is the 1st pulse wavelength of the WDT packet for all rates.

Table 6-1 Wavelengths of the pulses within the WDT packet at all data rates

Pulse wavelength (nm)	10 Gb/s	20 Gb/s	40 Gb/s	80 Gb/s	160 Gb/s
1st	1542.1	1537.9	1534.3	1532.1	1530.7
2nd	1544.3	1540	1535.7	1533.6	1532.1
3rd	1546.3	1542.1	1537.9	1535	1533.6
4th	1547.9	1543.6	1539.3	1537.1	1535.7
5th	1549.3	1545.7	1541.4	1538.6	1537.1
6th	1550	1547.1	1542.9	1540.7	1539.3
7th	1550.7	1548.6	1545	1542.9	1542.1
8th	1551.4	1550	1547.1	1545.7	1545
9th	1552.1	1551.4	1550	1549.3	1548.6
10th	1552.9	1552.9	1555	1555.7	1556.4

The previous section highlighted that there is no vital need to apply more than 10 pulses in the investigation; however, at data rates > 10 Gb/s, the variations of gain depletion after the 10th pulse cannot be neglected. The injection of more number of pulses in the packet at each higher data rate is necessary. Therefore, in the following investigation, the number of pulses per packet is increased at each data rate maintaining the packet duration of 1 ns. The SOA gain response when a 1 ns packet of 20 Gaussian pulses at 20 Gb/s is applied to the SOA is displayed in Fig. 6.9. Figure 6.9 shows the further depletion of SOA gain after the 10th pulse and it is clear that applying more than 20 pulses does not affect the gain depletion envelope.
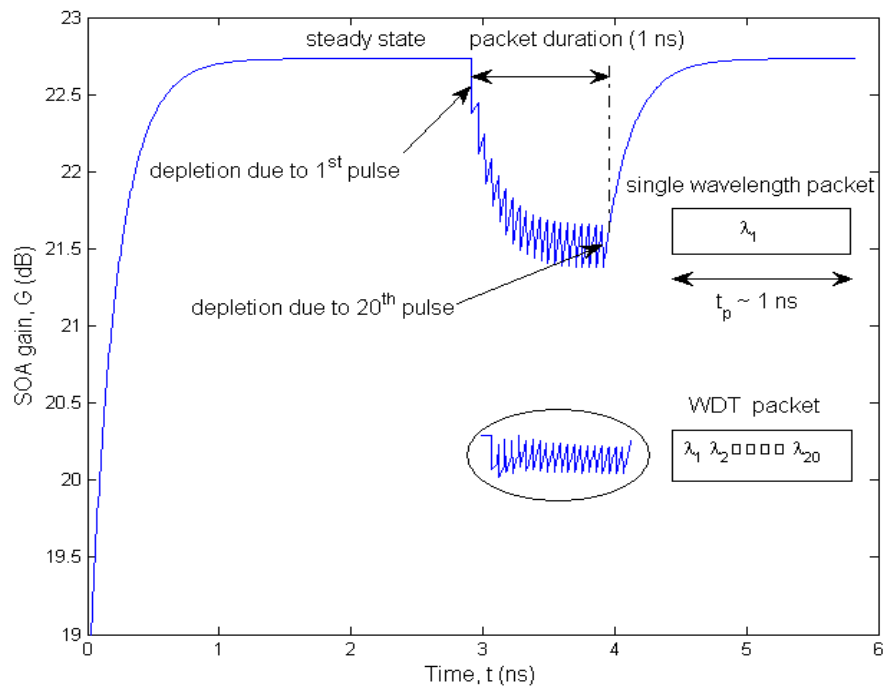
Figure 6.9 SOA Comparison between SOA gain responses to a 20 pulses packet of single wavelength and WDT at 20 Gb/s

Figure 6.9 also illustrates the response of the SOA gain when the WDT is applied to the 20 pulses packet (circled) in order to confirm the enhanced uniformity of the gain depletion envelope (compared to using a single wavelength). A reduction of 7.5 dB in σ is achieved employing the WDT. The wavelengths used for pulses 1 to 20 are 1537.9, 1539.3, 1541.4, 1542.9, 1545, 1545.7, 1547.1 1547.9, 1548.6, 1549.3, 1550, 1550.7, 1551.4, 1551.4, 1552.1, 1552.1, 1552.9, 1553.6, 1553.6 and 1553.6, respectively.

As it can be seen from Fig. 6.9, the last few pulses of the packet using the single wavelength technique cause the gain of the SOA to drop to levels with small gain differences. This response explains the small wavelength spacing between these pulses. Some of the pulses use the same wavelength however; the minimum spacing between pulses using two different wavelengths is 0.7 nm.

The same approach is repeated using 1 ns packet containing 40, 80 and 160 pulses at 40, 80 and 160 Gb/s. An improvement of 8 dB in the gain uniformity is achieved using the proposed technique at 40 Gb/s. By applying the WDT for 80 and 160 Gb/s packets, the wavelengths of pulses 1 to 15 and 1 to 4, respectively are < 1530 nm which determines the lower boundary of the C-band wavelength range. In this thesis, only wavelengths within the C-band range are considered.

6.5.   Boundaries of WDT

The boundaries and limitations of the proposed wavelength diversity technique are studied in this section in order to efficiently enhance the SOA gain uniformity. The wavelengths of the input pulses are chosen according to the wavelength band

used in the high speed application. This study focuses on the C-band range and therefore the minimum and maximum wavelength boundaries are 1530 and 1565 nm, respectively.

From Fig.6.3, it is also clear that G_m is another gain boundary (maximum) value by which the WDT can be used (i.e. all input pulses achieve the same gain level). Therefore, it is of interest to investigate the impact of I on G_m. Figure 6.10 depicts the maximum uniform SOA gain achieved corresponding to the applied bias current at all input data rates.
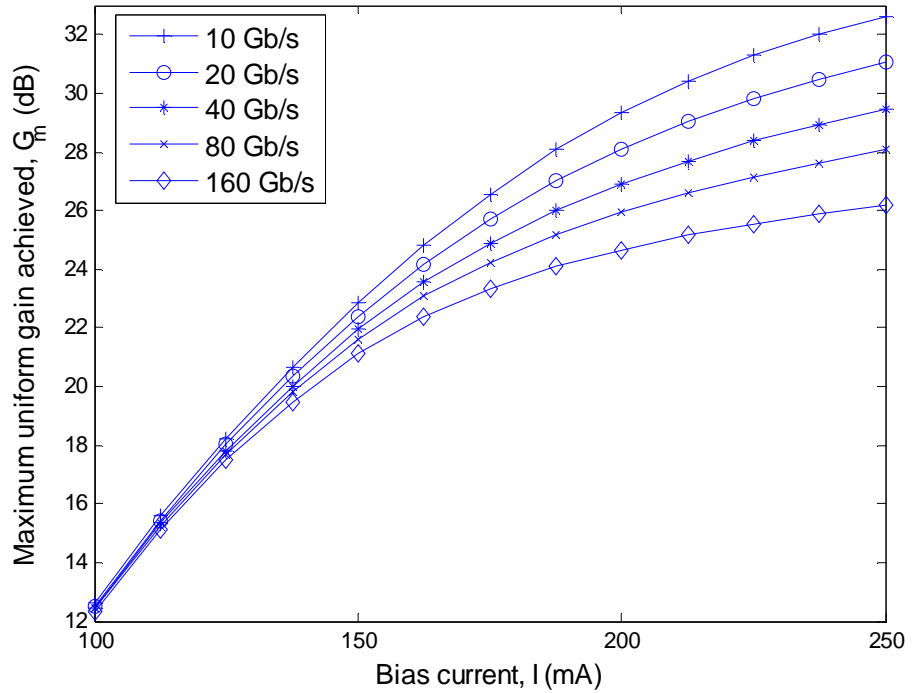
Figure 6.10 Maximum uniform gain achieved corresponding to the SOA applied bias current at all input data rates

As a result of the excitation of more electrons in the conduction band (i.e. higher N), it is anticipated that I is proportional to G_m which is observable in Fig. 6.10.

Figure 6.10 also shows that G_m has a lower value at higher data rates for any biasing current value due to the limited time available for the gain to recover at higher data rates.

6.6.   Summary

This chapter showed improvement in the gain uniformity of the SOA at high speed data rates employing a proposed wavelength diversity technique. In this chapter a gain standard deviation equation is introduced in order to measure the SOA gain uniformity. The impact of the wavelength diversion characteristics of a packet of Gaussian pulses on the SOA gain and gain uniformity is investigated. The least gain uniformity appeared at the peak gain wavelength while the best uniformity is achieved at 1530 nm within the C-band range.

The chapter compared the SOA gain uniformity using a single wavelength and a proposed wavelength diversity technique for the same input packet. The obtained results verified the ability of the WDT to enhance the SOA gain uniformity at different data rates. The average gain standard deviation improvement is 7.82 dB at data rates investigated in this chapter up to 160 Gb/s. The same comparison between both techniques is repeated maintaining a fixed packet time duration of 1 ns (similar to 10 Gb/s packet). The WDT also achieved a 7.5 and 8 dB reductions in gain standard deviation at 20 and 40 Gb/s. The limitations of the proposed technique regarding the wavelength and the applied bias current at all the input data rates are studied to set the boundary conditions.

Finally, it is important to note that the implementation of the proposed technique is complex due to the different wavelength for each pulse within the packet. The proposed technique would be possible if it is within the C-band range as investigated in the paper since most WDM systems have narrow channel spacing of 0.4 nm or less [142]. For that reason, a different approach is proposed in the next chapter to improve the SOA gain uniformity for high speed data rates in order to reduce power system penalties. Non-uniform electrical signal patterns are used as a replacement for the uniform current to bias the SOA.

Chapter 7   SOA Gain Uniformity Improvement Employing Classical Non-Uniform Biasing Technique for High Speed Optical Routers

7.1.   Introduction

The previous chapter highlighted the importance of the SOA amplification gain flatness in order to minimise the patterning effect. This chapter introduces a different technique to overcome the disturbance of the output SOA gain uniformity at high speed data rates. Non-uniform periodic signals are proposed to electrically bias the SOA as a substitute of the uniform bias current.

In this chapter, biasing the SOA with non-uniform bias current patterns, namely, triangular and sawtooth electrical patterns are proposed. The impacts of both

uniform and non-uniform biasing on the SOA gain responses and the corresponding gain standard deviations are analysed. The SOA gain uniformity is measured and compared for all the biasing patterns for input data speed up to 40 Gb/s.

The optical packet which consists of ten successive Gaussian pulses that was injected to the SOA in the previous chapter is also used as the input packet in this chapter. The same packet is used for consistency at different time separations between the pulses.

7.2.   Uniform Bias Current

The SOA gain response to the input 10 pulses packet is previously investigated and explained in Chapter 6 using a uniform bias current I of 150 mA (see Fig. 6.1). However, further analysis is required in order to understand the role of the bias current and N rate of change (i.e. dN/dt) on the gain profile. In this section, the applied uniform current is maintained the same. Prior to the entry of the first pulse of the packet, N is almost constant and therefore, the change of the carrier density in (3.6) is neglected. Equation (3.6) is presented here to aid the discussion.

$$\frac{dN}{dt} = \frac{I}{q \cdot V} - (A \cdot N + B \cdot N^2 + C \cdot N^3) - \frac{\Gamma \cdot g \cdot P_{av} \cdot L}{V \cdot h \cdot f}$$

With no input pulse entering the SOA, only the 1st and 2nd terms of (3.6) are considered due to the absence of the input power. The instant decrease in the carrier density due to the entrance of the first pulse results in a high negative dN/dt value. This is explained with reference to the 3rd term in (3.6), which depends on

the power of the input pulse and the material gain coefficient, thus causing dN/dt to have a high negative value.

When the pulse exits the SOA, the 3rd term returns to zero value. Therefore, dN/dt becomes a positive value which creates a gap between the 1st and the 2nd term of the rate equation; hence the carrier density starts to increase (i.e. SOA gain recovery). As described earlier, the next pulses entering the SOA before full recovery introduce further gain depletions. The 1st term of (3.6) is always constant due to the uniform biasing of the SOA and therefore, it is not possible to control the changes of the carrier density. Consequently, to minimise σ (i.e. to achieve a flat gain profile), it is important to control the rate of change of N, thus it is of interest to apply non-uniform biasing current to the SOA. In order to bias the SOA with non-uniform bias currents, refer to Section 4.3, specifically Figs. 4.3 and 4.4 to appreciate the influence of the applied bias current on the SOA gain.

In following sections, non-uniform current patterns are proposed to bias the SOA in order to study their impact on the SOA gain uniformity. The non-uniform bias currents applied to the SOA have an average value of 150 mA (equivalent to uniform bias current) in order to maintain the same power used in both cases.

7.3.   Triangular Bias Current

There are two criteria to control the pattern of the non-uniform bias current applied to the SOA. 1) The need to increase the value of the 1st term of the rate equation (3.6) to accelerate the gain recovery of the SOA. Therefore, a steep increase in the bias current is required following the departure of the pulse from the SOA. 2)

To maintain the average bias current (power) similar to the uniform current value (i.e. at 150 mA). Therefore, the bias current should decelerate at the same acceleration rate but in the opposite direction. Hence, a triangular pattern bias current is proposed to meet the required criteria in this section.
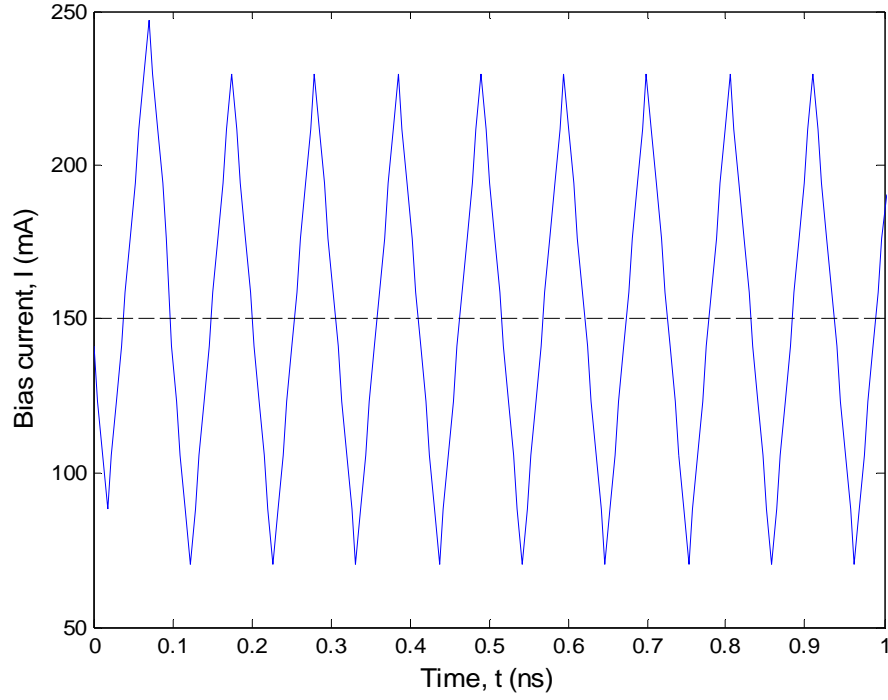
Figure 7.1 Triangular bias current

For an input packet with 10 Gb/s pulses rate, the bias current is adjusted to the same repetition rate of $1/T$. Over a triangular cycle T of 100 ps, the bias current can be represented as:

$$I = \begin{cases} m_1 \cdot t + C_1 & \text{for} \quad 0 \leq t \leq T/2 \\ m_2 \cdot t + C_2 & \text{for} \quad T/2 \leq t \leq T \end{cases},$$

(7.1)

where m_1 and m_2 are the slopes of the triangular biasing signal with values 30.26 and -30.26 mA/ns, respectively. C_1 and C_2 are 70.55 mA and 388.25 mA, respectively. It will take the bias current almost 50 ps to increase from ~70 mA to 230 mA as shown in Fig. 7.1 which displays the triangular bias current.

The 10 pulses packet at 10 Gb/s is applied to the SOA biased by the triangular current in Fig. 7.1. The corresponding gain response of the SOA is illustrated in Fig. 7.2. From Fig. 7.2, one can see the oscillations of the SOA gain due to the alternating bias current prior to the entry of the 1st pulse of the input packet. Similarly in uniform biasing, the entry of the input pulse results in a rapid depletion in the SOA gain within the 5.83 ps. However, in the case of triangular biasing, this depletion is less effective compared to the uniform biasing. The corresponding profiles of the amplified Gaussian pulses are depicted on the bottom of Fig. 7.2.

It can be seen that the 1st pulse achieves the maximum gain due to depletion of the SOA gain from the steady state value, as expected. It is important to note that the non-uniform biasing current does not produce amplitude modulation to the optical pulses; on the contrary, the applied current pattern to the SOA avoids the divergence in amplitudes of these output pulses.
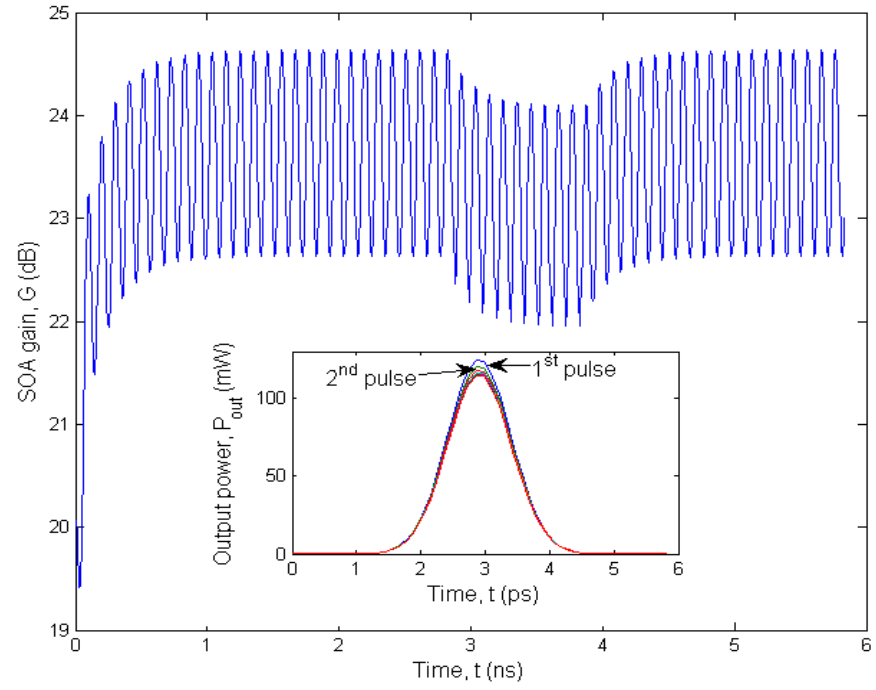
Figure 7.2 SOA gain response to a packet of 10 Gaussian pulses using triangular bias current and the corresponding profiles of the output pulses

When the input pulse propagates through the SOA, the 3rd term in rate equation (3.6) is the dominant term. That term is controlled by the time the input pulse enters to the SOA. There are two different conditions that affect that term. These conditions can be explained by plotting the change in N within the active region of the SOA when biased by a triangular bias current in Figs. 7.3 (a) and (b).
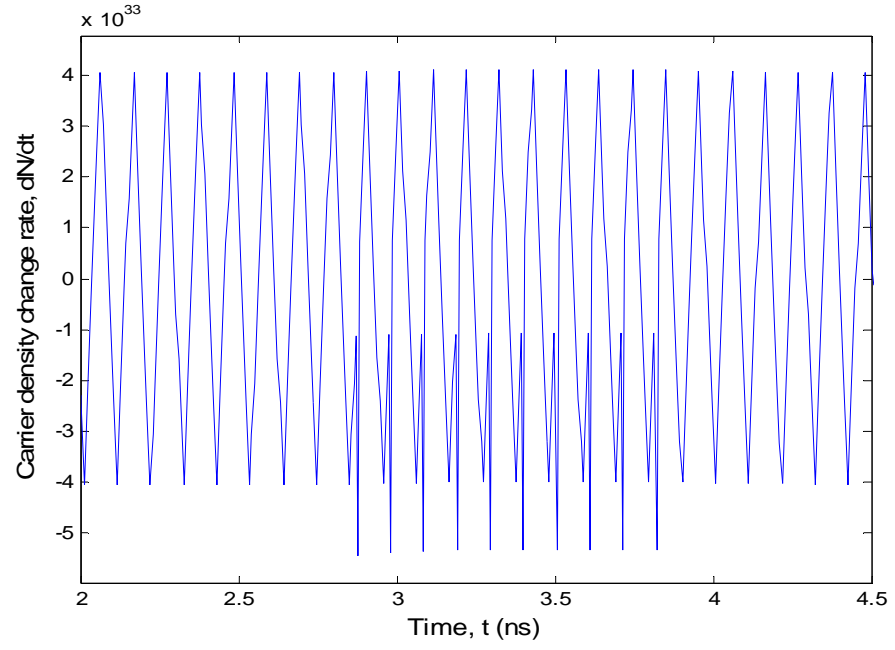
(a)
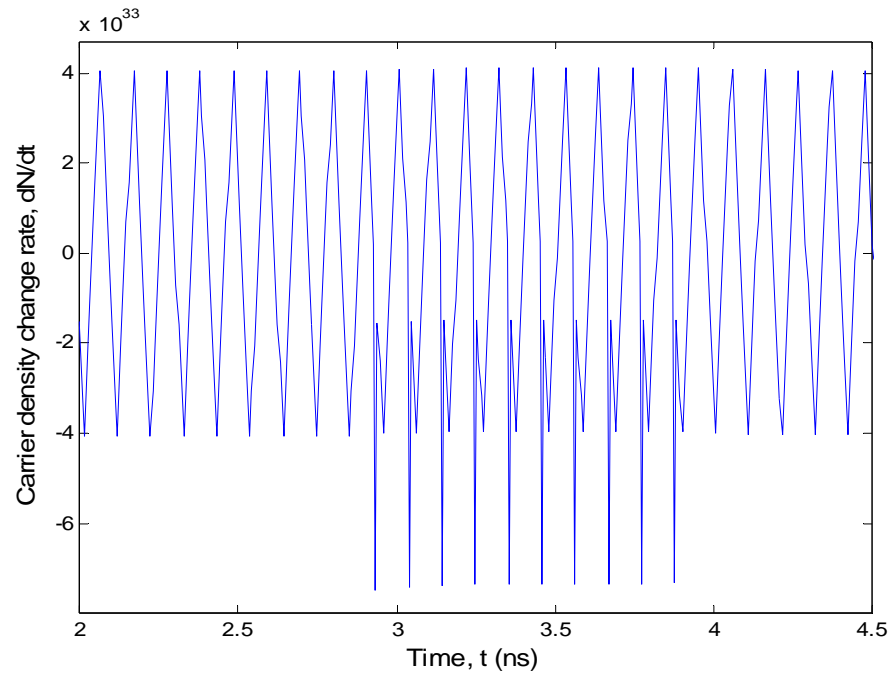
(b)

Figure 7.3 Carrier density change rate within the SOA active region due to triangular biasing corresponding to input packet of Gaussian pulses (a) at lower carrier density values and (b) at higher carrier density values

93

From (3.1) (and correspondingly (3.7)) and (3.2), one can see the dependence of the material gain coefficient and the net gain coefficient on N. In the first case (see Fig. 7.3 (a)), the 3rd term in (3.6) has less impact on the depletion of N and the total gain when the input pulse first enters the SOA at a lower value of N. Therefore, the effect of the subsequent pulses is minimised resulting in enhanced output gain uniformity. N has lower values for $0 \leq t \leq T/2$, where dN/dt is initially negative and at the same time the bias current increases (i.e. positive slope m_1 of I) which results in the overall increase of dN/dt.

Figure 7.4 shows the carrier density of the SOA which is directly proportional to the SOA gain as shown in Fig. 7.2. On the bottom left of Fig. 7.4, one can see that the input pulse is launched at a lower value of N which results in low gain depletion. On the other hand (see Fig. 7.3 (b)), when the input pulse enters the SOA at a higher value of N (i.e. $T/2 \leq t \leq T$) which can be seen on the bottom right of Fig. 7.4, higher gain depletion is introduced.
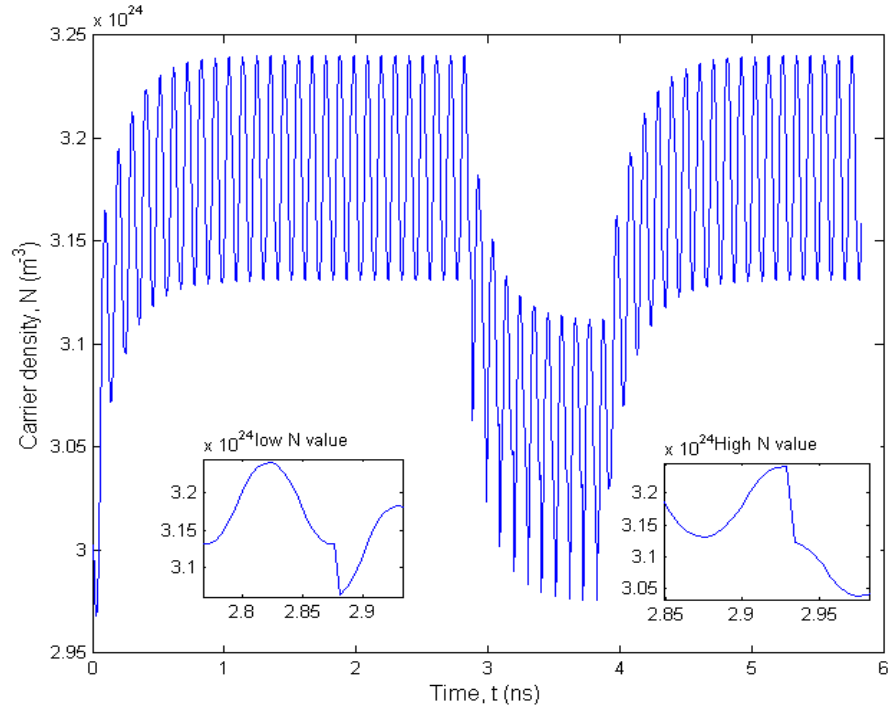
Figure 7.4 Carrier density of the SOA when the input pulse is launched at lower (bottom left) and higher values (bottom right) for triangular biasing

Figure 7.5 shows the comparison of σ for uniform and both cases of triangular (for input pulse at lower and higher values of N) biasing conditions at 10 Gb/s. Figure 7.5 is plotted against the pulse peak to realise the validity of the study at any input power. The figure shows that improved gain uniformity compared to uniform biasing is achieved when the input pulses are injected at lower N values in case of triangular biasing. However; at higher N values, less gain uniformity is achieved regardless of the input power levels. At higher input power, the fluctuation of σ is less perturbed. As predicted, σ has a higher value when more input signal power is applied which further increases the 3rd term of (3.6).
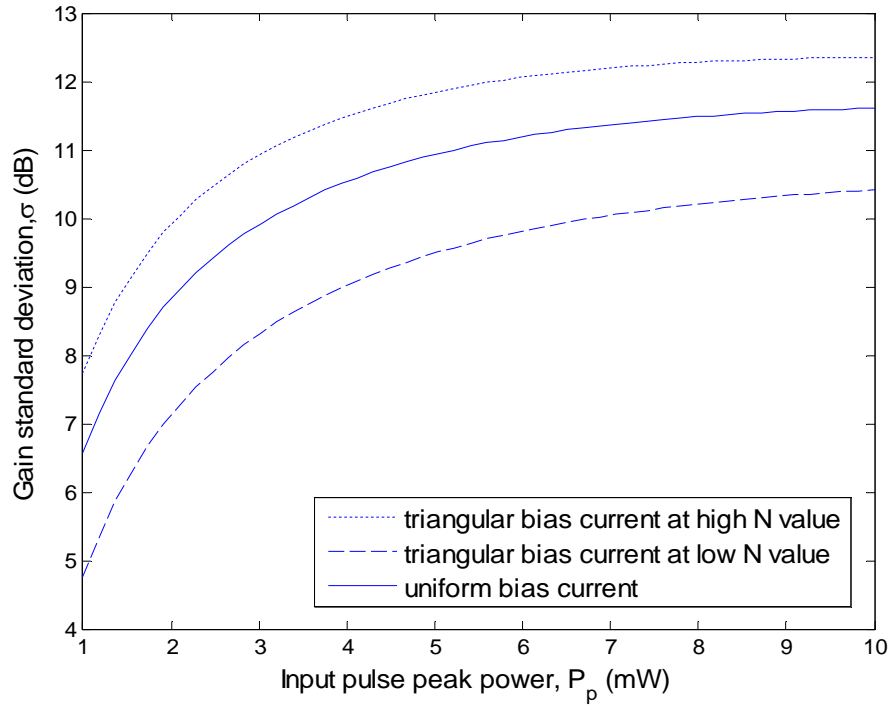
Figure 7.5 Comparison of gain standard deviation between uniform and both triangular biasing cases (at lower and higher carrier density values) against peak power of input pulses at 10 Gb/s

7.4.   Sawtooth Bias Current

In the previous section, it was clear that the SOA gain is more linear during the positive slope of the triangular bias current. For this reason, the criteria to control the non-uniform pattern for biasing the SOA is different in this section. The bias current is required to have a steep increase (i.e. positive slope) for a longer time maintaining the rising rate and an average current of 150 mA. Consequently, a sawtooth current is proposed to bias the SOA.
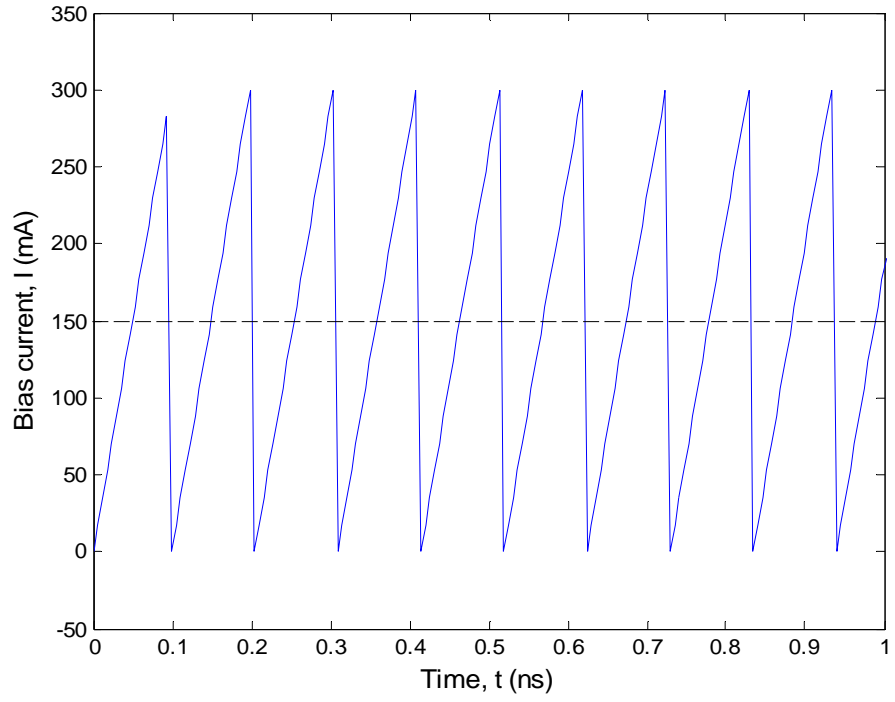
Figure 7.6 Sawtooth bias current

For $T = 100$ ps, the sawtooth bias current can be expressed by:

$$I = m_1 \cdot t,$$
(7.2)

where m_1 is the same positive slope used in triangular biasing. The sawtooth biasing current rising from 0 to 300 mA is plotted in Fig. 7.6. The SOA gain and the corresponding output profiles of the input pulses due to sawtooth bias current are shown in Fig. 7.7.
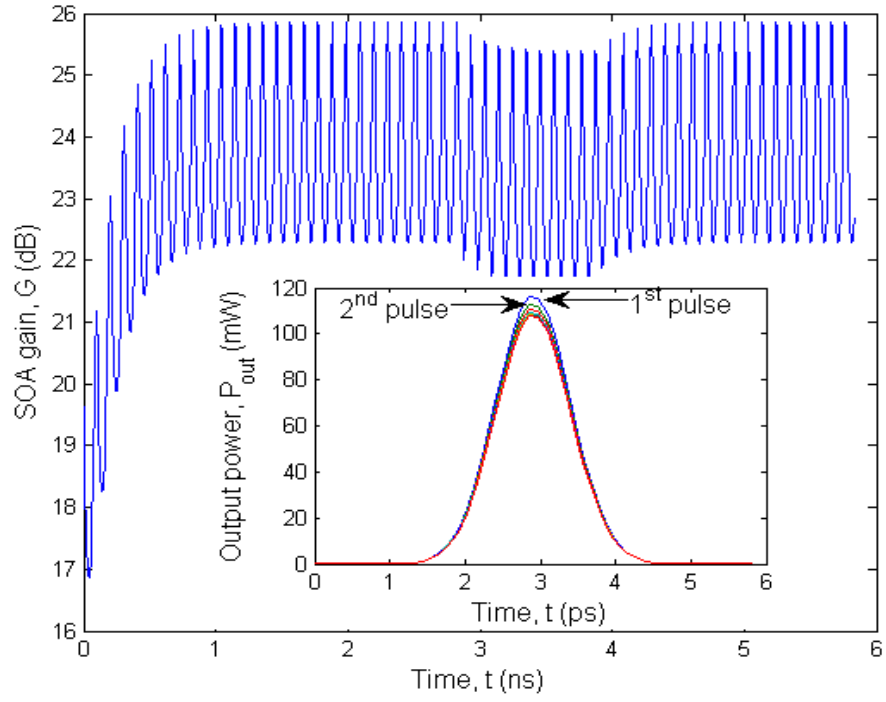
Figure 7.7 SOA gain response to a packet of 10 Gaussian pulses using sawtooth bias current and the corresponding profiles of the output pulses

From the figure, the SOA gain processes higher oscillations compared to triangular biasing prior to the entry of any input pulse. Such response is due to the variation of a larger range of the bias current (0 to 300 mA). The depletion of the SOA gain due to the input packet is detected from $t \sim$ 3 to 4 ns. Less gain fluctuations are observed in the SOA gain depletion envelope (i.e. more gain uniformity) in Fig. 7.7 compared to the uniform biasing illustrated in Fig. 6.1. However, the impact of the input pulses on the SOA in case of sawtooth bias current depends on the time they are applied to the SOA (similar to the triangular biasing case). This can be more obvious in Fig. 7.8 which depicts the effect of the

input pulse on the carrier density of the SOA when launched at lower and higher values.
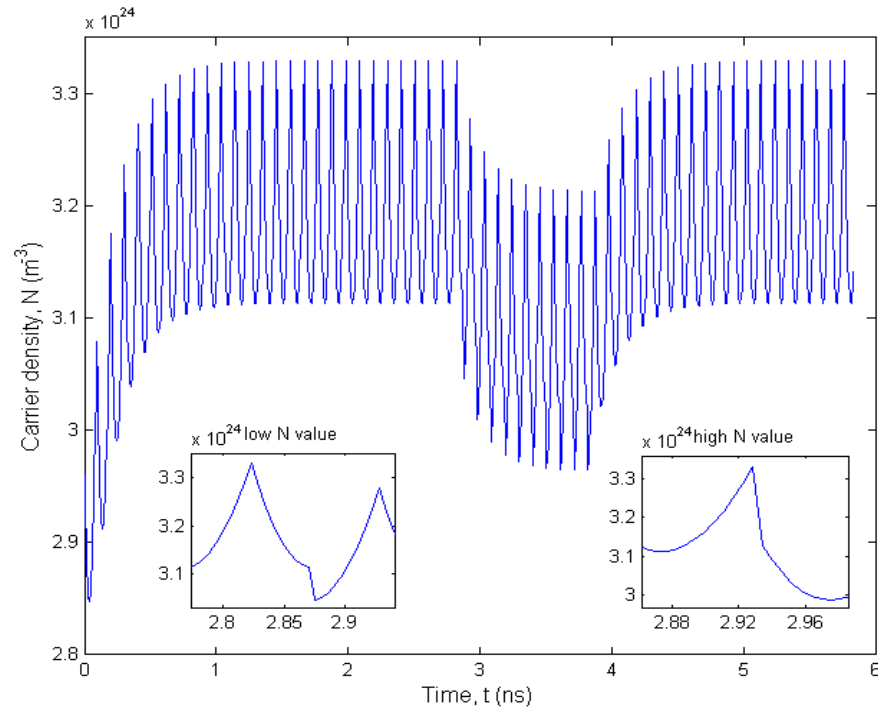
Figure 7.8 Carrier density of the SOA when the input pulse is launched at lower (inset left) and higher values (inset right) for sawtooth biasing

Similarly to triangular bias current, Fig. 7.8 (inset left) shows small impact of the input pulse when applied to the SOA at lower N. Alternatively, high N depletion occurs when the pulse is applied at a higher value (Fig. 7.8, inset right). Therefore, to view the impact of these two different conditions on the SOA gain uniformity, Fig. 7.9 is plotted comparing them to uniform biasing.

In spite of the power of the input pulse, the SOA shows an improved gain uniformity employing sawtooth bias current when the input packet arrives to the SOA at a lower N compared to uniform biasing.
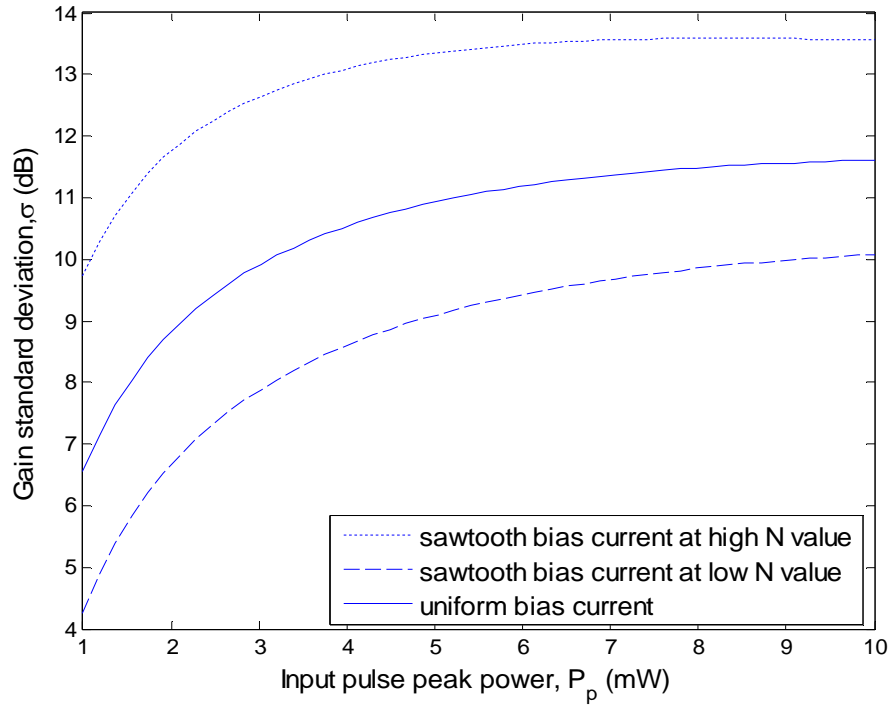
Figure 7.9 Comparison of gain standard deviation between uniform and both sawtooth biasing cases (at lower and higher carrier density values) against peak power of input pulses at 10 Gb/s

In order to appreciate the bias current pattern that results in the best achieved gain uniformity, the following section compares all the investigated biasing techniques (for lower N values) at different input packet data rates.

7.5. SOA Gain Uniformity Comparison for Uniform and Non-uniform Techniques

This section concludes the differences of all the investigated biasing techniques regarding the SOA gain uniformity.
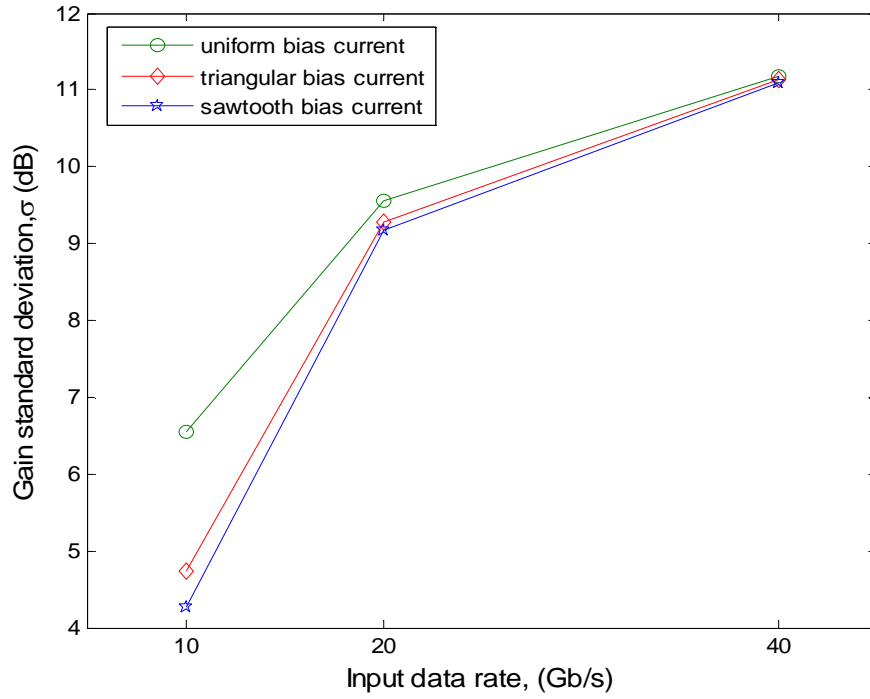
Figure 7.10 Comparison of gain standard deviation between all biasing techniques at different input data rates

Figure 7.10 compares the gain standard deviation of the uniform and non-uniform biasing techniques at different input data rates (i.e. 10, 20 and 40 Gb/s). Maintaining the number of pulses at all data rates, the achievement of lower σ at lower data rates is because the recovery of the SOA gains is more restricted at high speed input data rates. The sawtooth bias current shows a lower gain standard deviation (better gain uniformity) than the triangular biasing at all data rates as seen in Fig. 7.10. For all cases, σ is lower for the non-uniform biasing particularly at 10 Gb/s data rate. At 20 and 40 Gb/s, minimum improvements are achieved. The reason is that, at higher data rates and for the same number of pulses, the output gain has a higher σ due to the reduced separation period (i.e.

short time available for the SOA to recover as a result of each input pulse). For 10, 20 and 40 Gb/s data rates, σ for triangular and sawtooth biasing are 4.7, 9.3 and 11.1 dB, and 4.3, 9.2 and 11.1 dB respectively. For uniform biasing these are 6.6, 9.6 and 11.2 dB, respectively.

The advantage of using non-uniform techniques over uniform biasing is more evident in Fig. 7.11. The figure illustrates the improvement of the gain standard deviation for using non-uniform (triangular and sawtooth) bias currents as a replacement of the uniform current.
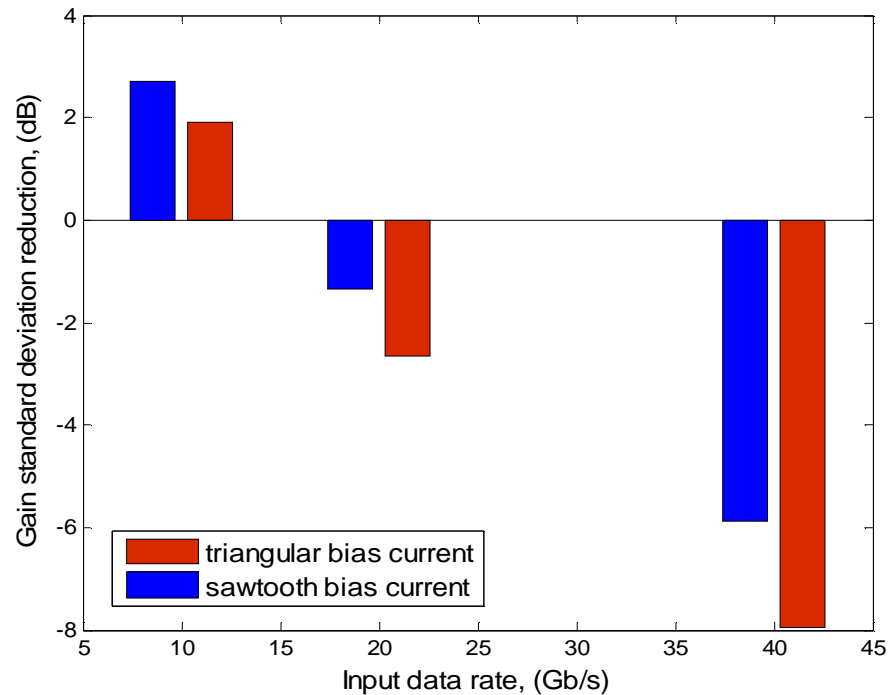
Figure 7.11 Gain standard deviation improvement for using triangular and sawtooth bias currents over uniform bias current at different input data rates

At a data rate of 10 Gb/s the non-uniform biasing techniques result in a gain standard deviation improvement of 1.9 and 2.7 dB for the triangular and sawtooth

biasing schemes, respectively. Meanwhile at 20 Gb/s, these improvements are only -2.7 and -1.3 dB (i.e. 0.54 and 0.73 absolute values), respectively. At the speed of 40 Gb/s minimum improvement is achieved.

7.6.   Summary

This chapter focused on the impact of the electrical current characteristics which is used to bias the SOA on the carrier density and the gain uniformity of the SOA. The chapter proposed non-uniform techniques for biasing the SOA that were able to improve the SOA gain uniformity at high speed data rates under certain conditions.

The chapter analysed the carrier density rate of change and the SOA gain when biased by the proposed triangular and sawtooth patterns. The uniform bias current is compared to the non-uniform biasing techniques when the same input packet is applied to the SOA at 10, 20 and 40 Gb/s. The gain uniformity comparison showed a reduction in the gain fluctuation (i.e. gain standard deviation) for both non-uniform currents compared to the uniform biasing. This reduction occurs at the condition when the pulses are injected at low carrier density level. The sawtooth biasing technique appeared to have the best gain uniformity at all investigated data rates. The obtained results show an enhancement in the SOA gain uniformity of 1.9 and 2.7 dB employing the triangular and sawtooth bias currents at 10 Gb/s, respectively. This improvement was only -2.7 and -1.3 dB (i.e. 0.54 and 0.73 absolute values) for the triangular and sawtooth currents at 20 Gb/s, respectively. However, minimum reduction in the gain standard deviation is obtained at 40 Gb/s.

Finally there is a need to synchronise the non-uniform biasing with the incoming pulses so that they coincide with low carrier density level.

Few limitations were observed employing the proposed non-uniform biasing techniques in this chapter. None of the proposed bias currents were able to enhance the gain uniformity beyond 40 Gb/s. The gain standard deviation showed a minimum improvement at high data rates, particularly 40 Gb/s. In addition, the non-uniform current needed to be adjusted at the same repetition rate as the input data rate. For that reason, the following chapter optimises the non-uniform bias current pattern in order to maximise the SOA gain uniformity improvement. The proposed pattern is able to achieve more uniform SOA gain for data rates reaching 160 Gb/s at a repetition rate of only 1 GHz.

Chapter 8   Optimised Biasing for SOA (OBS)

8.1.   Introduction

Improving the SOA gain uniformity was the main focus of the previous chapter which proposed applying non-uniform (i.e. triangular and sawtooth) currents to bias the SOA. However, few limitations were observed employing the previous proposed biasing patterns and minimum improvements were achieved in the SOA gain uniformity at high speed data rates up to 40 Gb/s. For these reasons, this chapter proposes a general equation that optimises the non-uniform bias current pattern in order to maximise the SOA gain uniformity improvement for all conditions.

This chapter investigates the SOA gain profile when the same input packet used in the previous chapter enters the SOA. The chapter analyses the impact of the bias current on the SOA gain responses in order to optimise the non-uniform bias current pattern for input data speed up to 160 Gb/s. The uniform bias current is replaced by the optimised non-uniform pattern to compare the SOA gain uniformity for both techniques for all conditions which include different number of input pulses, input pulse sequences and data rates. The chapter also compares the average output power of the pulses between both biasing techniques to further evaluate the proposed technique.

8.2.   Optimising Non-uniform Bias Current Pattern

The same non-uniform SOA gain problem is previously stated in Chapter 6.2 which shows the SOA gain response to the 10 pulses packet at 10 Gb/s when biased with a uniform 150 mA current. The all '1's bit sequence will be simulated in this chapter to present the worst case scenario for SOA gain depletion. The all '1's sequence is also a commonly used bit sequence in optical applications employing polarisation modulation techniques such as, SOA-based ultrafast all-optical switches [146-150]. In order for all pulses to achieve the same output gain, bias current characteristics are used so that these pulses enter the SOA at the same carrier density. Based on the direct temporal relationship of the bias current on the SOA gain shown in (3.6), this chapter proposes applying a non-uniform bias current pattern to the SOA, where each Gaussian pulse enters the SOA at a different biasing value in order to improve the output gain uniformity.

Consequently, in order to optimise the non-uniform bias current pattern that would achieve the best gain uniformity, the SOA gain response of all the input pulses for a range of bias current values are investigated (see Fig. 8.1).
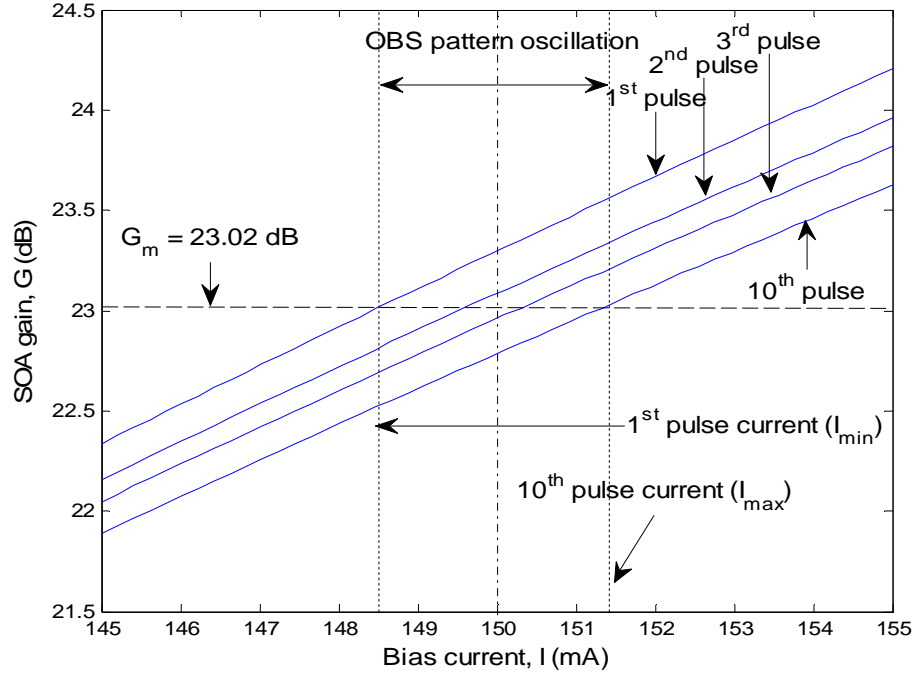
Figure 8.1 SOA gain response of all pulses within the packet to the uniform bias current

From Fig. 8.1, one can see that the same gain (i.e. uniform output gain) can be achieved by the input pulses at different bias current values. However, it is important for the non-uniform bias current applied to the SOA to have an average value equivalent to the uniform bias current in order to maintain the same power used in both cases. For 10 Gb/s input data rate, this uniform output gain condition occurs at G_m = 23.02 dB (horizontal dashed line in Fig. 8.1). This gain value intersects with all pulses at different biasing values while maintaining an average bias current I_{av} = 150 mA where I oscillates between the minimum, I_{min} and

maximum, I_{max} bias currents corresponding to the 1st and 10th pulses respectively. Similarly, input packets are applied to the SOA at higher data rates maintaining the packet duration of 1 ns in all cases. The SOA gain responses to the 1 ns packets of 20, 40, 80 and 160 successive Gaussian pulses at 20, 40, 80 and 160 Gb/s are displayed in Figs. 8.2 (a), (b), (c) and (d), respectively.
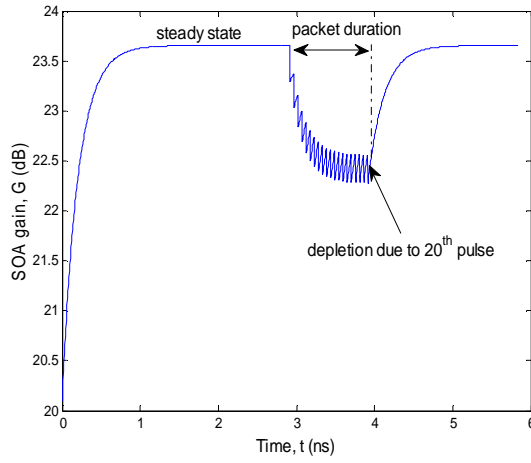
(a)
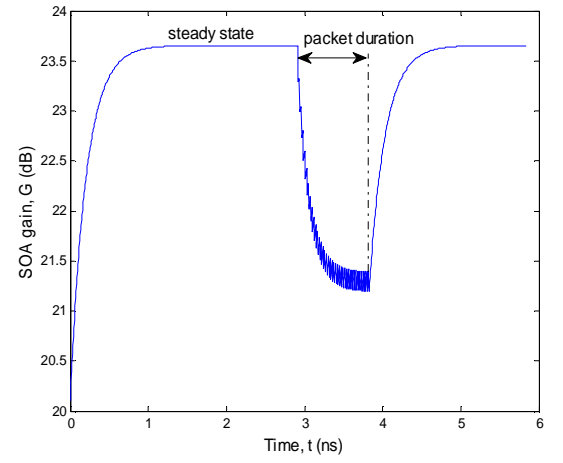
(b)
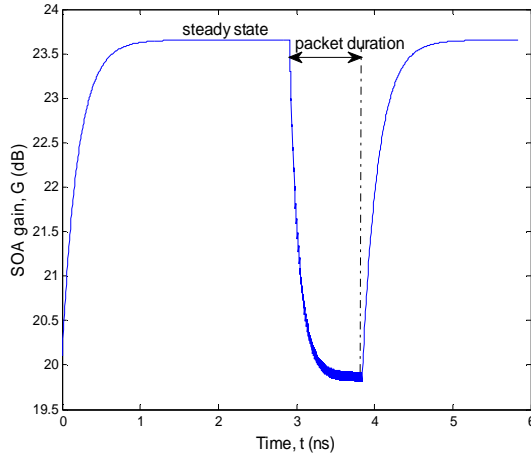
(c)
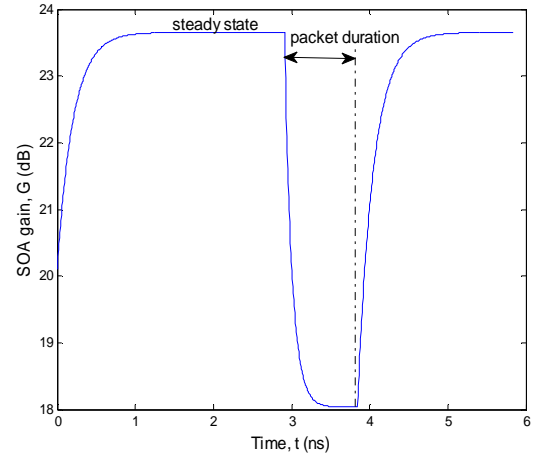
(d)

Figure 8.2 SOA gain responses to the input packets at (a) 20, (b) 40, (c) 80 and (d) 160 Gb/s

The appropriate responses of the non-uniform bias currents should be the inverse to the SOA gain depletion envelopes shown in Figs. 6.1 and 8.2 for all investigated data rates in order to obtain uniform amplitudes for the output pulses. Consequently, this chapter proposes a general equation for the optimised non-uniform biasing pattern at any input data rate and for any number of pulses based on the scheme approached in Fig. 8.1 for all the pulses to achieve the same output gain G_m.

8.3. General Optimised Biasing for SOA (OBS)

In this section, the general optimised biasing for SOA (OBS) equation is derived from the rate equation (3.6) which take in three different scenarios into account. The initial state is represented in the 1st scenario where N depletes from the steady state value due to the propagation of the 1st pulse through the SOA in time t_{int} (i.e. 5.83 ps). Accordingly, (3.6) is rewritten as:

$$\frac{dN}{dt} = \frac{I}{q \cdot V} - \left(A \cdot N_{ss} + B \cdot N_{ss}^2 + C \cdot N_{ss}^3 \right) - \frac{\Gamma \cdot g_{ss} \cdot L \cdot P_{av1}}{V \cdot h \cdot f} , \qquad (8.1)$$

where N_{ss} and g_{ss} are the carrier density and gain coefficient at the steady state value, respectively, while P_{av1} is the average power of the 1st pulse. The carrier density depletes from N_{ss} to N_1 after the 1st pulse is amplified by the SOA gain G_1 (due to the 1st order material gain coefficient g_1) and they are given by:

$$N_1 = N_{ss} + \frac{dN}{dt} \cdot t_{int} , \qquad (8.2)$$

$$g_1 = a_1 \left(N_1 - N_o \right), \qquad (8.3)$$

109

$$G_1 = e^{(\Gamma \cdot g_1 - \alpha_s)L}.$$ (8.4)

where α_s is the internal waveguide scattering loss. The 2nd scenario defines the recovery of N after the departure of the propagating pulse i from the SOA and before the injection of the following input pulse j, where $j=i+1$, at the level x (i.e. from N_i to N_{xj}). Each input pulse is separated by a period $t_{sep}=1$/bit-rate. Therefore, (3.6) is rewritten considering only the first two terms (due to the absence of the propagating signal in the SOA) as follows:

$$\frac{dN_i}{dt} = \frac{I}{q \cdot V} - \left(A \cdot N_i + B \cdot N_i^2 + C \cdot N_i^3\right),$$ (8.5)

where,

$$N_{xj} = N_i + \frac{dN_i}{dt} \cdot t_{int}.$$ (8.6)

Similarly, the corresponding material gain coefficient, g_{xj} and SOA gain, G_{xj} are defined as:

$$g_{xj} = a_1\left(N_{xj} - N_o\right),$$ (8.7)

$$G_{xj} = e^{(\Gamma \cdot g_{xj} - \alpha_s)L}.$$ (8.8)

The 3rd scenario is described by the propagation of the ith pulse along the SOA length. The corresponding rate, carrier density and gain equations are presented as follows:

$$\frac{dN_{xj}}{dt} = \frac{I}{q \cdot V} - \left(A \cdot N_{xj} + B \cdot N_{xj}^2 + C \cdot N_{xj}^3 \right) - \frac{\Gamma \cdot g_{xj} \cdot L \cdot P_{avi}}{V \cdot h \cdot f}, \qquad (8.9)$$

$$N_j = N_{xj} + \frac{dN_{xj}}{dt} \cdot t_{int}, \qquad (8.10)$$

$$g_j = a_1 \left(N_j - N_o \right), \qquad (8.11)$$

$$G_j = e^{\left(\Gamma \cdot g_j - \alpha_s \right) L}. \qquad (8.12)$$

A generalised equation for N is formed from the different scenarios to reflect the gain depletion envelope. Therefore, the instantaneous carrier density N_k to amplify the input pulse k by the gain G_k is described by:

$$N_k = N_{ss} + \frac{dN}{dt} \cdot t_{int} + \sum_{i=1}^{k-1} \frac{dN_i}{dt} \cdot t_{sep} + \sum_{j=2}^{k} \frac{dN_{xj}}{dt} \cdot t_{int}. \qquad (8.13)$$

Hence, the instantaneous 1st order gain coefficient:

$$g_k = g_{ss} + a_1 \left(\frac{dN}{dt} \cdot t_{int} + \sum_{i=1}^{k-1} \frac{dN_i}{dt} \cdot t_{sep} + \sum_{j=2}^{k} \frac{dN_{xj}}{dt} \cdot t_{int} \right). \qquad (8.14)$$

Taking Γ, α_s and L into account in the exponential, (8.14) becomes

$$G_k = G_{ss} \cdot \exp \left(\Gamma \cdot a_1 \cdot L \cdot t_{int} \left(\frac{dN}{dt} + \sum_{i=1}^{k-1} \frac{dN_i}{dt} \cdot \frac{t_{sep}}{t_{int}} + \sum_{j=2}^{k} \frac{dN_{xj}}{dt} \right) \right), \qquad (8.15)$$

where, G_{ss} is the SOA gain at steady state condition (i.e. before the entry of any pulse) derived from the net gain coefficient g_{Tss} and is defined as:

$$G_{ss} = e^{g_{Tss} \cdot L}. \qquad (8.16)$$

Let

$$\frac{dN}{dt} = \frac{I}{q \cdot V} - D_1 , \tag{8.17}$$

$$\frac{dN_i}{dt} = \frac{I}{q \cdot V} - D_2 , \tag{8.18}$$

$$\frac{dN_{xj}}{dt} = \frac{I}{q \cdot V} - D_3 , \tag{8.19}$$

where,

$$D_1 = \left(A \cdot N_{ss} + B \cdot N_{ss}^2 + C \cdot N_{ss}^3 \right) - \frac{\Gamma \cdot g_{ss} \cdot L \cdot P_{av1}}{V \cdot h \cdot f} , \tag{8.20}$$

$$D_2 = \left(A \cdot N_i + B \cdot N_i^2 + C \cdot N_i^3 \right) , \tag{8.21}$$

$$D_3 = \left(A \cdot N_{xj} + B \cdot N_{xj}^2 + C \cdot N_{xj}^3 \right) - \frac{\Gamma \cdot g_{xj} \cdot L \cdot P_{avi}}{V \cdot h \cdot f} . \tag{8.22}$$

Therefore, G_k can be rewritten as:

$$G_k = G_{ss} \cdot \exp\left(\Gamma \cdot a_1 \cdot L \cdot t_{\text{int}} \left(\frac{I}{q \cdot V} - D_1 + \frac{I}{q \cdot V} \cdot \frac{t_{sep}}{t_{\text{int}}} - \sum_{i=1}^{k-1} D_2 \cdot \frac{t_{sep}}{t_{\text{int}}} + \frac{I}{q \cdot V} - \sum_{j=2}^{k} D_3 \right) \right). \tag{8.23}$$

Consequently, from (8.23), the final OBS equation is given by:

$$I_k = \frac{q \cdot V}{\left(2 \cdot t_{\text{int}} + t_{sep} \right)} \left(\frac{1}{\Gamma \cdot a_1 \cdot L} \ln\left(\frac{G_k}{G_{ss}} \right) + t_{\text{int}} \left(D_1 + \sum_{i=1}^{k-1} D_2 \cdot \frac{t_{sep}}{t_{\text{int}}} + \sum_{j=2}^{k} D_3 \right) \right). \tag{8.24}$$

The OBS pattern will repeat periodically after the packet duration t_p. The OBS pattern for 10 Gb/s input data rate using equation (8.24) is shown in Fig. 8.3. On the contrary to the previous chapter, the bias current cycle (repetition rate) covers all the packet duration (i.e. 1 ns which is only 10% of the input data rate in the current investigation) and varies between 148.5 and 151.5 mA.
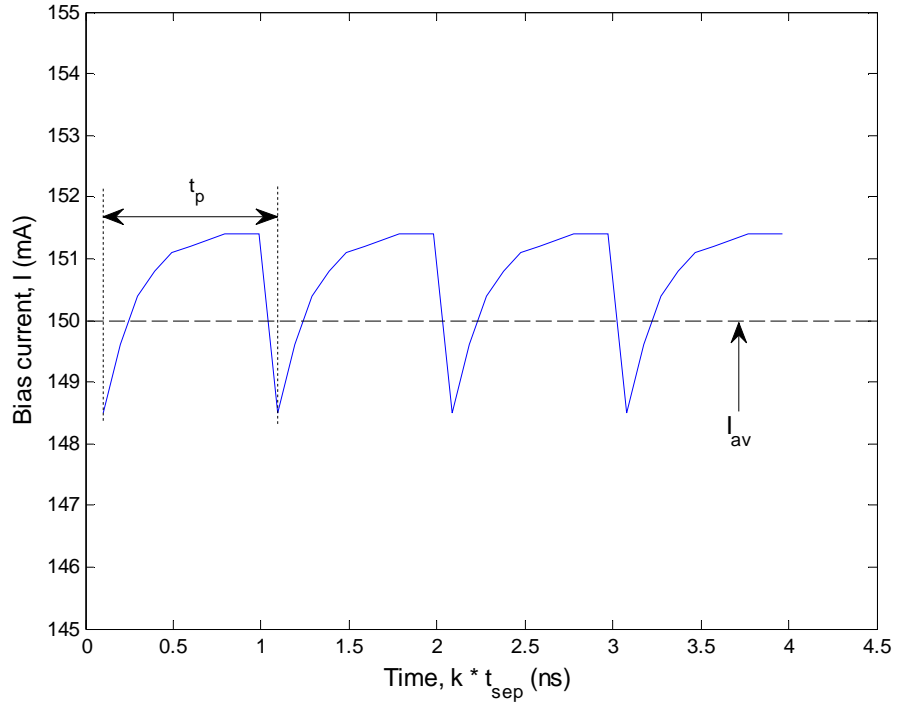
Figure 8.3 OBS pattern for input packet at 10 Gb/s

The corresponding OBS patterns of the biasing currents at 20, 40, 80 and 160 Gb/s input packets are plotted in Figs. 8.4 (a), (b), (c) and (d), respectively. The repetition rate of the periodic OBS pattern is at 1 GHz regardless of the input data rate (i.e. < 1% of 160 Gb/s data rate). The proposed OBS pattern confirms the ability to overcome the repetition rate constraint presented in the previous chapter.
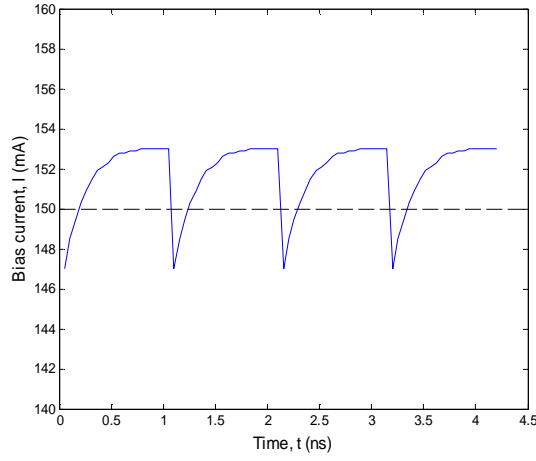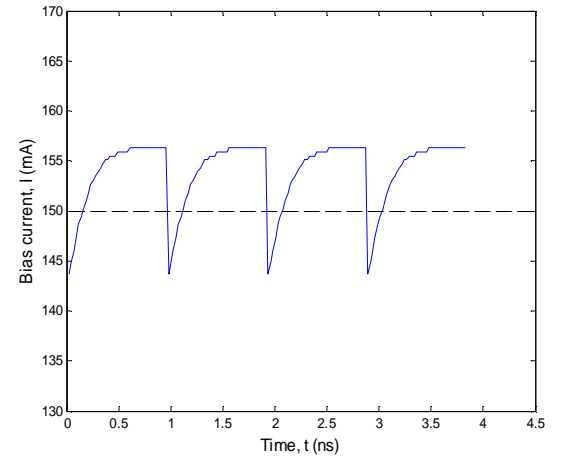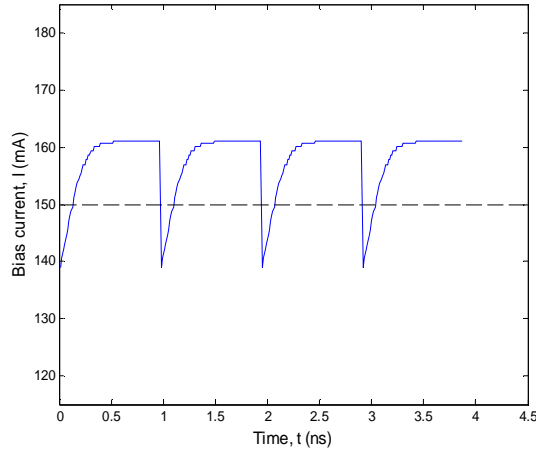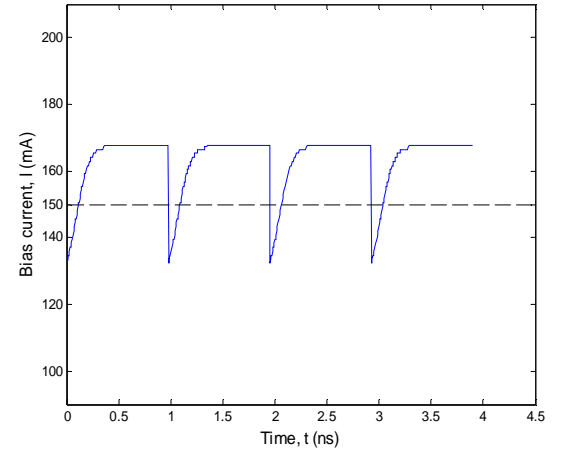
Figure 8.4 OBS patterns for input packets at (a) 20, (b) 40, (c) 80 and (d) 160 Gb/s

Figure 8.4 shows that the OBS pattern fluctuates within a higher range as the data rates increase. These current fluctuation ranges are 6, 12.6, 22 and 35.6 mA at 20, 40, 80 and 160 Gb/s, respectively maintaining I_{av} = 150 mA. It is also clear from Fig. 8.4 that biasing pattern at higher input rates have steeper slope to reach the maximum current value I_{max}. This response refers to the slope of the gain

depletion envelope of the first few pulses of the input packet. The reason for the steep slope at higher rates is due to the limited recovery time.

8.4. Impact of the Applied Bias Current on OBS Pattern

For the non-uniform technique, the maximum current value of the biasing OBS pattern should not exceed the practical SOA biasing limit of 300 to 400 mA [151]. This study focuses on the 300 mA as the maximum (boundary) current limit for safe SOA operation. Therefore, further investigations are carried out for higher I_{av} i.e. 200 and 250 mA at all data rates to find the boundary condition for the proposed OBS technique. Results obtained show that in case of maintaining I_{av} = 200 mA, the I_{max} for the OBS are 206.7, 213, 224, 235.1 and 247.8 mA as illustrated in Figs. 8.5 (a), (b), (c), (d) and (e) at 10, 20, 40, 80 and 160 Gb/s, respectively.
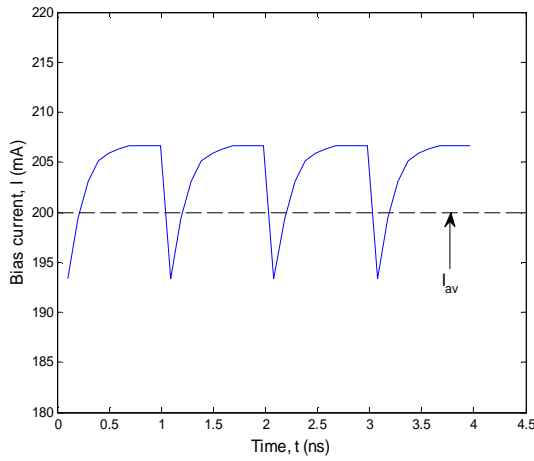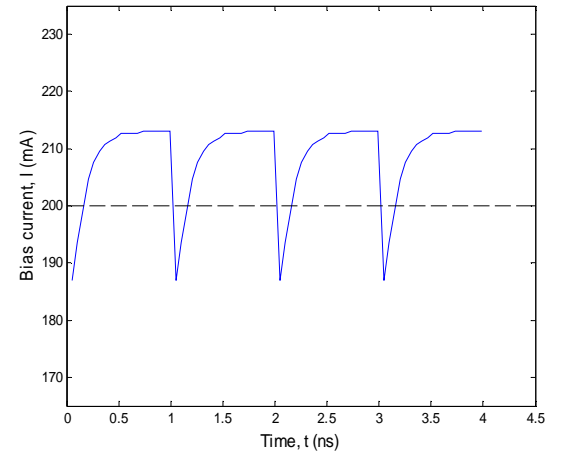
(a)   (b)
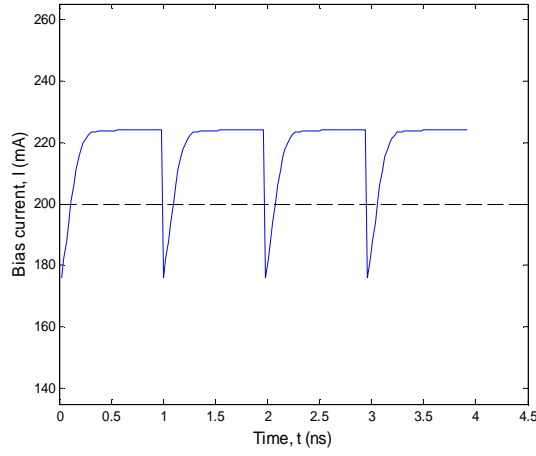
(c)
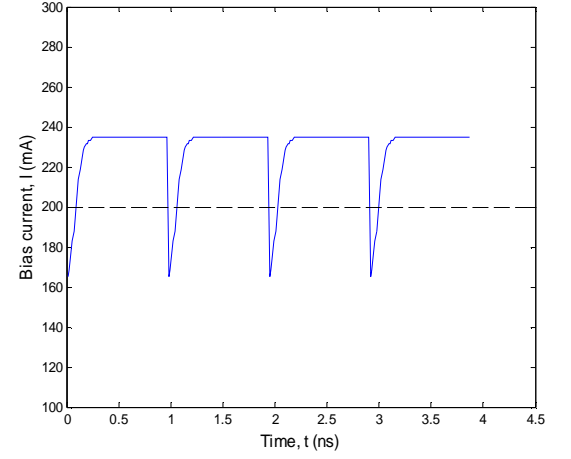
(d)
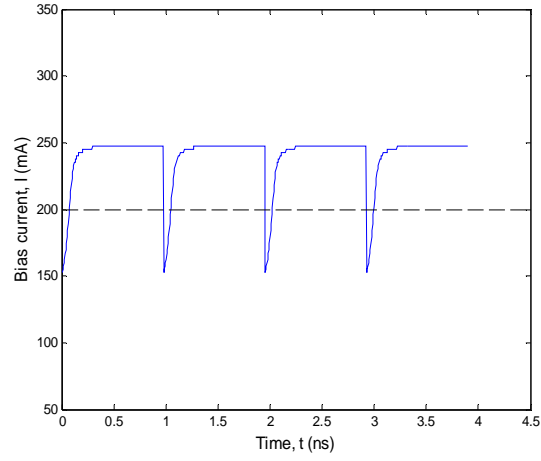
(e)

Figure 8.5 OBS patterns for input packets at (a) 10, (b) 20, (b) 40, (c) 80 and (d) 160 Gb/s maintaining average biasing current of 200 mA

On the other hand, for I_{av} = 250 mA, the I_{max} values are beyond 300 mA at 80 and 160 Gb/s. Nevertheless, the SOA gain uniformity is improved employing the OBS patterns in all cases.

8.5. SOA Gain Uniformity Comparison Between Uniform and the Non-uniform OBS Patterns

In order to emphasise the capability of the proposed OBS pattern to improve the SOA gain uniformity, this section compares the gain standard deviations of the output pulses when the SOA is biased by uniform and the non-uniform OBS patterns.

This comparison between both biasing techniques at all investigated packet speeds is displayed in Fig. 8.6 for I_{av} = 150 and 200 mA. Figure 8.6 confirms the improvement in the SOA gain uniformity achieved employing the proposed OBS technique for all input data rate or the average bias current I_{av}.
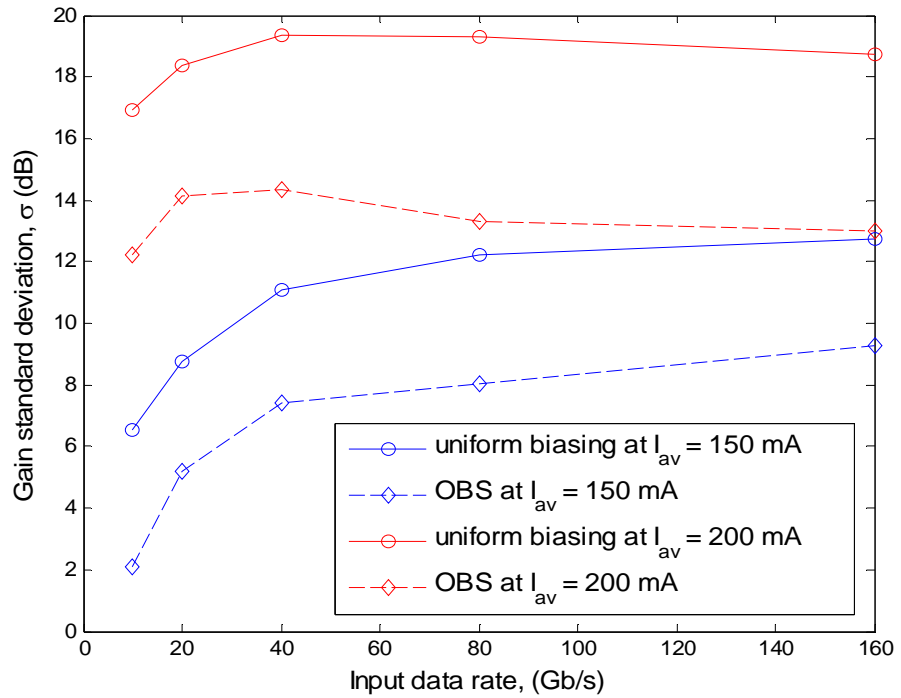
Figure 8.6 Comparison between the gain standard deviation of a packet when the SOA is biased by uniform and the OBS currents at all data rates

In contrast to the previous chapter where the SOA gain uniformity improvement was limited to only 40 Gb/s, the OBS pattern in this chapter is able to maximise the SOA gain uniformity for data speeds up to 160 Gb/s. Results show that the OBS pattern has lower σ compared to the uniform curves at any input rate. The higher curves of the 200 mA I_{av} are predictable due to the higher differences between the output powers achieved by the pulses. As a result, the 200 mA I_{av} will show better gain uniformity improvements in the following figure.

Figure 8.7 shows the advantage of using the OBS pattern over uniform biasing depicted in a bar chart of σ improvement when the uniform bias current is replaced by the proposed technique at I_{av} = 150 and 200 mA for all rates. At higher input rates, more improvement in the SOA gain uniformity is achieved. Figure 8.7 also shows that fluctuation of σ improvement is less perturbed at rates > 40 Gb/s for both I_{av} cases. The reason for the small differences in σ improvement at higher rates (> 40 Gb/s) for different I_{av} level is due to shorter time spacing between input pulses hence, smaller gain differences. An enhancement of 4.6, 6.3, 8.7, 10.1 and 10.2 dB in the SOA gain uniformity when biased with the OBS pattern is achieved at input rates of 10, 20, 40, 80 and 160 Gb/s, respectively for 150 mA I_{av}. On the other hand, these values reach 15.2, 16.3, 17.7, 18 and 17.4 dB at 200 mA.
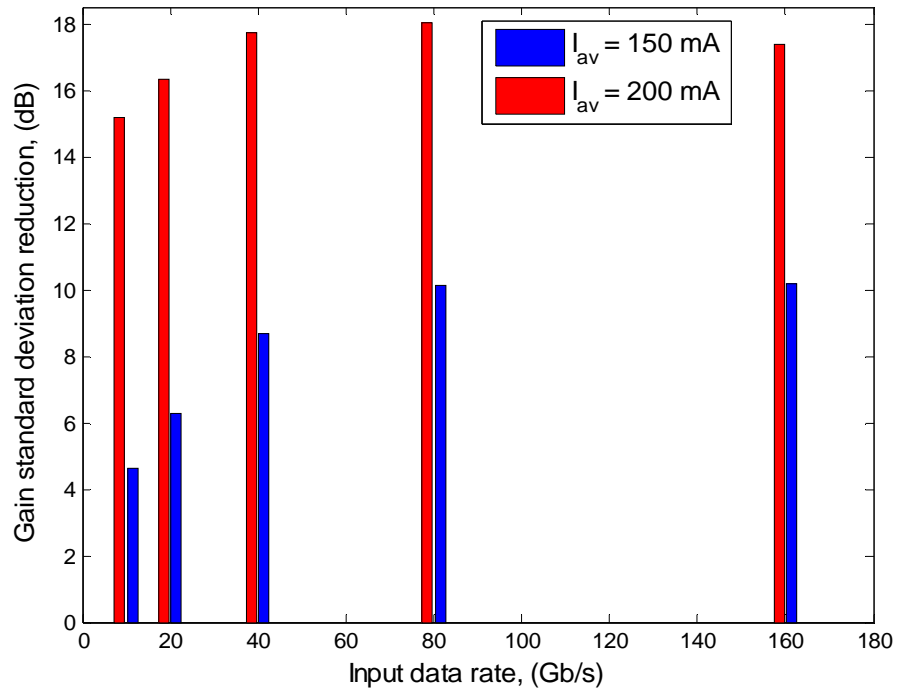
Figure 8.7 Gain standard deviation reduction employing the OBS pattern for all '1's bit sequence packet

8.6. Average Output Power Comparison Between Uniform and OBS Techniques

This chapter presents another key advantage of employing the OBS pattern to the SOA which is the higher average output power. Although both biasing techniques supply the same power to the SOA, the proposed technique offers higher power amplifications for the input pulses. The average output peak powers P_{poav} of the pulses within the packet are plotted in Fig. 8.8 to compare both biasing techniques.
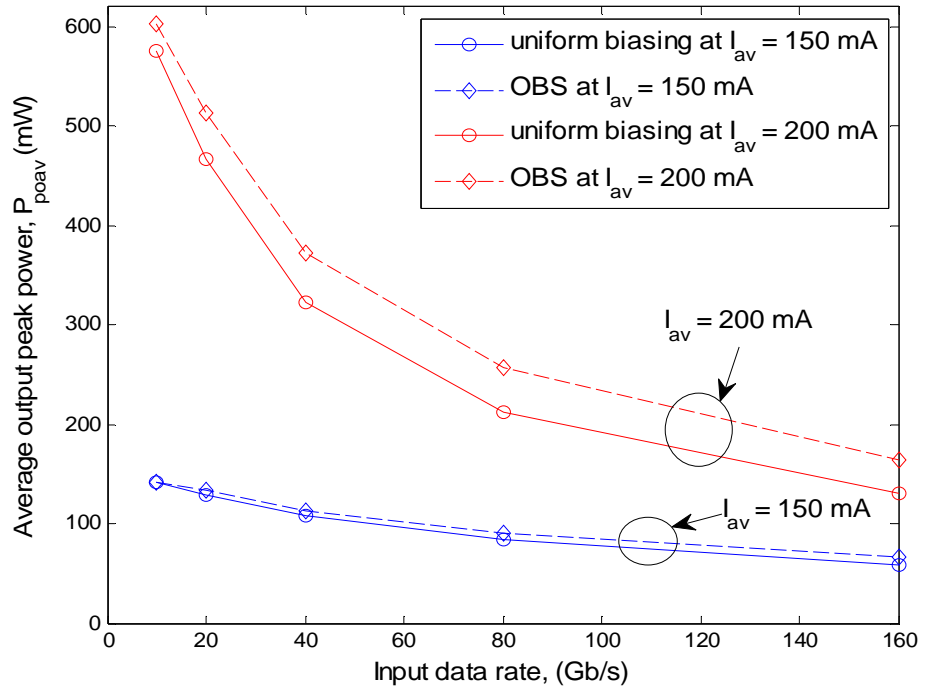
Figure 8.8 Comparison between the average output peak powers of a packet with all '1's bit sequence when the SOA is biased by uniform and the non-uniform OBS patterns at all data rates

In Fig. 8.8, the comparison is carried out at 10, 20, 40, 80 and 160 Gb/s for I_{av} of 150 and 200 mA. From Fig. 8.8, one can see that the average output powers are higher at lower data rates for all curves. The comparison in Fig. 8.8 shows the higher output power achieved by the pulses when the applied bias current to the SOA is optimised using OBS equation for all input data rates and for both I_{av} cases. Figure 8.9 introduces the increase in P_{poav} for using OBS pattern instead of the uniform current at 150 and 200 mA I_{av}.
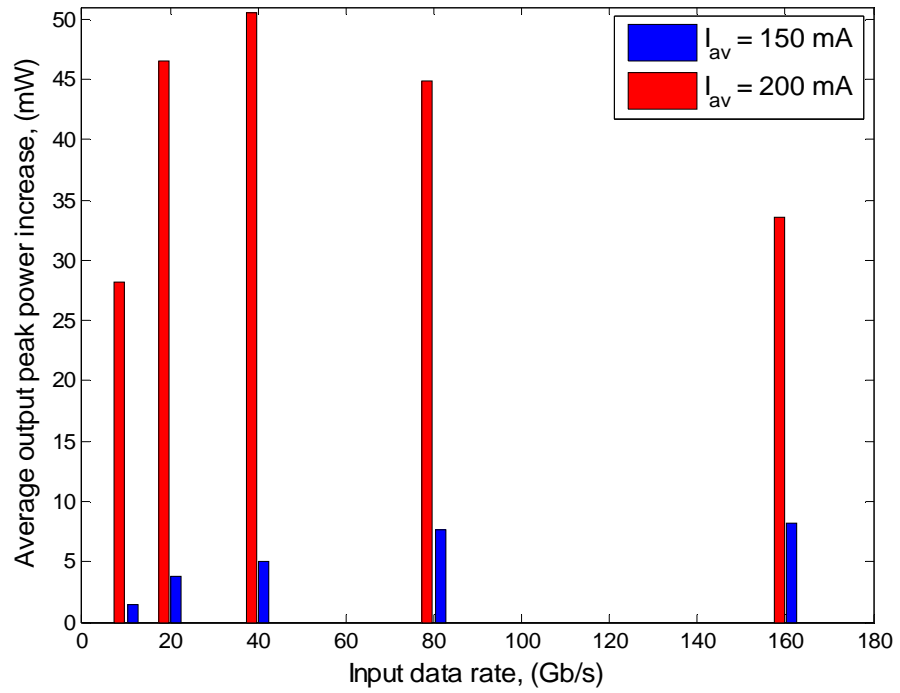
Figure 8.9 Average output peak power increase employing the OBS pattern as a replacement of the uniform current for all '1's bit sequence packet

Figure 8.9 shows that biasing the SOA with the proposed OBS pattern amplify the input pulses with higher power regardless of the pulses speed rate. At 150 mA I_{av}, P_{poav} is increased by 1%, 3%, 5%, 9% and 14% at 10, 20, 40, 80 and 160 Gb/s, respectively. The reason for such response is due to the continuous saturation in case of uniform biasing. Figure 8.9 also verifies the higher increase in P_{poav} at 200 mA I_{av} of 5%, 10%, 16%, 21% and 26% at 10, 20, 40, 80 and 160 Gb/s, respectively. The maximum increase in P_{poav} of 50.5 mW appears at 40 Gb/s maintaining $I_{av} = 200$ mA.

121

8.7.　SOA Gain Uniformity and Average Output Power Comparisons Between Uniform and Non-uniform OBS patterns for Random Bit Sequences

It is of interest to measure the impact of the OBS pattern on other optical applications that use random bit sequences.
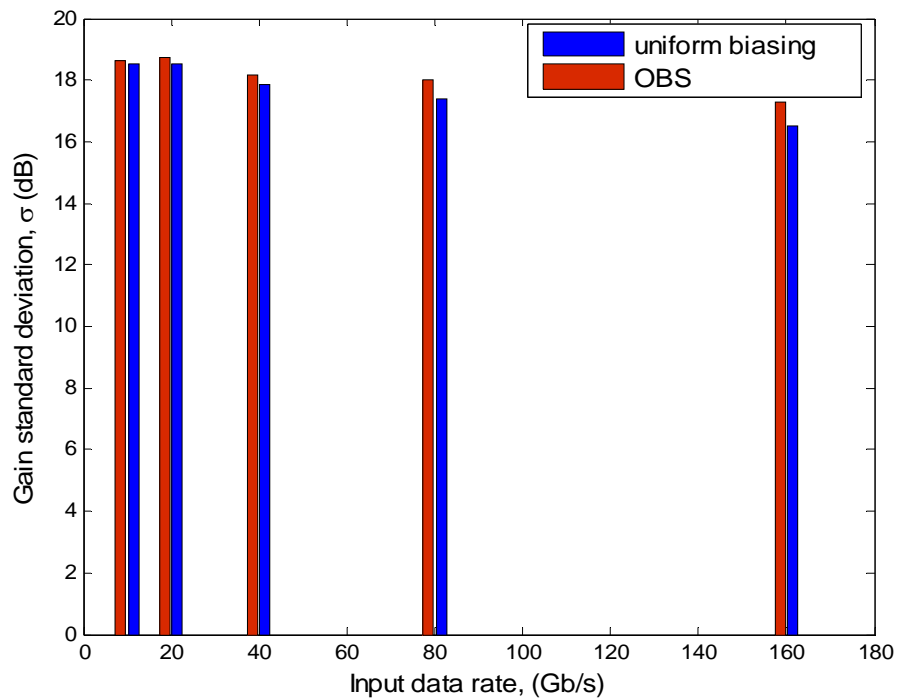
Figure 8.10 Comparison of gain standard deviation between uniform and non-uniform OBS patterns for random bit sequence packet

For that reason, we have applied input packets with the same random bit sequence to SOA biased with both techniques at all data rates. Figure 8.10 illustrates a comparison of the gain standard deviation between uniform and non-uniform OBS patterns for random bit sequence packet.

122

Results obtained from the comparison in Fig. 8.10 show that σ is similar for both biasing cases. However, the proposed technique improves (i.e. increases) the average output power of the packet regardless of the data rate or the average biasing current. This conclusion is more obvious in Fig. 8.11 which depicts a comparison between both biasing techniques for the average output peak powers when an input packet with random bit sequence enters the SOA.
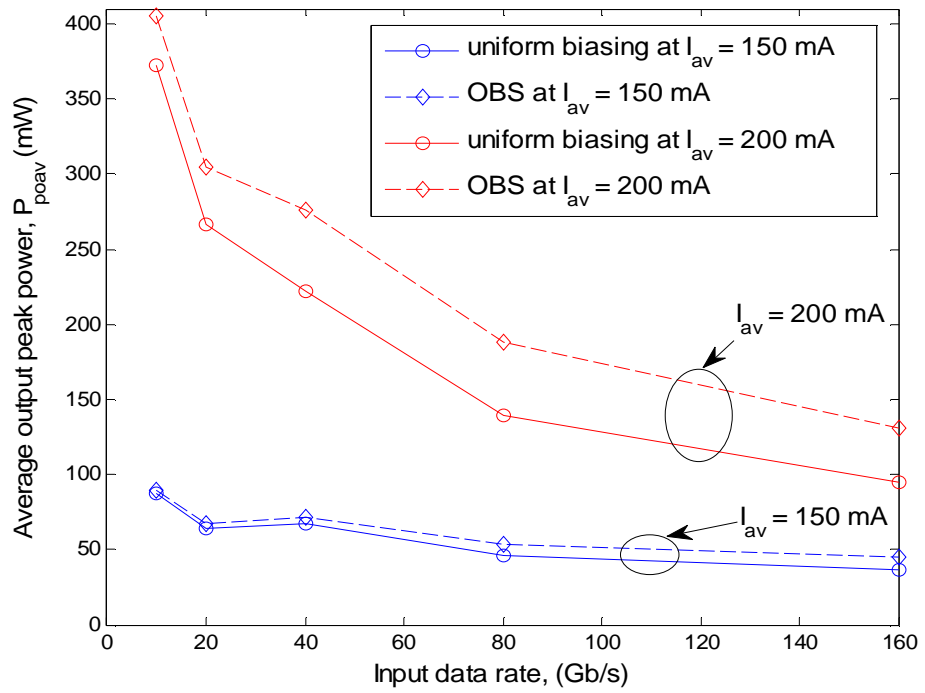
Figure 8.11 Comparison between the average output peak powers of a packet with random bit sequence when the SOA is biased by uniform and the OBS patterns at all data rates

Similarly to the input packet with all '1's bit sequence, the average output show higher powers when the SOA is biased by the OBS pattern at any input data rate and for I_{av} of 150 and 200 mA. P_{poav} also appear to have higher values at low input data rates and at higher I_{av} values as in Fig. 8.8.

123
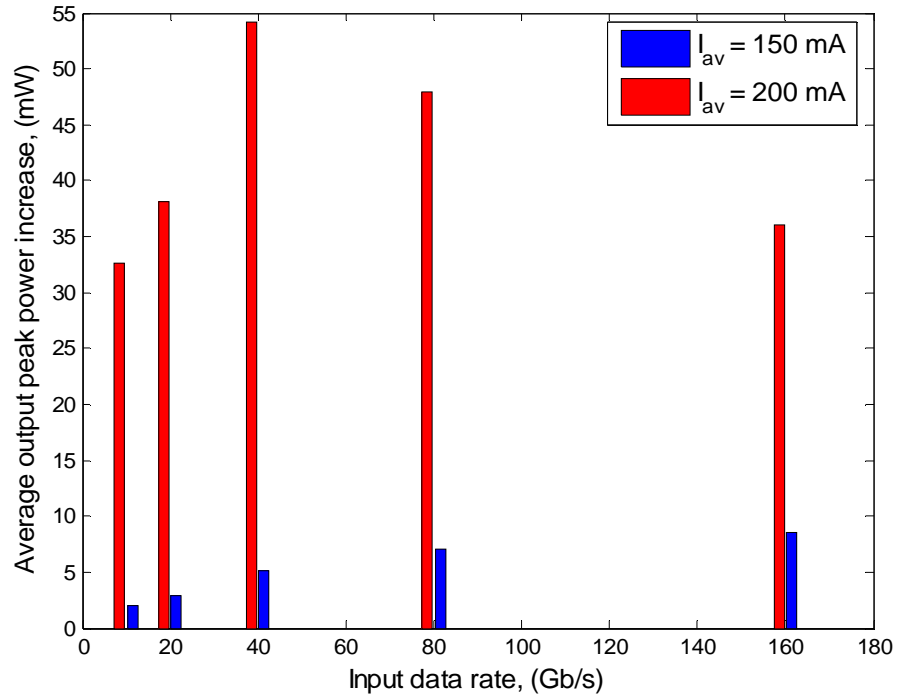
Figure 8.12 Average output peak power increase employing OBS pattern as a replacement of the uniform current for random bit sequence packet

In the same way, Fig. 8.12 depicts the improvement (i.e. increase) in the average output power of the random pulses using the OBS pattern. P_{poav} is increased by 2%, 4%, 8%, 15% and 23% at 150 mA I_{av} while at 200 mA, these improvements are 9%, 14%, 24%, 34% and 38% at 10, 20, 40, 80 and 160 mA, respectively. Results show that applying input packets with random sequence result in higher P_{poav} achievements compared to all '1's sequence at all input data rates (see Fig. 8.9).

8.8. Summary

This chapter proposed an optimised biasing for SOA (OBS) in order to maximise the SOA gain uniformity at high speed data rates. The proposed technique was able to overcome the constraints of the previous chapter regarding the high speed of the non-uniform current and the limited improvement at 40 Gb/s speed. The OBS pattern of only 1 ns time duration significantly improved the SOA gain uniformity at high speed data rates up to 160 Gb/s.

In this chapter, the carrier density and corresponding SOA gain uniformity dependence on the applied bias current are analysed. Accordingly, the current pattern for biasing the SOA was optimised in order to linearise the gain of the input pulses. An OBS equation to maximise the gain uniformity at any input data rate and for any number of pulses is also proposed.

The chapter compared the uniform bias current to the OBS pattern for the same input packet in order to highlight the advantages of employing the proposed technique. The SOA gain uniformity comparison confirmed the reduction in the gain standard deviation at all investigated data rates. In the case of using the OBS pattern, the average σ improvements are 8 and 16.9 dB for 150 and 200 mA I_{av}, respectively at all the data rates investigated.

This chapter also introduced another evaluation scheme, namely the average output power of the pulses P_{poav} between both biasing techniques. The OBS pattern offered higher power amplifications for the input pulses regardless of the packet bit rate or sequence. The average percentage increase in P_{poav} achieved at

all investigated data rates employing the proposed technique for all '1's bit sequence was 6% and 15% at 150 mA and 200 mA average biasing current, respectively. On the other hand, for the random bit sequence these average improvements were 11% and 24% for the 150 mA and 200 mA average currents, respectively. The boundaries of the proposed technique are studied regarding the maximum current limit that should be reached by the OBS pattern. Results showed that the average output power will improve employing the proposed OBS pattern regardless of the input bit sequence while the gain uniformity will either show improvement or remain unaffected.

In the following chapter, the OBS pattern is practically generated at 1 GHz. Different experimental developments of the OBS pattern are demonstrated in order to verify the improvements of the SOA gain uniformity.

Chapter 9 Experimental Implementation of Optimised Biasing for SOA (OBS) Pattern

9.1. Introduction

In this thesis, different techniques were proposed in chapters 6, 7 and 8 to improve the uniformity of the output pulses due to the propagation along the SOA at high data rates. In chapter 8, the OBS equation (8.24) was proposed and showed significant improvements to the SOA gain uniformity at all investigated data rates. Experimental demonstration is necessary to validate the improvement offered by the proposed OBS technique.

This chapter presents the laboratory experimental setup and the obtained results. All the experimental setup, from input optical pulses generation, SOA connections

to the biasing circuits are described. The proposed OBS pattern in the previous chapter is generated with 1 GHz repetition rate and is used to bias the SOA. The experiments executed at 10 and 20 Gb/s data rates for all '1's (the worst case scenario) and random bit sequences apply both uniform and the OBS patterns to bias the SOA. The output power standard deviation from the experiments are analysed in order to compare both biasing techniques. The chapter also discusses the factors that affected the practical achieved results.

9.2. Experimental Setup

After the simulation of the SOA and its applied bias current to improve the SOA gain uniformity, the corresponding experiment setup is implemented to verify the principle of the proposed technique. A general block diagram of the experimental setup is shown in Fig. 9.1. The experiment can be divided into three parts: generation of optical pulses, SOA-based Mach-Zehnder interferometer (SOA-MZI) connections and the biasing circuit. The following sections describe the equipments used, connections and the output signals of the experiment setup. These output signals are then analysed.
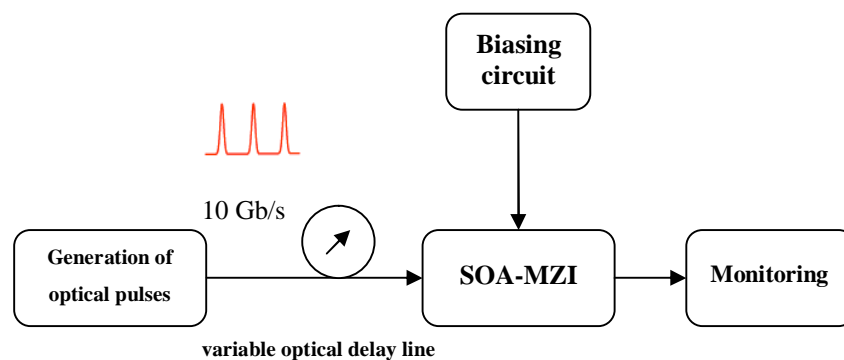
Figure 9.1 General block diagram of the experimental setup

The variable optical delay lines are used in order to synchronise the optical input pulses with the OBS pattern when they enter into the SOA-MZI active region. This synchronisation is explained later in Section 9.3. All the optical connections of the experiment use single mode fibre (SMF) patch cords that operate at 1550 nm. However, these patch cords are polarisation maintaining (PM) fibres and have high attenuation.

From Fig. 9.1, a SOA-MZI is used in the experimental setup in place of a single SOA due to the availability of such module in the laboratory. Consequently, there are few limitations in the experimental results that are discussed later in Section 9.3.

9.2.1. Generation of optical pulses

A block diagram for the generation of optical pulses setup is shown in Fig. 9.2. The input optical pulses are generated using an optical pulse source, Calmar Optcom picosecond pulsed fibre laser (PSL-101TNUU12). This optical pulse generator will be referred to as 'PSL' for the rest of this chapter. The PSL is a mode-locked fibre laser that generates a near Gaussian shaped optical pulse train with a pulse width < 2 ps at 10 GHz (specifically, 9.95328 GHz) repetition rate.
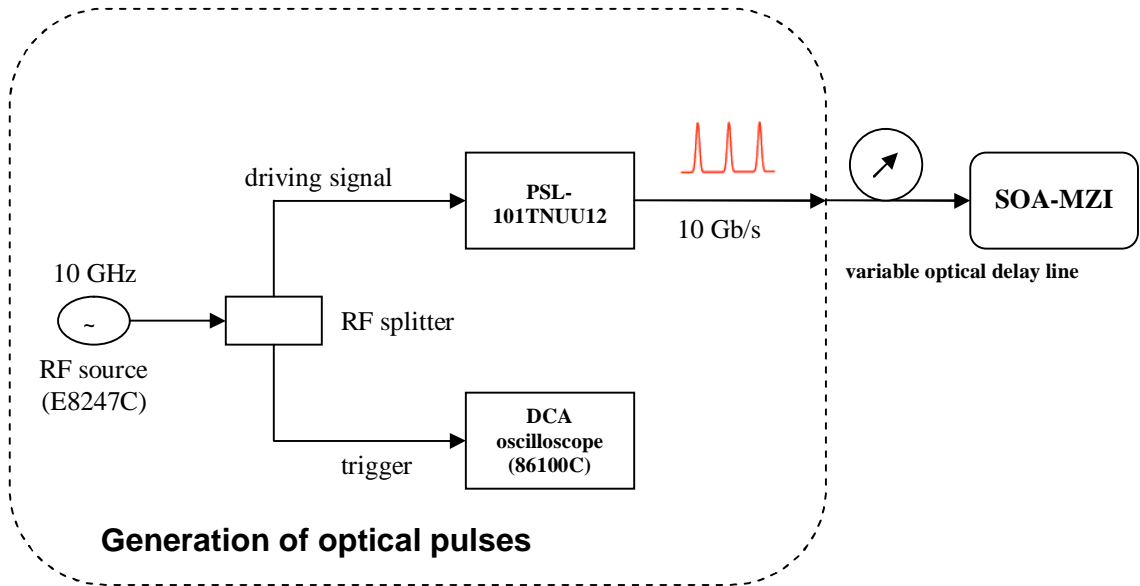
Figure 9.2 Block diagram of the generation of optical pulses setup

In order for the PSL to achieve a stable mode-locking (i.e. ensure a stable operation) at 1550 nm wavelength, three parameters must first be adjusted. These PSL mode-locked operating parameters are listed in Table 9-1.

1. **Pump current;** which is the current in the EDFA within the PSL that provides optical pump to excite the gain medium. Adjustment of the pump laser current changes the output power.

2. **Bias;** which is the electro-optic modulator that modulates the loss in the laser cavity. It is controlled by externally supplied bias voltage.

3. **Phase;** which controls the phase of the radio frequency (RF) drive in a phase locked loop circuit that fine-tunes the laser cavity length.

Table 9-1 PSL mode-locked operating parameters

Parameter	Value
Wavelength	1550.583 nm
Pump current	0.599 A
Bias	5.29 V
Phase	3.98 V

In order to initiate the PSL operation, an external RF source is required with a driving frequency between 9 and 13 GHz and a driving power level between -1 and 2 dBm. Therefore, the RF source used to drive the PSL is the Agilent Technologies (AT) PSG CW signal generator (E8247C). The frequency and power of the RF source are adjusted to 9.95328 GHz and 0 dBm, respectively.

A high speed 'DCA oscilloscope' (AT-86100C) is used to monitor the output optical pulses from the PSL that will then propagate through the variable optical delay line to the SOA-MZI. In order to monitor these high speed optical pulses, the DCA requires a synchronised RF trigger. Therefore, the RF source output signal is split into two parts using a RF splitter: one used as a driver to the PSL and the other as a trigger to the DCA.
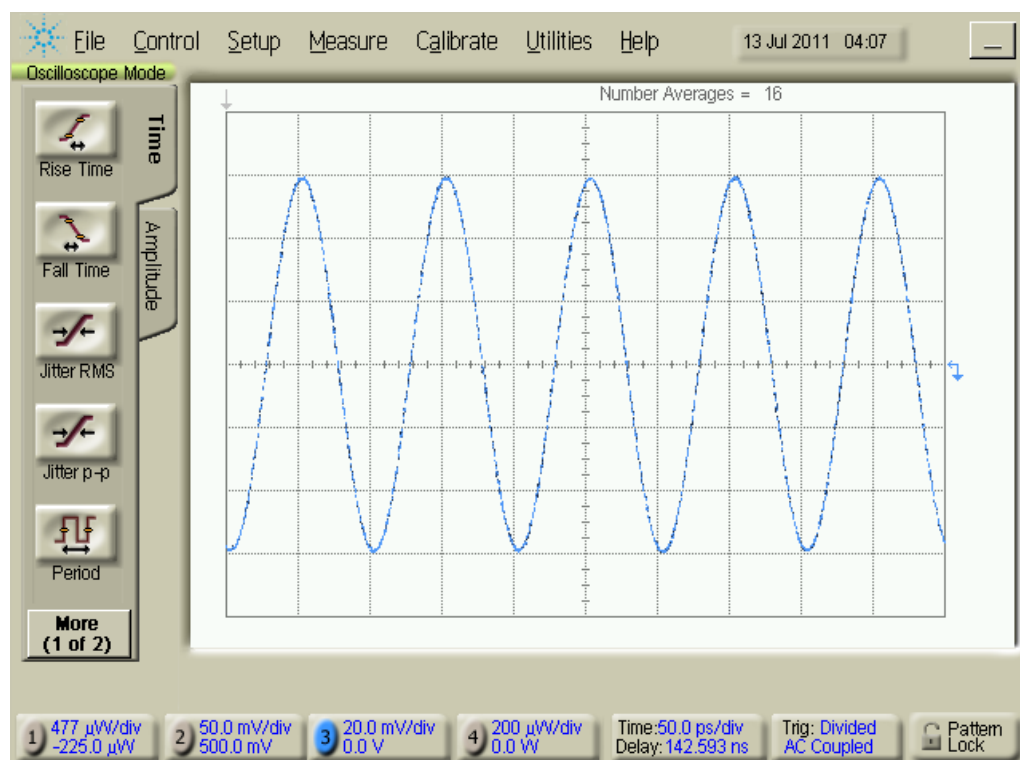
Figure 9.3 RF signal used to drive the PSL and trigger the DCA oscilloscope
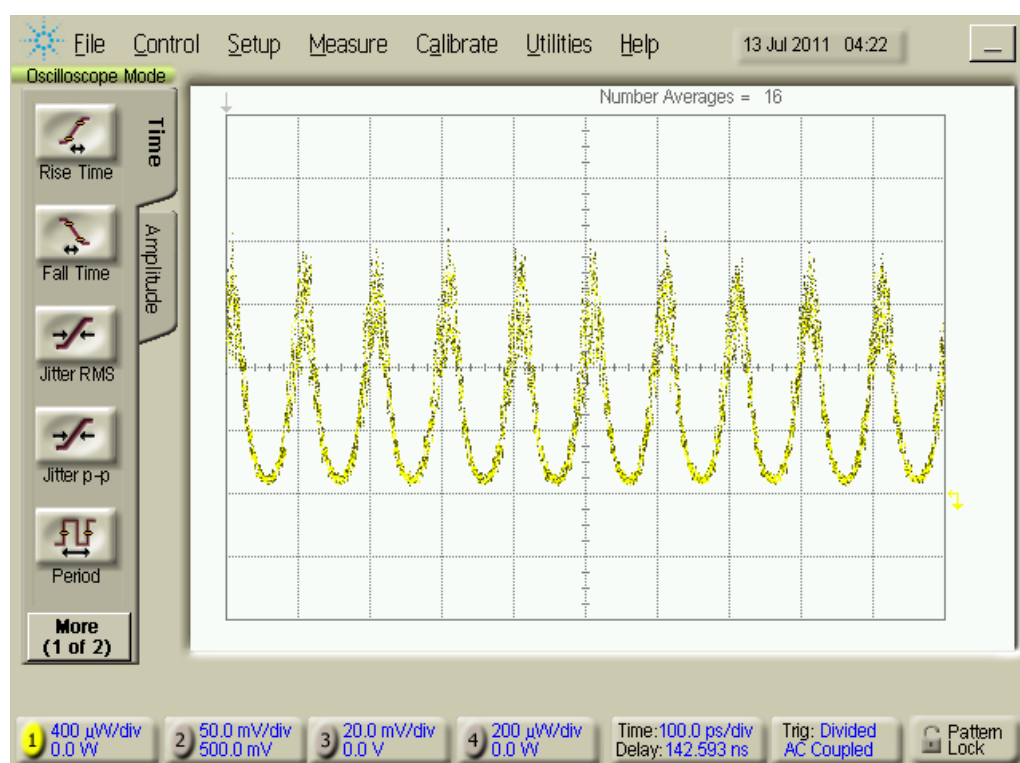
Figure 9.4 PSL generated output optical pulse train

The 10 GHz sinusoidal RF signal used to drive the PSL is shown in Fig. 9.3, while the PSL output optical pulse train with 10 GHz repetition rate (i.e. 100 ps separation) is displayed in Fig. 9.4. The adjusted wavelength of these generated optical pulses is monitored using the optical spectrum analyser (AT-86146B).

9.2.2. SOA-MZI connections

Due to the available resources in the laboratory, the experimental demonstration uses a SOA-MZI (Quad 40 Gb/s 2R Optical Regenerator) made by The Centre of Integrated Photonics (CIP) Technologies. The optical module is a hybrid integrated device consisting of four planar silica MZIs with two quad arrays of non-linear SOAs in the interferometer arms. The module includes Peltier and thermistor electrical pins for temperature control due to the high rise in temperature during operation. The SOA-MZI also contains other electrical pins for SOA bias currents and phase shifters. The independent thermo-optic phase shifters are incorporated to allow precise phase control of the interferometers. However, these phase shifters result in dramatic increase in the module temperature and requires additional cooling system. For that reason, in this experiment, the phase shifter pins are not connected. The input and output optical pulses are fed to and from the SOA-MZI via optical fibres.

For stable performance, the operating temperature of the SOA-MZI should be 25°C. In order to control the temperature, the resistance between the electrical thermistor pins is maintained 10 kΩ by adjusting the voltage across the Peltier

pins. This is achieved using the thermoelectric temperature controller (Thorlabs TED200C).

In the laboratory, for this experimental setup, a box was specially designed to house the SOA-MZI module for easier access to the connections from the top of the box and in order to avoid electrostatic contact or damage. A picture of the SOA-MZI module inside the designed box can be seen in Fig. 9.5. The schematic diagram of the SOA-MZI part of the experiment is illustrated in Fig. 9.6.
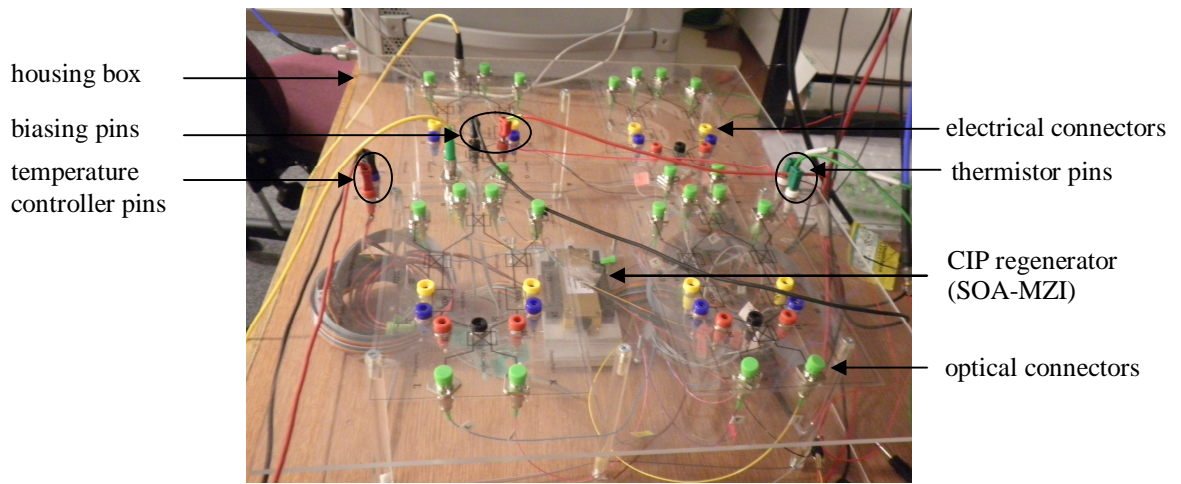
Figure 9.5 SOA-MZI module within the designed box

Although each SOA-MZI module contains two identical SOAs (one in each interferometer arm as shown in Fig. 9.6), this practical experiment is setup to compare the gain uniformity of the output pulses of a single SOA when biased with uniform and the OBS patterns. For that reason, only one SOA device within the module is biased (i.e. operating).

134
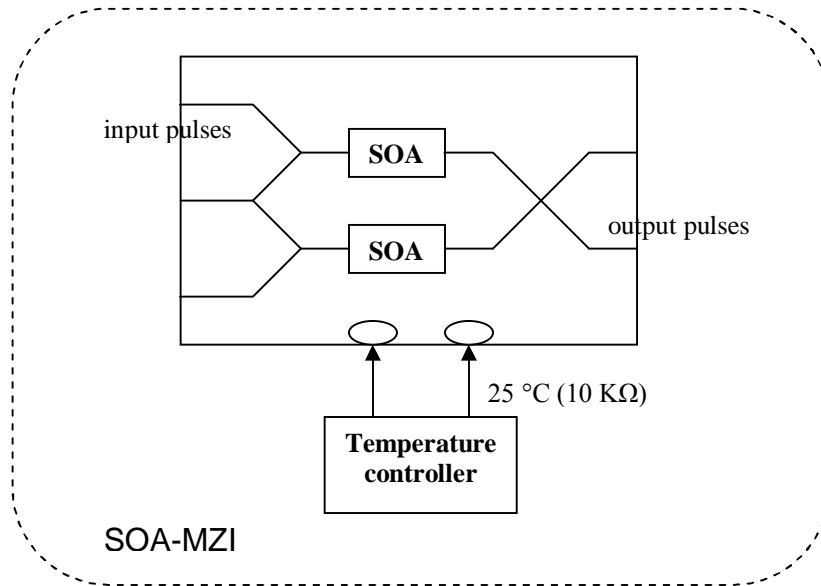
Figure 9.6 Schematic diagram of the SOA-MZI setup

9.2.3.   SOA-MZI biasing circuits

This section presents the different approaches used to practically bias the SOA. Comparing the output results that are obtained by applying these different bias currents on the same experimental demonstration is the main aim of this chapter.

9.2.3.1   Uniform pattern

Since this experiment focuses on the differences between the biasing methods, it is necessary to apply a stable current source for biasing the SOA using Thorlabs 'multi laser controller module' (MLC8200CG). This biasing current source will be referred to as 'MLC' for the rest of this chapter. The block diagram for the uniform biasing setup is displayed in Fig. 9.7. In order for the MLC module to operate, it is biased with 5 V and -5 V using two power supplies as shown in Fig. 9.7. The MLC

will bias the SOA with a stable 150 mA electrical bias current as in the simulation in the previous Chapters.
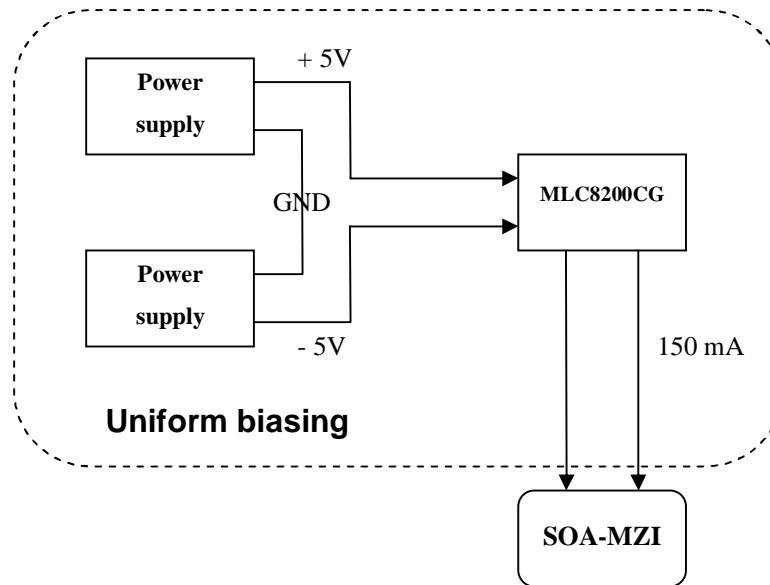
Figure 9.7 Block diagram of the uniform biasing setup

9.2.3.2 OBS pattern

The aim of this section is to practically generate OBS pattern depicted in Fig. 8.3 (for 10 Gb/s inputs) and bias the SOA. However, producing such signal is challenging at the desired 1 GHz repetition rate. An electronic circuit is designed in order to help achieving the required signal. This section introduces the proposed method to achieve OBS pattern and its demonstration.

The OBS pattern that varies between 148.5 and 151.5 mA (i.e. 3 mA) within 1 ns in Fig. 8.3 can be divided into two signals: a uniform current of 150 mA and a non-uniform current fluctuating from −1.5 to 1.5 mA (see Section 8.2). The setup

136

presented in the previous section (see Fig. 9.7) to bias the SOA with uniform 150 mA is used for providing the uniform part of the desired biasing pattern.

On the other hand, in order to produce the non-uniform part, a square wave signal with 1 GHz repetition rate (specifically 1.0625 GHz) generated from AT 'serial bit error rate tester (BERT N4906B)' is used. The block diagram of the OBS setup is depicted in Fig. 9.8. To monitor these high speed signals via the DCA oscilloscope, RF splitter is used to trigger the DCA with a synchronised signal from the BERT. The output square wave from the BERT is displayed in Fig. 9.9. Although the practical signal generated in Fig. 9.9 is not a pure square shape (due to input impedance mismatch between the BERT and the DCA), the output signal from the electronic circuit illustrated in Fig. 9.10 shows a non-uniform pattern as required.

The voltage of the square wave from the BERT is tuned so that the non-uniform current pattern oscillate from -1.5 to 1.5 mA to match the simulated OBS pattern in Fig. 8.3 when added to the uniform 150 mA. It can be seen From Fig. 9.10 that the amplitude of the signal is presented in 2 division where the DCA channel has a 50 Ω resistance and is adjusted to 75 mV/division. The conversion of the available square wave at such high speed in the laboratory (i.e. 1 GHz) to the desired pattern is achieved by the electronic circuit. This circuit consists of a diode to operate only in the positive part of the square wave, 15 pF capacitor, 1 kΩ and 22 Ω resistors.

From Fig. 9.10, one can see that the generated non-uniform current pattern decays within 50% from the entire 1 ns signal duration which is the main difference to the simulated signal illustrated in Fig. 8.3 that makes an impact on the obtained results and will be discussed in Chapter 9.3.6. Practically, generating the desired signal with an instantaneous drop is complex because a synchronised high speed switch is required to allow the capacitor to discharge to a different resistor.

The output non-uniform signal from the electronic circuit is then added to the 150 mA current using a 'bias-T' component to produce the desired OBS pattern.
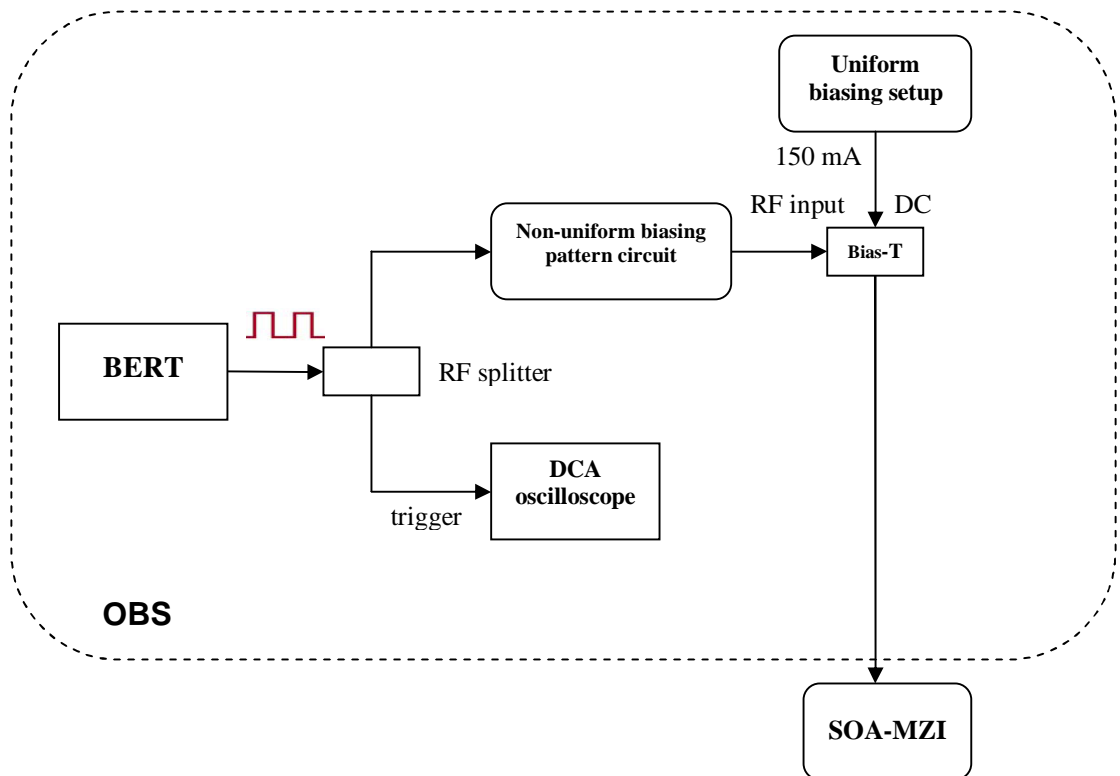
Figure 9.8 Block diagram of the OBS setup
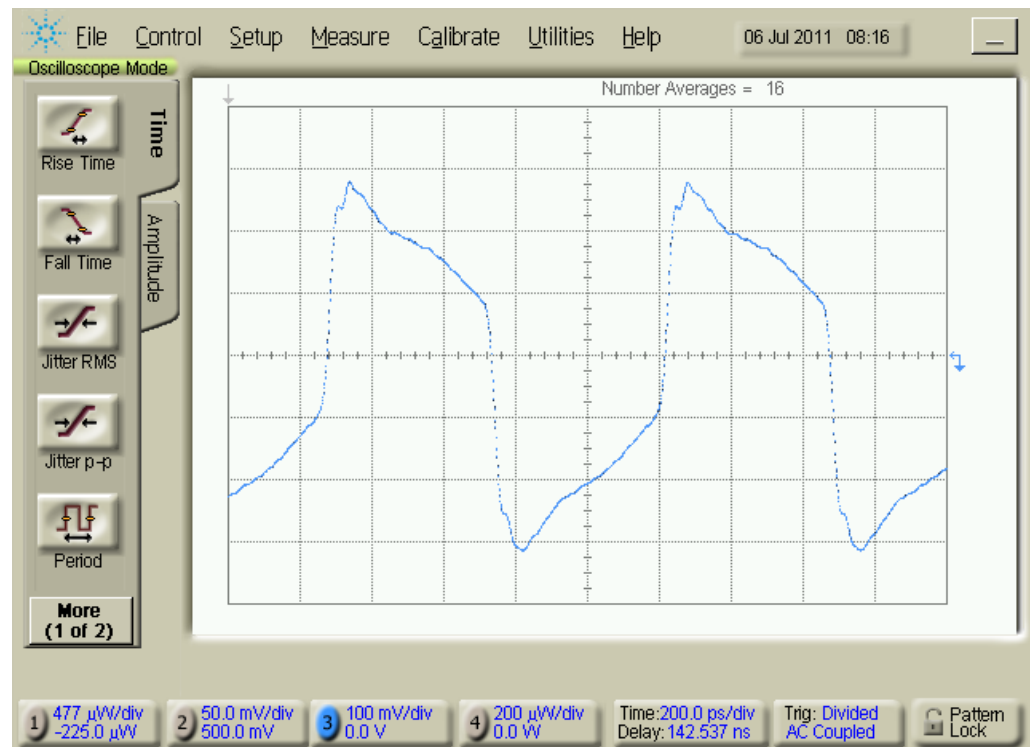
Figure 9.9 Generated square wave from the BERT
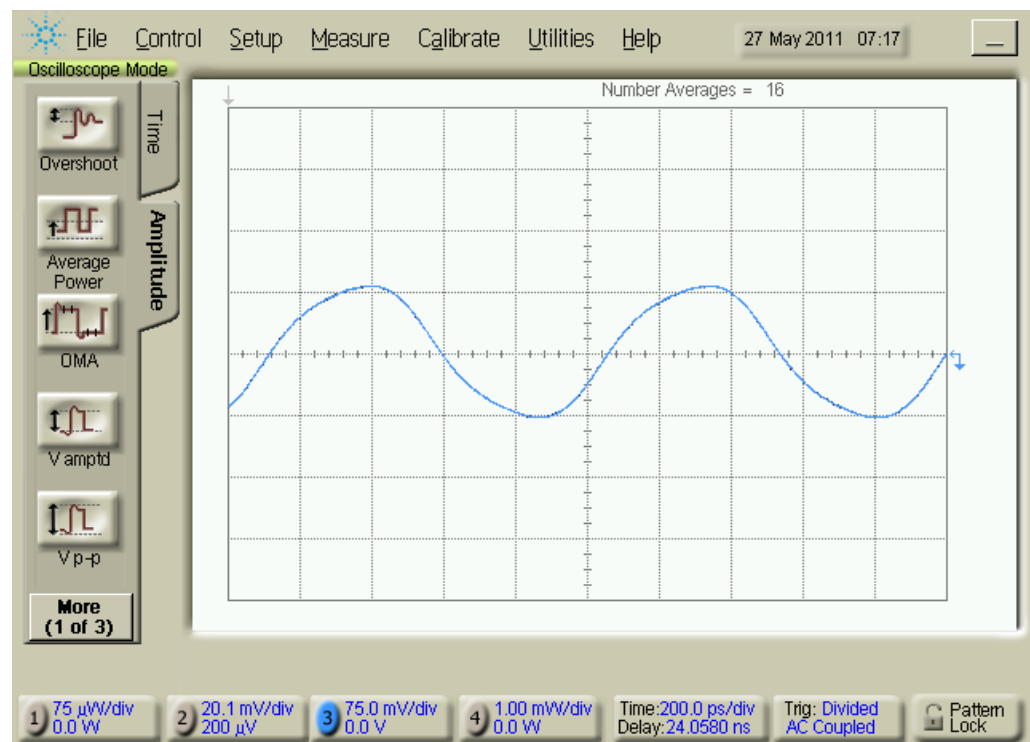
Figure 9.10 The non-uniform bias current added to the 150 mA to form the OBS pattern at 10 Gb/s input data rate

139

9.3. Experimental Measurements and Results

This section presents the practical experiments executed in the laboratory. All the experiments are connected according to the basic setup shown in the block diagram in Fig. 9.1. Any changes to the experiment setup will be discussed in the corresponding section. For each experiment, the SOA is first biased using the uniform 150 mA current while the variable optical delay line is adjusted to zero delay and the output signals are measured. The 1 GHz non-uniform signal is then added to the uniform current to form the OBS pattern. Synchronisation between the input pulses and OBS pattern is necessary to obtain the optimised output gain uniformity. This is achieved by manually adjusting the variable optical delay line which is tuned from zero delay and increased by a step of 5 ps. All the output data obtained from biasing the SOA with both uniform and OBS patterns are analysed and the output power standard deviation are calculated.

In this section, the standard deviation of the output power replaces the gain in equation (6.1) for calculating the uniformity of the output pulses due to the severe loss achieved by the input pulses instead of amplification as explained later.

9.3.1. Experiment 1: Comparing biasing techniques at 10 Gb/s

This section displays the results obtained from executing the first experiment where the input data are launched to the SOA with all '1's bit sequence (that presents the worst case scenario for SOA gain depletion) at 10 Gb/s. After the propagation of the input pulses through the uniform biased SOA, the output pulses are monitored via the DCA oscilloscope and displayed in Fig. 9.11.

140
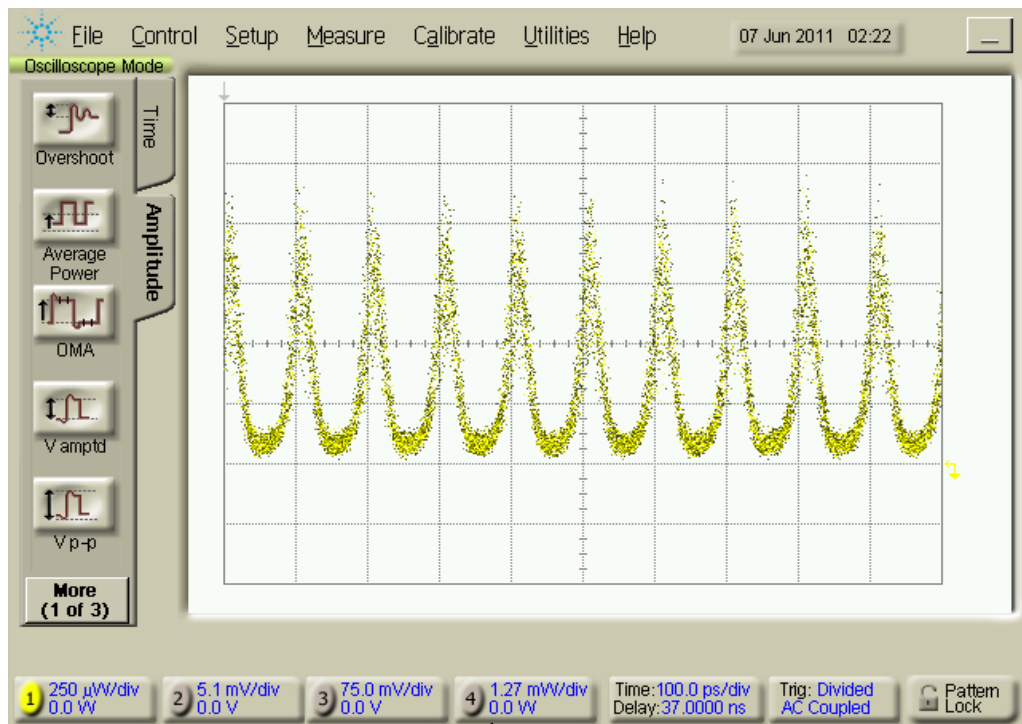
(a)
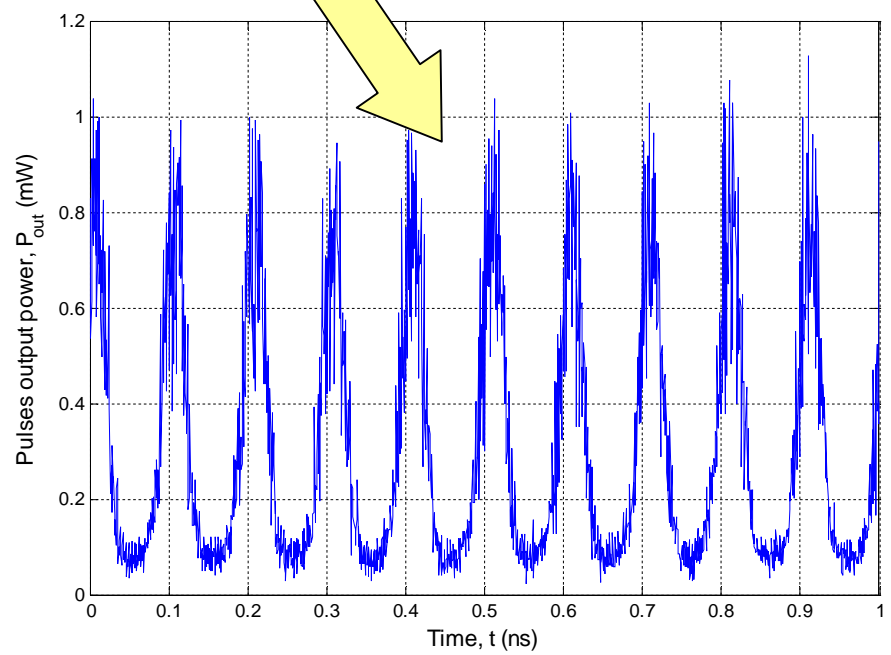
(b)

Figure 9. 11 Pulses output power employing uniform bias current at 10 Gb/s (a) from the DCA and (b) from the Matlab illustration

A frame of 10 pulses (in case of 10 Gb/s data rate) with 1 ns duration is considered as in the previous chapter. The peak power of the pulses from PSL is 25 mW each. The output pulses from the DCA and illustrated using Matlab^{TM} are shown in Figs. 9.11 (a) and (b), respectively. The results show a dramatic attenuation experienced by the input signals (generated from the PSL) in the experimental setup. Unlike theoretical simulations that investigated the SOA as a single unit, there are some factors in the experimental demonstration that result in the high power attenuations. The external connections to the SOA were not taken into account in simulation however; all these connections introduce power losses and have impact on practical output pulses. Consequently, these pulses suffer from power losses due to the repeated attenuations along the way. These losses are as a result of the optical connectors, fibres insertion losses, attenuations by the optical PM fibres and the variable optical delay line.

Using the SOA-MZI module instead of a single SOA device has caused additional attenuations to the power of the output pulses. The configuration of the optical regenerator module is the major reason for the severe power losses experienced by the input optical pulses. These pulses are launched to the symmetric SOA-MZI (SMZ) structure and propagate through optical couplers with 3 dB splitting ratios. The SMZ operation includes biasing both identical SOAs and therefore, the splitted signals from both branches interfere either constructively or destructively. However, due to biasing a single SOA in these experimental setups, the splitted signals from each coupler are lost. The SOA also introduces input and output coupling and excess losses. Moreover, the phase shifter pins that are responsible

142

for maximising the power of the pulses at the desired output port are not connected to avoid the temperature increase of the SOA-MZI module. As a result, a portion of the input pulses power propagates through the undesired output port. The experimental power losses experienced by the propagating pulses are summarised in Table 9-2 which includes the losses of the bit rate multiplier (BRM) that is used in Section 9.3.3.

Table 9-2 Experimental power losses

Parameter	Loss (dB)
1 m PM fibre attached to an optical connector	14
Maximum PM fibre insertion loss	1
Each SOA-MZI coupler	3
SOA input/output coupling loss	0.79/1.24
SOA input/output excess loss	0.7/2.4
Bit rate multiplier (BRM)	2.5

The output pulses are also affected by the amplified spontaneous emission (ASE) noise which is the noise that has been optically amplified in the SOA gain medium by the process of spontaneous emission. The ASE noise shows higher effects on the propagating signals when biased with high bias currents. However, in this experiment, average bias currents are applied to the SOA is fixed at 150 mA, therefore the impact of the ASE noise is the same in all cases.

As a result of these high attenuations, Fig. 9.11 shows that the peak powers of the output pulses are around 1 mW. The output pulses are then interpreted and the

143

uniformity of these 10 pulses is calculated using the output power standard deviation equation. The standard deviation of the output powers appears to be 54.38 µW that corresponds to -42.65 dB. In order to minimise the fluctuations on the output pulses power resulting from the ASE noise, hence the output uniformity results, the averaging feature in the DCA oscilloscope is used on the monitored signals. Consequently, the output pulses monitored in Fig. 9.11 after using the averaging feature of the DCA is re-illustrated in Fig. 9.12.
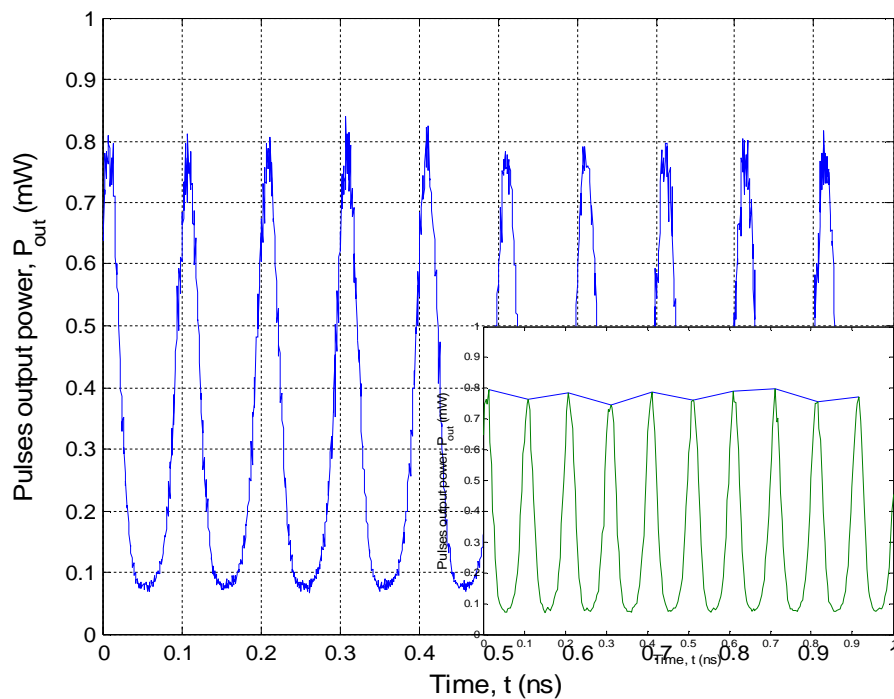
Figure 9.12 Pulses output power employing uniform bias current at 10 Gb/s using DCA averaging feature and (inset) interpolated signal.

From Fig. 9.12, it can be seen that the monitored output pulses are clearer (compared to Fig. 9.11) with minimum fluctuation. The attenuation throughout the experiment is more obvious in Fig. 9.12 where the pulses output peak powers are

144

shown around 0.8 mW. For that reason, for the rest of this chapter all the results shown will use the averaging feature of the DCA oscilloscope. Therefore, the output power uniformity of the pulses is calculated again using the averaged measurements to give 15.98 μW deviations (-47.96 dB). The interpolated output pulses are depicted in the inset of Fig. 9.12 showing the output peak powers envelope in order to highlight its non-uniform shape.

The proposed OBS pattern is then applied and is best synchronised with the input pulses using the adjustable variable optical delay line.
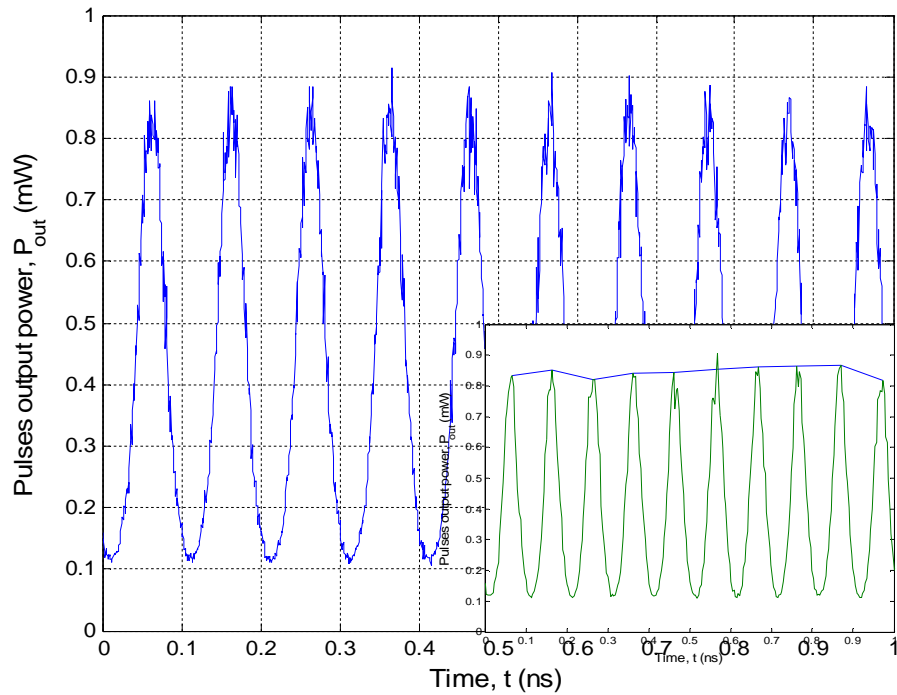
Figure 9.13 Pulses output power employing synchronised OBS pattern at 10 Gb/s and (inset) interpolated signal

The corresponding powers of the output pulses are depicted in Fig. 9.13 while the interpolated output pulses are plotted in the inset of the figure to show the more

145

uniform envelope response. Employing the proposed OBS pattern, a 3% drop in the output gain standard deviation (compared to uniform biasing) is achieved with a -63.85 dB improvement in the output power uniformity.

In order to further evaluate the proposed OBS pattern corresponding to the previous chapter, the average output peak powers (i.e. P_{poav}) for both biasing techniques were measured. These measurements show that replacing the uniform current with the OBS pattern results in 78 µW increase in P_{poav} (10% improvement). These outcomes justify the simulated results in the previous chapter and verify the validity of proposed OBS pattern to improve the output uniformity of the SOA and the average output powers.

9.3.2.   Experiment 2: Comparing biasing techniques at 10 Gb/s with EDFA amplification

Due to the continuous attenuation of the optical pulses along all connections and the SOA-MZI module, in this section, another experiment is performed where an erbium doped fibre amplifier (EDFA) is added to the Experiment 1 setup. The block diagram for this experiment in Fig. 9.14 shows the position of the EDFA used to amplify the output pulses from the SOA-MZI to ~ 1 mW.

The same input pulses used in the Experiment 1 are launched to the SOA-MZI module. The output pulses are monitored after being amplified by the EDFA in Figs. 9.15 and 9.16 when the SOA is biased by the uniform and the OBS patterns, respectively. Similarly, a frame of 10 pulses within 1 ns is measured and analysed.

From Fig. 9.15, it can be seen that the output pulses from the uniform biased SOA are amplified to reach ~ 1 mW with P_{poav} of 0.97 mW.
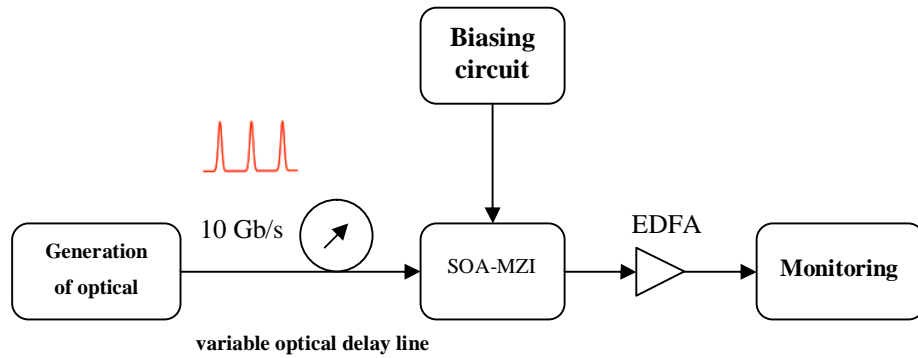
Figure 9.14 Block diagram of experimental setup 2
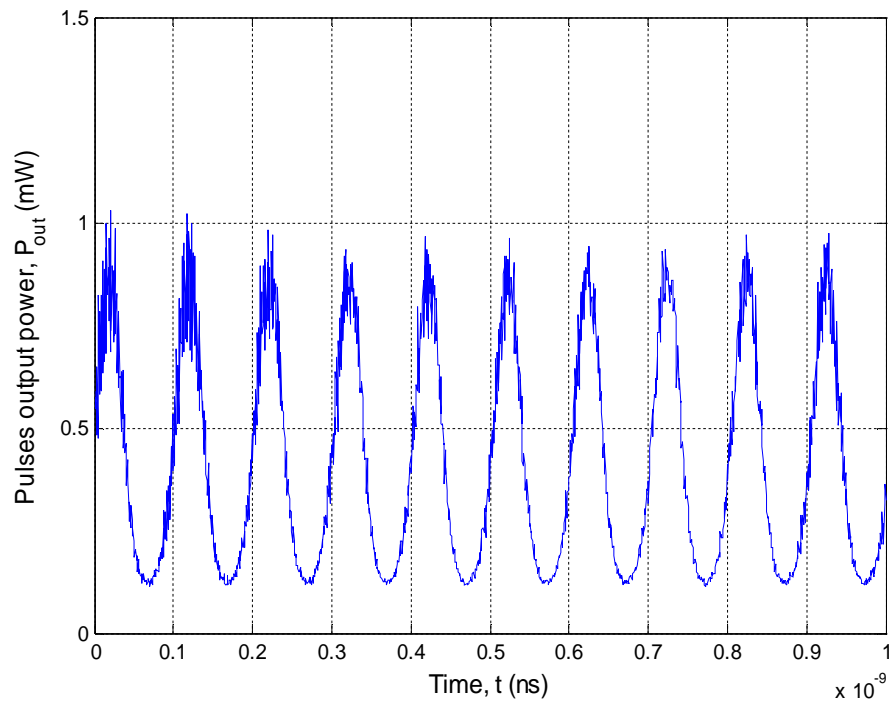
Figure 9.15 Amplified pulses output power employing uniform bias current at 10 Gb/s
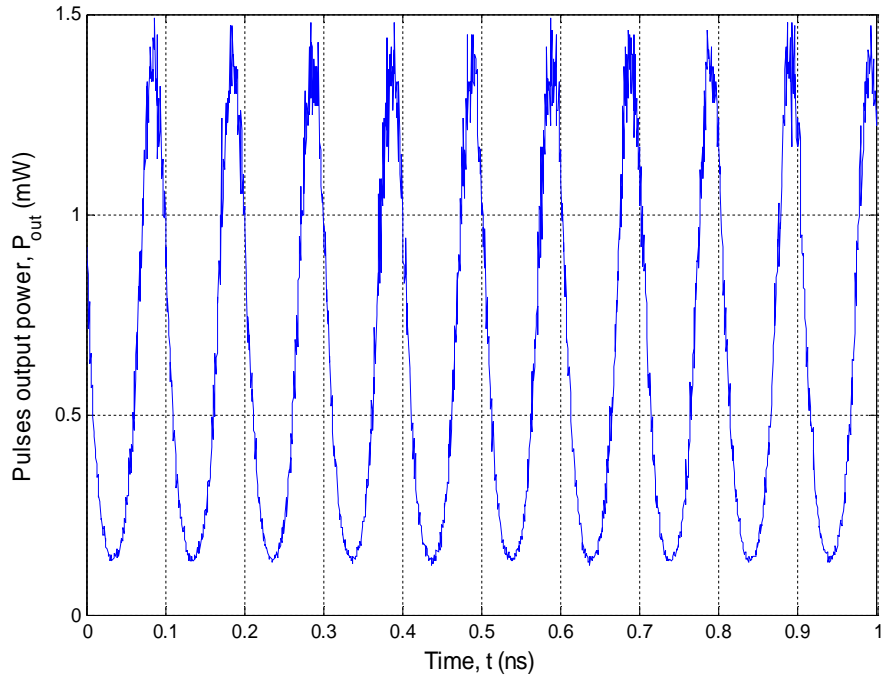
Figure 9.16 Amplified pulses output power employing OBS pattern at 10 Gb/s

Comparing the peak powers from Figs. 9.15 and 9.16, one can observe that the output pulses are more uniform and achieve higher average power level in case of using the OBS pattern. The proposed technique shows significant improvements which result in a reduction of -47.36 dB in σ (59% improvement) is achieved while P_{poav} is increased by 54% (i.e. 0.53 mW) to reach 1.5 mW.

9.3.3. Experiment 3: Comparing biasing techniques at 20 Gb/s with EDFA amplification

After the previous experiments verified the ability to improve the SOA output uniformity by employing the OBS pattern at 10 Gb/s, it was important to further carry out the practical investigation to higher input data rates. In this experiment, a

20 Gb/s frame with all '1's bit sequence pulses is generated the Calmar Optcom optical 'bit rate multiplier (BRM)' (BRN-T16).

The block diagram of this experimental setup illustrated in Fig. 9.17 is similar to the Experiment 2 with the addition of the BRM. However, the required OBS pattern for the 20 Gb/s frame will correspond to the simulated result in Fig. 8.4 (a). For that reason, the non-uniform current that varies from -3 to 3 mA shown in Fig. 9.18 is added to the uniform 150 mA to form the OBS pattern.
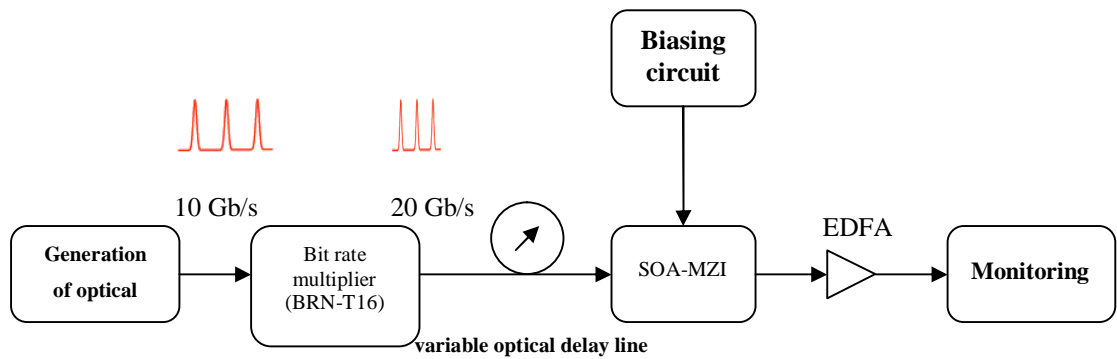
Figure 9.17 Block diagram of experimental setup 3
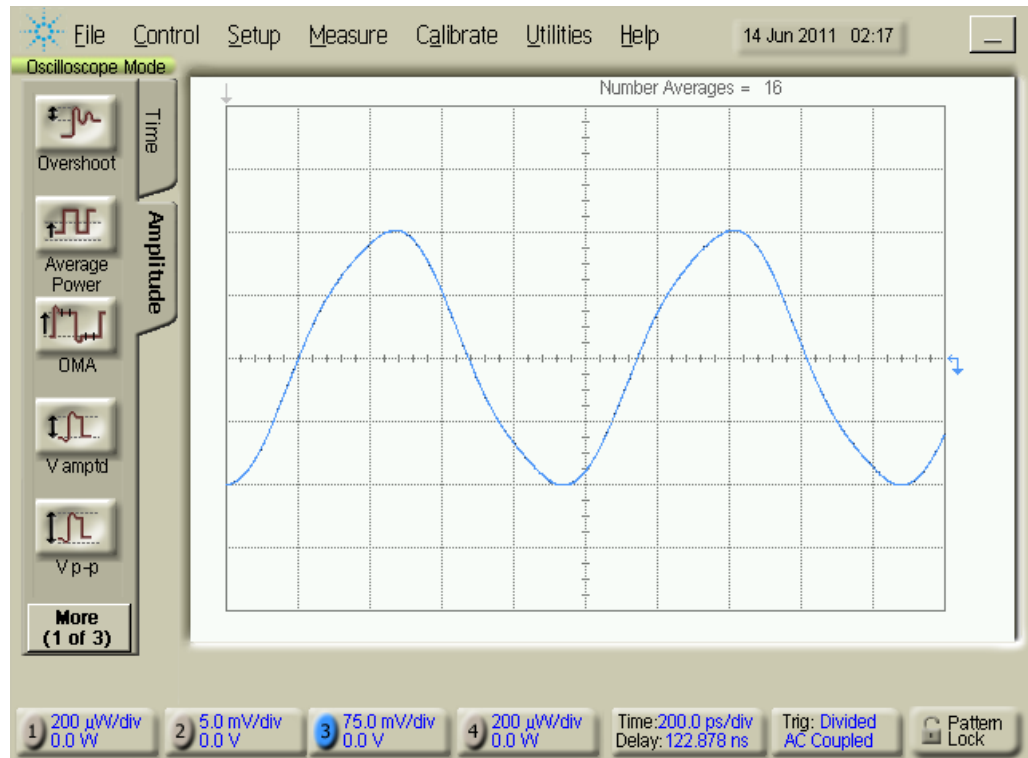
Figure 9.18 The non-uniform bias current added to the 150 mA to form the OBS pattern at 20 Gb/s input data rate

The BRM is a passive device that splits the input pulses into two identical images. One of these images is delayed and equalised manually in order to achieve twice the repetition rate with similar amplitudes. Consequently, the BRM results in 2.5 dB additional power loss to the input signals (see Table 9-2). For that reason, the EDFA pumping current in this experiment is adjusted to a higher level compared to Experiment 2 for the 20 Gb/s pulses to reach the same 1 mW peak powers at the output. Similar frame duration of 1 ns is measured where the 20 Gb/s frame contains 20 pulses (same as the simulation). These output pulses resulted from the uniform and OBS approaches are plotted in Figs. 9.19 and 9.20, respectively.

The comparison between the outcomes from both biasing techniques once again shows better results at a higher data rate using OBS pattern. The SOA output power uniformity is improved by 16% (i.e. σ is reduced -54.8 dB) with an increase of 21.85 µW in P_{poav} which corresponds to 2% improvement.
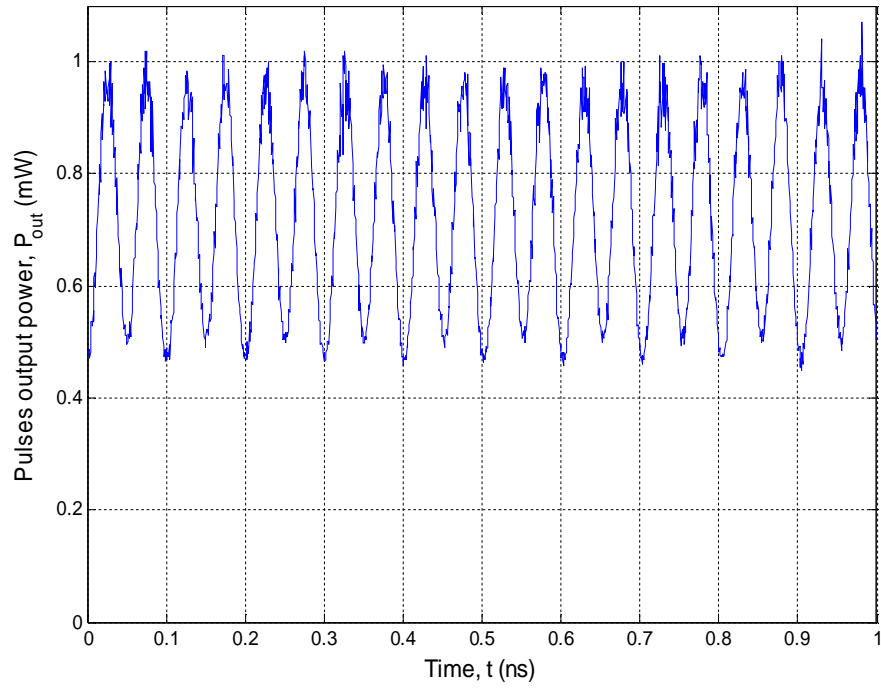
Figure 9. 19 Amplified pulses output power employing uniform bias current at 20 Gb/s
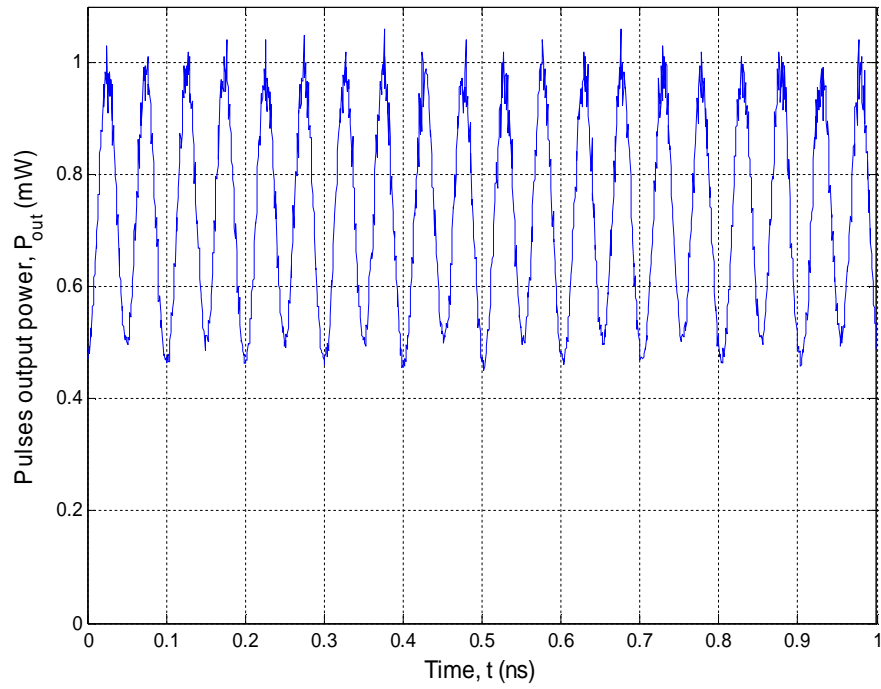
Figure 9.20 Amplified pulses output power employing OBS pattern at 20 Gb/s

9.3.4. Experiment 4: Comparing biasing techniques for the same random bit pattern used for simulated results

This experiment further examines the ability of the proposed biasing technique to improve the output results compared to the uniform biasing when a random input pulses are launched to the SOA. According to the PSL manual of operation, an RF sinusoidal wave is necessary to drive it. For that reason, when the BERT provided a random bit sequence to drive the PSL, the 'zero' bits showed certain peak powers. This PSL limitation will impact the practical output results.

In this section, a setup similar to Experiment 1 (i.e. at 10 Gb/s with no EDFA amplification) is implemented but with random input pulses sequence as in

simulation. The bit sequence used in this experiment is '1011011101'. Similarly to Experiments 1 and 2, the non-uniform current used is the pattern shown in Fig. 9.10. These output pulses are displayed in Fig. 9.21 where the SOA is uniformly biased while the output pulses corresponding to the OBS approach is depicted in Fig. 9.22.
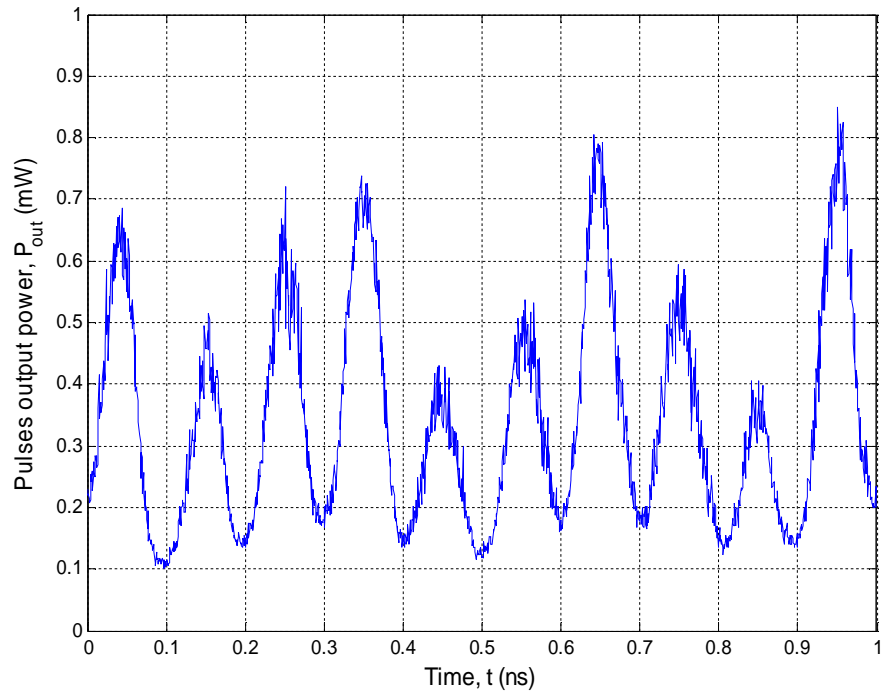
Figure 9.21 Pulses output power employing uniform bias current at 10 Gb/s for random bit sequence
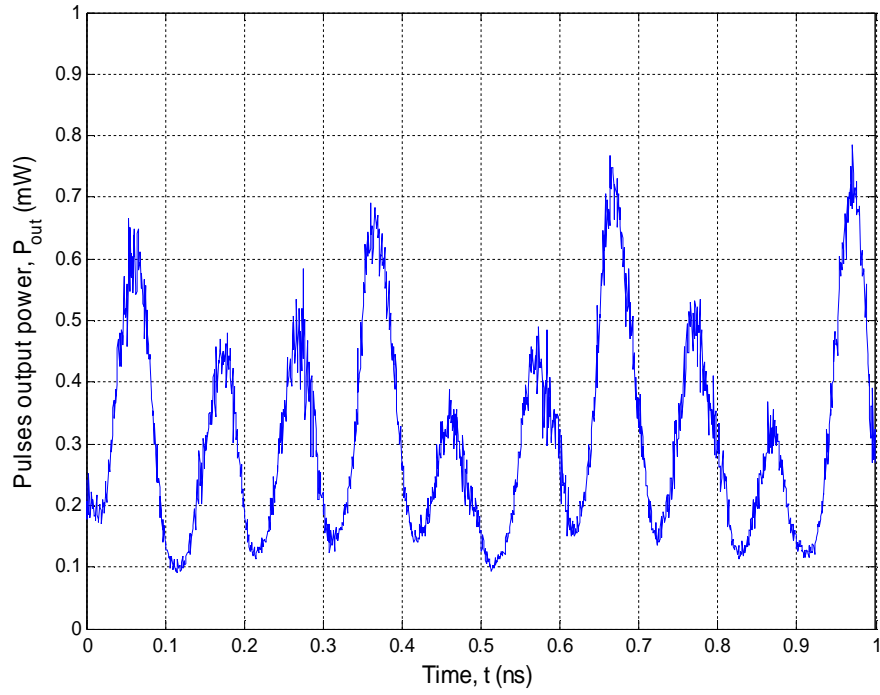
Figure 9.22 Pulses output power employing OBS pattern at 10 Gb/s for random bit sequence

In the simulation results there is no improvement in σ for OBS pattern at 10 Gb/s while there is a 2% increase in the average output power. The practical results however, achieved -45.92 dB (8%) improvement in σ with 41.4 µW reduction (i.e. 8% decrease) in P_{poav}.

At low output powers resulted from the severe power losses along the experimental demonstration, the uniformity of the output pulses is more perturbed due to the ASE noise. For that reason, applying the proposed OBS pattern has practically improved the power uniformity of the output pulses. On the other hand, the drop in P_{poav} that contradicts the simulation results is mainly caused by the PSL limitation in generating random sequences.

9.3.5. Experiment 5: Comparing biasing techniques for a different random bit pattern used for simulated results

In order to verify the random bit sequence practical results, Experiment 4 is repeated in this section with a different input sequence. The random sequence '1101110011' is launched to the SOA in this experiment. The corresponding output frames when the SOA is biased with the uniform and OBS patterns are displayed in Figs. 9.23 and 9.24, respectively.

The improved output uniformity and the reduction in P_{poav} of the random output pulses achieved in this experiment support the findings in Experiment 4. However, due to a more distinct random sequence (between '1's and 'zero's), compared to the random sequence used in Experiment 4, the proposed OBS pattern showed better σ reduction of -44.8 dB (10% improvement). However the P_{poav} reduced by 51.1 µW (i.e. 10% due to the PSL limitation).
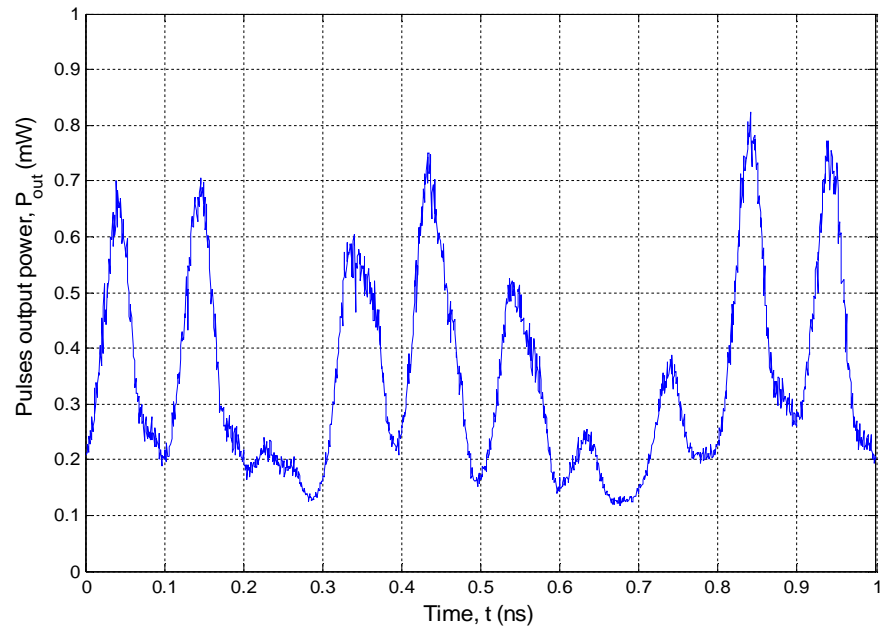
Figure 9.23 Pulses output power employing uniform bias current at 10 Gb/s for a different random bit sequence
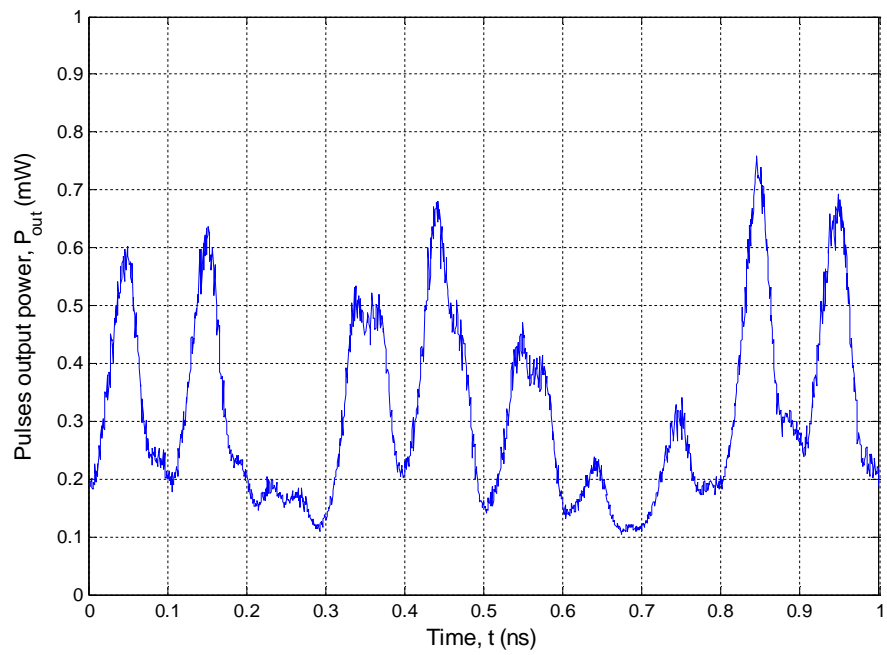
Figure 9.24 Pulses output power employing OBS pattern at 10 Gb/s for a different random bit sequence

9.3.6.   Summarised results

Overall, five different practical experiments are carried out in the laboratory and discussed in this chapter. A picture for the practical setup is displayed in Fig. 9.25. This section summarises the outcomes of all these experiments and highlights the achievements. Each experiment is executed with different variables and conditions and it is important to compare the practical results with the theoretical simulation.
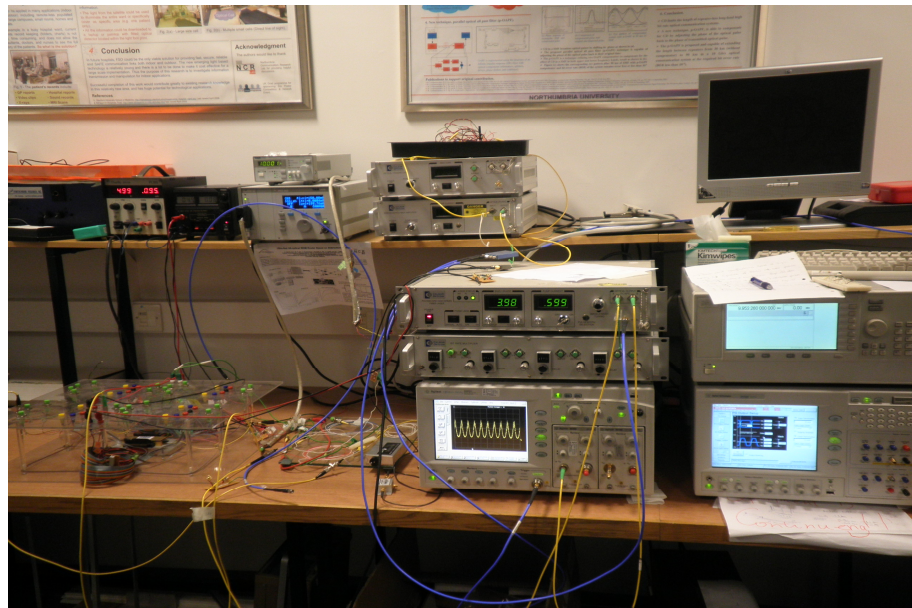
Figure 9.25 Output power standard deviation when the SOA is biased by uniform and the OBS patterns for all executed experiments

Figure 9.26 depicts the summary of the measured σ for all the five experiments using uniform and OBS patterns. The figure shows that the output pulses of all experiments achieved better power uniformity by applying OBS pattern compared to the uniform current.
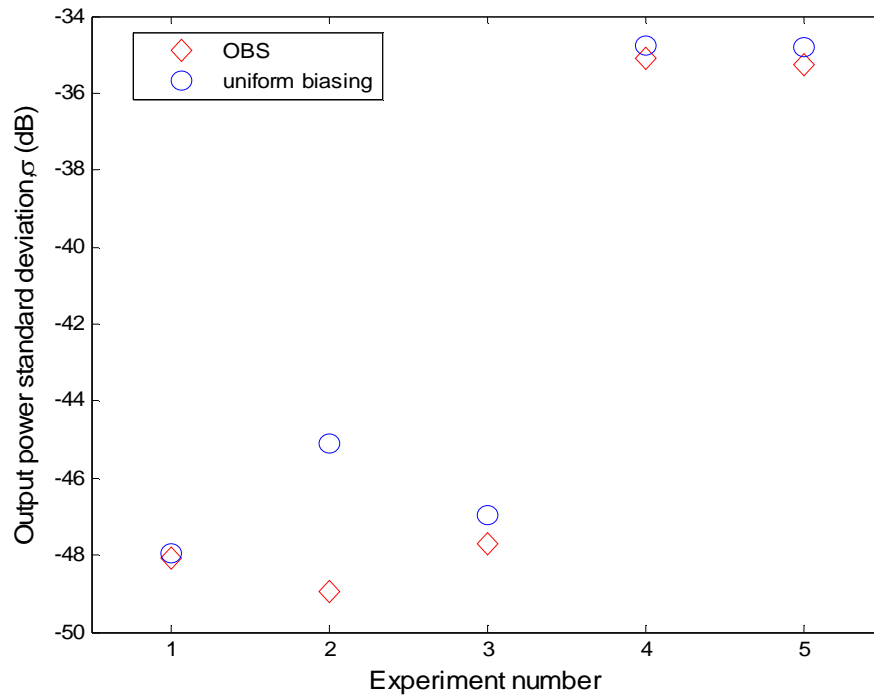
Figure 9.26 Output power standard deviation when the SOA is biased by uniform and the OBS patterns for all executed experiments

One can also observe from Fig. 9.26 that σ has higher values (i.e. > -36 dB) in Experiments 4 and 5 for both biasing approaches compared to all other experiments which are expected due to the input random sequences in both experiments that results in relatively low output uniformities. This observation corresponds to the simulated results that showed high σ values (i.e. >18 dB) compared to all '1's sequences for both biasing approaches. The lower power scale of the practical results compared to simulations is due to the high power losses discussed earlier.

On the contrary to simulations, the ASE noise that practically affected the low output pulses power for random sequences and decreased their uniformities

allowed the proposed technique to improve σ (see Section 9.3.4) as reflected in Fig. 9.27. The figure illustrates σ improvements in percentage while employing the OBS pattern compared to the uniform biasing for all experiments and its corresponding simulations. Figure 9.27 also shows that the bit sequence used in Experiment 5 is more sensitive than Experiment 4 to the proposed OBS pattern and achieves better results experimentally and in simulations.
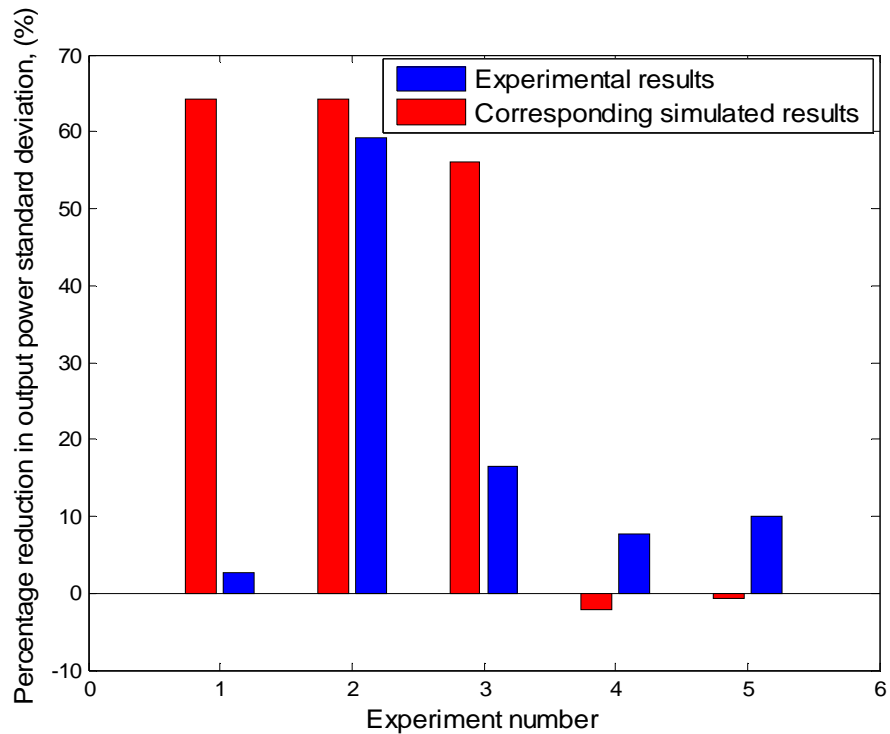
Figure 9.27 Percentage reduction in the output power standard deviation employing the OBS pattern as a replacement of the uniform current for all executed experiments and the corresponding theoretical simulations

Experiments 1 and 2 are executed at 10 Gb/s for all '1's bit sequences and that is the reason both experiments has the same corresponding theoretical simulations in Fig. 9.27. However, the only difference between both experiments is the use of EDFA in Experiment 2 which has closer σ improvements to the simulated results.

From Fig. 9.27 it can be seen that the experiments that use EDFA (i.e. Experiments 2 and 3 corresponding to 10 and 20 Gb/s, respectively) achieved larger improvements. Experiments 2 and 3 also show that higher data rates achieve less σ percentage improvements which agree with the theoretical simulations. The percentage of σ improvement is less in practical experiments compared to the simulations for the case of all '1's bit sequence due to the fact that in the practical OBS pattern, the charging and discharging cycle requires the same amount of time as shown in Fig. 9.10. As a result, half of the pulses in the frame will experience lower gains.
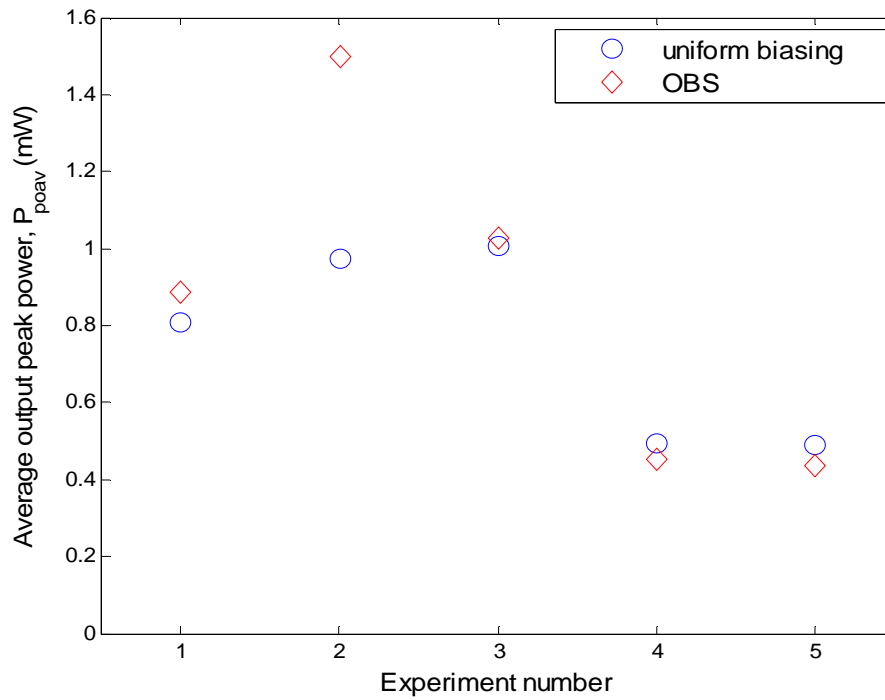
Figure 9.28 The average output peak powers when the SOA is biased by uniform and the OBS patterns for all executed experiments

In the same way, the average output powers of the monitored pulses from all five experiments are assembled for both biasing currents in Fig. 9.28. However, in this evaluation scheme, the severe power losses achieved by the optical pulses throughout the experimental setup makes it difficult to compare with the simulated results. Moreover, the use of EDFA in Experiments 2 and 3 in order to amplify the output pulses by gain values of 1.25 and 2.2, respectively to reach 1 mW peak powers has a significant influence on the obtained results.

It can be seen from Fig. 9.28 that P_{poav} when uniform biased is ~ 0.8 mW for Experiment 1 (see Section 9.3.1) which is amplified by EDFA to reach ~ 1 mW (specifically 0.97 mW) in Experiment 2. Similarly, Experiment 3 uses EDFA with a higher gain level to overcome the 2.5 dB power lost by the BRM in order for P_{poav} to reach the 1 mW. These experiments with all '1's bit sequences have achieved an increased P_{poav} (similarly to the simulated results) to reach 0.89, 1.5 and 1.03 mW, respectively employing the proposed OBS pattern. Another resemblance to the theoretical results presented in Fig. 8.8 is observed in Fig. 9.28 which confirms the higher P_{poav} that are > 0.8 mW (140 mW in simulations) offered by the all '1's input sequence at 10 Gb/s (Experiment 1) compared to random sequences in Experiments 4 and 5 that show P_{poav}.< 0.5 mW (90 mW in simulations).

However, due to the losses presented in Table 9-2, the ASE noise and the different EDFA gains, the percentage increase in P_{poav} of 10%, 54% and 2% for all '1's sequences in Experiments 1, 2 and 3 is different from the corresponding results of 1% and 3% at 10 and 20 Gb/s, respectively. On the other hand, due to

the PSL limitation regarding the amplitudes of the 'zero' bits in random sequences (see Section 9.3.4), Experiments 4 and 5 experience 8% and 10% reductions, respectively to P_{poav} as shown in Fig. 9.29. These results disagree with the simulations that show 2% increase in P_{poav} for the corresponding random bit sequence.
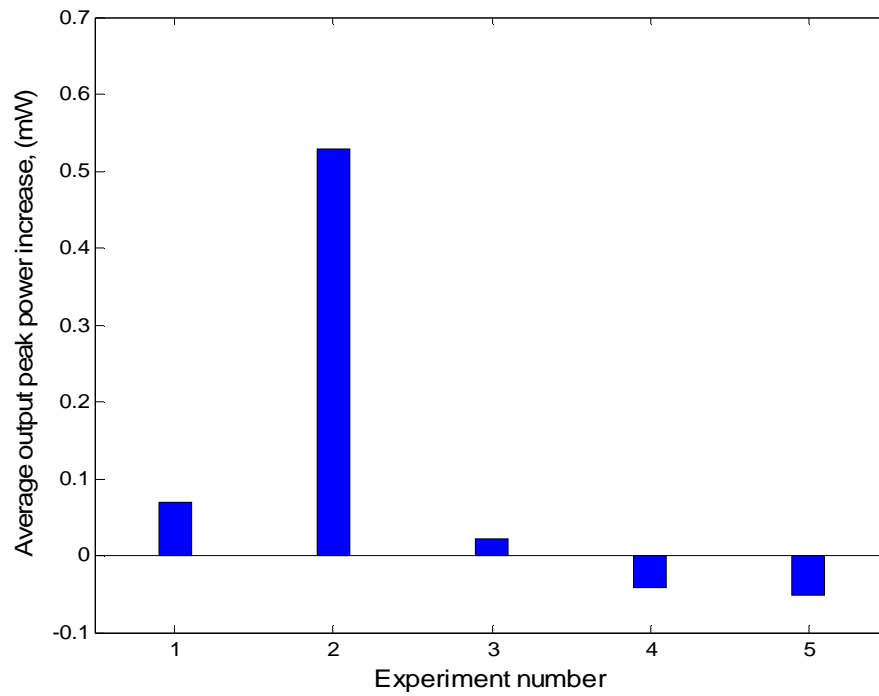
Figure 9.29

Figure 9. 29 Average output peak power increase employing the OBS pattern as a replacement of the uniform current for all executed experiments

9.4.   Summary

In the previous chapter, the output gain uniformity was theoretically maximised at high speed data rates by applying an optimised biasing for SOA (OBS) pattern. The proposed technique achieved significant improvements at different data rates

and for different input bit sequences. This chapter presented the different experimental demonstrations that were implemented in the laboratory corresponding to the theoretical investigations in order to practically validate the achievements of the previous chapter. All experiments show improved output pulses' uniformity when employing the OBS pattern and justified the theoretical simulation results.

This chapter first presented the experimental demonstration and introduced the equipments used. The optical and electrical connections of the different experimental parts are described including the circuit involved for generating the OBS pattern at 1 GHz. In the practical work, there are some factors affected the output powers. These factors that result in severe losses in the output signal powers are discussed in this chapter in order to clarify the differences between the achieved results. Five different experiments were carried out in the laboratory while exploring input signals with all '1's and random bit sequences at rates of 10 and 20 Gb/s.

The comparison made between the uniform and the OBS techniques in all experiments verified the ability of the proposed OBS patterns to practically generate the output pulses from the SOA with more uniform power. The obtained results has corresponded to the theoretical simulations and showed lower σ percentage improvements at higher data rates for all '1's bit sequences. It was also shown that experiments using EDFA to overcome the severe losses achieved better output uniformities. Although the output uniformity of the random bit sequence was not affected in the simulation results employing the OBS pattern,

163

the corresponding practical experiments achieved 8% improvement using the same bit sequence and 10% using a different random sequence.

As in the theoretical investigations, this chapter furthermore investigated the average output powers between the two biasing techniques. The output results corresponded to the simulated results for the all '1's input sequences and showed an increase in average output powers at the different data rates although the percentage increase was different because of the attenuations, the ASE noise and use of different EDFA gains in some experiments. However, due to the PSL limitation to 'zero' bits, experiments with random sequences achieved lower average output powers.

Considering the practical factors and limitations in the experiments, the obtained results in this chapter confirms the achievements of the previous chapter employing the proposed OBS technique. The following chapter concludes all the findings and contributions made in this thesis.

Chapter 10 Conclusions and Future Work

10.1.   Conclusions

As the need for capacity in optical transmission systems and networks increases, all-optical processing became the key for the design of an all-optical router for today and future high speed photonic networks. Such systems benefit from employing optical signal processing for relatively simple functionalities. The building block of all-optical routers is SOA-based interferometers (SOA-MZI) that is able to perform such tasks due to the attractive features of the SOA such as the multi-functional capability, low power consumption, compactness, broad gain bandwidth and ability to be integrated [37, 40, 43, 48]. This thesis therefore aims to characterise the SOA features and optimise its performance in order to execute

different tasks within the optical router and to propose new solutions that overcome the limitations that appear at high speed data rates. This section summarises all of the important findings of the work and discusses the achieved outcomes throughout the research.

The thesis began with a comprehensive review of the high speed photonic networks demands and the vital role of SOAs in all-optical routing and switching. The different structures and types of the SOA were introduced in this research. A comprehensive study on the SOA fundamental characteristics and its major non-linear effects that are useful for high speed optical communication networks was presented in Chapter 2. The principles of operation of the SOA including the different processes that occur when input optical signals propagate along its active region are explained. Accordingly, the type and material structure of the SOA used in this study is chosen. Chapter 2 also presented some of the literature main applications that depend on the SOA in all-optical signal processing such as switching and wavelength conversion.

The entire mathematical models that describe the SOA features utilising the complete rate, propagation and phase equations necessary for the SOA operation were presented in Chapter 3. A segmentation model of the SOA was proposed employing the mathematical analysis in basis of understanding the small variations that occur within the short length of each segment. An accurate and efficient identification to the changes of SOA gain and the propagating input signals were achieved using the 10 µm segments model. This segmentation model presented in Chapter 3 was then used for all theoretical investigations simulated in this thesis.

This thesis presented the optimised input parameters and the required conditions for the SOA to efficiently perform different tasks within the optical router. In Chapter 4, it was shown that for maximum SOA amplification function, the propagating signals are required to be close to the peak gain wavelength with low input powers. The biasing current is directly proportional to amplification and therefore, higher currents are needed. Maximum amplifications are achieved at an optimum SOA length which is dependent on its physical parameters. On the other hand, in Chapter 5, it was shown that for an efficient SOA switching operation less input power is required for achieving the 180^0 desired phase shift in case of applying higher bias currents which induces more phase shifts.

At high speed operations, the saturation gains of the SOA result in degradation to the power of the output pulses (i.e. patterning effect). These non-uniform output powers from the SOA will induce higher system power penalties. In this study a gain standard deviation equation was introduced in order to measure the uniformity of the SOA gain. This thesis proposed different new techniques in order to overcome the speed limitation of the SOA and improve the SOA gain uniformity.

Chapter 6 had used the wavelength diversion characteristics of the input pulses to propose a wavelength diversity technique (WDT) that was able to improve the SOA gain uniformity at high speed data rates up to 160 Gb/s within the C-band spectrum. The uniformity of the output pulses were compared using a single wavelength and the proposed WDT at the investigated data rates. An average improvement of 7.82 dB in the SOA gain uniformity employing WDT at input rates up to 160 Gb/s were achieved. Chapter 6 also studied the wavelength and biasing

current limitations to set the boundary conditions for the WDT. The complexity of applying a different wavelength for each pulse was the main limitation for implementing the proposed technique practically. However, the rapid increase in wavelength conversion technologies and the narrow spacing between channels in WDM systems would make it possible.

A different method was then approached in Chapter 7 utilising the biasing characteristics of the applied current in order to achieve lower gain standard deviations. This thesis proposed applying non-uniform current patterns (i.e. triangular and sawtooth) that improved the gain uniformity under certain conditions compared to the uniform bias current. The non-uniform biasing techniques were able to improve the gain uniformity employing the triangular and sawtooth bias currents at 10 Gb/s and 20 Gb/s. However, no significant improvements were achieved beyond 40 Gb/s. Moreover, the non-uniform current patterns needed to be adjusted at the same repetition rate as the input data rate.

In chapter 8, the non-uniform biasing current shape was optimised in order to overcome the above limitations and constraints observed to the proposed techniques in Chapter 7. The optimised biasing for SOA (OBS) pattern was able to maximise the uniformity of the output pulses for data rates reaching 160 Gb/s at a repetition rate of only 1 GHz. A general OBS equation to maximise the gain uniformity at any input data rate and for any number of pulses was proposed. The OBS patterns based on the proposed equation had achieved 8 and 16.9 dB average improvements to the gain uniformity at investigated rates for 150 and 200 mA average currents, respectively. The obtained results showed that the gain

uniformity was either improved (in case of all '1's bit sequence) or remain unaffected (in case of random bit sequence). Another measurement scheme was introduced in Chapter 8 in order to further evaluate the proposed technique regarding the average output power achieved by the emerged pulses. The OBS pattern offered higher power amplifications compared to uniform biasing for the input pulses regardless of the packet bit rate or sequence.

In order to validate all the improved SOA output power uniformities theoretically simulated at different data rates and with different input sequences in Chapter 8, five different experimental demonstrations corresponding to the theoretical investigations (at 10 and 20 Gb/s for all '1's and random input sequences) were implemented in the laboratory and the results were presented in Chapter 9. The obtained results from all experiments verified the ability of the OBS patterns to practically improve the uniformity of the output pulses from the SOA. The results obtained from the different executed experiments corresponded to the theoretical simulations. Moreover, an improvement to the random sequences output gain uniformity was shown. On the other hand, by applying the average output power evaluation scheme, all executed experiments have corresponded to simulated results at a much lower scale and different percentage improvements due to the attenuations. Nevertheless, the practical results at random input sequences showed reductions in the average output power due to the limitation of the laser source to 'zero' bits. Overall, taking the practical limitations and attenuations that affected the practical demonstrations into account, the practical outcomes confirmed the achievements of the simulated results.

10.2. Future work

This section discusses the future work that can use the thesis outcomes and carry out further investigations as an extension for this study.

All the theoretical results simulated are based on the proposed segmentation model that employed the complete rate equations of the SOA. However, in this work the ASE noise effect on the emerged output pulses from the SOA was not considered in order to study the direct impacts of the investigated parameters and techniques independently. Adding the ASE noise parameters to this mathematical model is the next step forward in the verification and evaluation of the proposed techniques. Moreover, this segmentation model was based on a bulk TW-SOA therefore; different SOA types (such as multi-quantum-well) and structures (such as FP-SOA) can be investigated in order to validate the proposed contributions.

All investigations carried out in this thesis used Gaussian shaped optical pulses with fixed pulse width. Further analyses are required to all the proposed techniques employing different optical pulses shapes and pulse widths. These factors will also affect the required conditions for the SOA to perform amplification and switching functions.

The direct impacts of the input signals wavelength on the carrier density and the corresponding SOA gain were studied in order to optimise the SOA performance to execute different tasks. Only signals with wavelengths within the C-band spectrum (1530 to 1565 nm) were investigated. This research also proposed a new WDT that was able to improve the SOA gain uniformity within the same

wavelength range at data rates up to 160 Gb/s. It is therefore important to further extend these investigations to different optical wavelength bands such as the S-band (1460 to 1530 nm) and the L-band (1565 to 1625 nm) in order to evaluate the concept.

Due to the absence of a single unit SOA device in the laboratory, all executed practical experiments in this thesis used a SOA-MZI module that cause dramatic attenuations to the input pulses due to 3 dB couplers and the biasing of only one SOA from the SMZ structure. It is very beneficial to execute these experiments using a single unit SOA in order to fairly compare the obtained outcomes with theoretical simulated results. Moreover, direct comparisons can be made if the laboratory contains optical pulse source equipment that is sensitive to random bit sequences.

All the theoretical and practical work presented in this thesis used co-propagating signals through the active region of the SOA. It is therefore important to launch the input pulses to the SOA from the counter-propagation direction in order to confirm the achievements of this thesis despite the propagation direction of the optical signals.

REFERENCES

[1]   M. Y. Jeon, Y. A. Leem, D. C. Kim, E. Sin, S. B. Kim, H. Ko, D. S. Yee, and K. H. Park, "40 Gbps all-optical 3R regeneration and format conversion with related InP-based semiconductor devices," vol. ETRI Journal, pp. 633-640, 2007.

[2]   E. F. Burmeister and J. E. Bowers, "Integrated gate matrix switch for optical packet buffering," *Photonics Technology Letters, IEEE,* vol. 18, pp. 103-105, 2006.

[3]   R. Maher, P. M. Anandarajah, and L. P. Barry, "Generation and Characterisation of 40 GHz Picosecond Optical Pulses Generated Using an EAM," in *Transparent Optical Networks, 2006 International Conference on*, pp. 201-204, 2006.

[4]   G. P. Agrawal, *Fibre-Optic Communication Systems*. New York, USA: Willey Interscience, 1997.

[5]   P. J. Delfyett, "Hybrid WDM - OTDM technologies using semiconductor optical amplifiers for networking, instrumentation and signal processing," in *Semiconductor Device Research Symposium, 2001 International*, p. 589, 2001.

[6]   H. F. Chou and J. E. Bowers, "High-Speed OTDM and WDM Networks Using Traveling-Wave Electroabsorption Modulators," *Selected Topics in Quantum Electronics, IEEE Journal of,* vol. 13, pp. 58-69, 2007.

[7]   R. Ramaswami and N. Sivarajan, *Optical network – a practical perspective*, 2 ed. USA: Morgan Kaufmann, 2002.

[8]   N. S. Bergano, "Wavelength division multiplexing in long-haul transoceanic transmission systems," *Lightwave Technology, Journal of,* vol. 23, pp. 4125-4139, 2005.

[9]   G. P. Agrawal, *Lightwave Technology - Telecommunication System*. New Jersey, USA: John Wiley & Son, Inc., 2005.

[10]   R. Medina, "Photons vs. electrons [all optical network]," *Potentials, IEEE,* vol. 21, pp. 9-11, May 2002 2002.

[11]   D. Adami, S. Giordano, M. Pagano, and L. Gustavo Zuliani, "MCP-RWA: A novel algorithm for QoT-guaranteed online provisioning in Photonic Networks," in *Ultra Modern Telecommunications and Control Systems and Workshops (ICUMT), 2010 International Congress on*, pp. 141-147, 2010.

[12]   C. Schubert, J. Berger, S. Diez, H. J. Ehrke, R. Ludwig, U. Feiste, C. Schmidt, H. G. Weber, G. Toptchiyski, S. Randel, and K. Petermann, "Comparison of interferometric all-optical switches for demultiplexing applications in high-speed OTDM systems," *Lightwave Technology, Journal of,* vol. 20, pp. 618-624, 2002.

[13]   E. Kehayas, J. Seoane, Y. Liu, J. M. Martinez, J. Herrera, P. V. Holm-Nielsen, S. Zhang, R. McDougall, G. Maxwell, F. Ramos, J. Marti, H. J. S. Dorren, P. Jeppesen, and H. Avramopoulos, "All-optical network subsystems using integrated SOA-based optical gates and flip-flops for label-swapped networks," *Photonics Technology Letters, IEEE,* vol. 18, pp. 1750-1752, 2006.

[14]   S. L. Jansen, S. Spalter, G. D. Khoe, W. Huug de, H. E. Escobar, L. Marshall, and M. Sher, "16×40 gb/s over 800 km of SSMF using mid-link spectral inversion," *Photonics Technology Letters, IEEE,* vol. 16, pp. 1763-1765, 2004.

[15]   A. Barbieri, G. Colavolpe, T. Foggi, E. Forestieri, and G. Prati, "OFDM versus Single-Carrier Transmission for 100 Gbps Optical Communication," *Lightwave Technology, Journal of,* vol. 28, pp. 2537-2551, 2010.

[16]   A. Paraskevopoulos, S. H. Voss, M. Talmi, and G. Walf, "High speed (>100 Gbps) key components for a scalable optical data link, to be implemented in future maskless lithography applications," *Mask and Lithography Conference (EMLC), 2009 25th European,* pp. 1-8, 2009.

[17]   H. Uemura, H. Hamasaki, H. Furuyama, H. Numata, C. Takubo, and H. Shibata, "Extremely-compact and high-performance (160Gbps = 20GB/s) optical semiconductor module using lead frame embedded optoelectronic ferrule," in *Electronic Components and Technology Conference, 2008. ECTC 2008. 58th*, pp. 1936-1940, 2008.

[18]   A. V. Nguyen, H. P. Nguyen, N. B. Le, and V. L. Dang, "Digital lightwave receiver employing parallel-DSP-based equalization technique for 100 Gbps 1000-km RZ-DQPSK optical communication system," in *Advanced Technologies for Communications (ATC), 2011 International Conference on*, pp. 152-155, 2011.

[19]   J. M. Martinez, J. Herrera, F. Ramos, and J. Marti, "All-optical correlation using cascaded logic XOR gates based on active Mach-Zehnder interferometers," in *Optical Communication, 2005. ECOC 2005. 31st European Conference on*, vol.1, pp. 103-104, 2005.

[20]   L. Vikrant, L. M. Milan, A. S. Joseph, F. Greg, and J. B. Daniel, "Monolithic Wavelength Converters for High-Speed Packet-Switched Optical Networks," *Selected Topics in Quantum Electronics, IEEE Journal of,* vol. 13, pp. 49-57, 2007.

[21]   C. Porzi, N. Calabretta, M. Guina, O. Okhotnikov, C. A. Bogoni, and L. Poti, "All-Optical Processing for Pulse Position Coded Header in Packet Switched Optical Networks Using Vertical Cavity Semiconductor Gates,"

Selected Topics in Quantum Electronics, IEEE Journal of, vol. 13, pp. 1579-1588, 2007.

[22] D. Apostolopoulos, O. Zouraraki, D. Petrantonakis, P. Bakopoulos, D. Tsiokos, E. Kehayas, and H. Avramopoulos, "Bit- and packet-level self-synchronization for all-optical label-switched network nodes with transparency to network-traffic," in *Optical Fiber Communication Conference and the National Fiber Optic Engineers Conference. OFC*, p. 3, 2006.

[23] H. Le Minh, "All-optical router with PPM header processing high speed photonic packet switching networks," Northumbria University, 2007.

[24] J. Leuthold, P. A. Besse, J. Eckner, E. Gamper, M. Dulk, and H. Melchior, "All-optical space switches with gain and principally ideal extinction ratios," *Quantum Electronics, IEEE Journal of,* vol. 34, pp. 622-633, 1998.

[25] K. Morito, J. Leuthold, and H. Melchior, "Dynamic analysis of MZI-SOA all optical switches for balanced switching," in *Integrated Optics and Optical Fibre Communications, 11th International Conference on, and 23rd European Conference on Optical Communications (Conf. Publ. No.: 448)*, vol.2, pp. 81-84, 1997.

[26] N. Pleros, P. Zakynthinos, A. Poustie, D. Tsiokos, P. Bakopoulos, D. Petrantonakis, G. T. Kanellos, G. Maxwell, and H. Avramopoulos, "Optical signal processing using integrated multi-element SOA-MZI switch arrays for packet switching," *Optoelectronics, IET,* vol. 1, pp. 120-126, 2007.

[27] A. Maziotis, B. Schrenk, M. Bougioukos, and H. Avramopoulos, "Cognitive Routing in Converged Access-Metro Environment via Selective SOA-MZI Switch," *Photonics Technology Letters, IEEE,* vol. PP, pp. 1-1, 2011.

[28] D. Petrantonakis, D. Apostolopoulos, M. Spyropoulou, N. Pleros, K. Vyrsokinos, and H. Avramopoulos, "40 Gb/s NRZ wavelength conversion

with enhanced 2R regeneration characteristics using a differentially-biased SOA-MZI switch," in *LEOS Annual Meeting Conference Proceedings, 2009. LEOS '09. IEEE*, pp. 781-782, 2009.

[29]   J. Kurumida, Y. Tatara, H. Uenohara, and K. Kobayashi, "All-optical Header Recognition Sub-system Based on SOA-MZI Switches," in *Lasers and Electro-Optics, CLEO/Pacific Rim. Pacific Rim Conference on*, pp. 1790-1791, 2005.

[30]   S. Gupta, M. Presi, N. Calabretta, G. Contestabile, and E. Ciaramella, "Operational Equivalence of Self-Switching Effect in SOA-based Nonlinear Polarization and MZI Switches," in *Lasers and Electro-Optics Society, LEOS. The 20th Annual Meeting of the IEEE*, pp. 810-811, 2007.

[31]   S. Nakamura, K. Tajima, and Y. Sugimoto, "Experimental investigation on high-speed switching characteristics of a novel symmetric Mach-Zehnder all-optical switch," *Applied Physics Letter,* vol. 65, pp. 283-385, 1994.

[32]   X. Chen, M. Yao, J. Zhang, Y. Li, L. Xu, M. Chen, and Y. Gao, "All-optical switch based on an ultrafast nonlinear interferometer (UNI)," in *Communication Technology Proceedings, 2000. WCC - ICCT 2000. International Conference on*, vol.1, pp. 206-209, 2000.

[33]   C. Bintjas, K. Vlachos, N. Pleros, and H. Avramopoulos, "Ultrafast nonlinear interferometer (UNI)-based digital optical circuits and their use in packet switching," *Lightwave Technology, Journal of,* vol. 21, pp. 2629-2637, 2003.

[34]   H. Le Minh, Z. Ghassemlooy, and N. Wai Pang, "Characterization and performance analysis of a TOAD switch employing a dual control pulse scheme in high-speed OTDM demultiplexer," *Communications Letters, IEEE,* vol. 12, pp. 316-318, 2008.

[35]   J. M. Tang, P. S. Spencer, P. Rees, and K. A. Shore, "Enhanced TOAD performance by negative frequency-detuned signal and control picosecond

optical pulses," *Quantum Electronics, IEEE Journal of,* vol. 36, pp. 574-582, 2000.

[36] J. Wei, Z. Min, and P. Ye, "All-Optical-Packet Header and Payload Separation for Unslotted Optical-Packet-Switched Networks," *Lightwave Technology, Journal of,* vol. 25, pp. 703-709, 2007.

[37] E. S. Awad, C. J. K. Richardson, P. S. Cho, N. Moulton, and J. Goldhar, "Optical clock recovery using SOA for relative timing extraction between counterpropagating short picosecond pulses," *Photonics Technology Letters, IEEE,* vol. 14, pp. 396-398, 2002.

[38] R. Giller, R. J. Manning, and D. Cotter, "Gain and phase recovery of optically excited semiconductor optical amplifiers," *Photonics Technology Letters, IEEE,* vol. 18, pp. 1061-1063, 2006.

[39] J. Moerk, M. Nielsen, and T. Berg, "The dynamics of semiconductor optical amplifiers-modeling and applications," *Optics and Photonics News,* vol. 14, pp. 42-48, 2003.

[40] E. Tangdiongga, Y. Liu, H. Waardt, G. Khoe, A. Koonen, and H. Dorren, "All-optical demultiplexing of 640 to 40 Gbits/s using filtered chirp of a semiconductor optical amplifier," *Optics Letters,* vol. 32, pp. 835-837, 2007.

[41] A. Perez-Pardo, T. T. Ng, P. Petropoulos, S. Sales, and D. J. Richardson, "Analysis of the Dynamic Responses of SOA Wavelength Converters Using Linear Frequency Resolved Gating Technique," *Photonics Technology Letters, IEEE,* vol. 20, pp. 1079-1081, 2008.

[42] M. Matsuura, N. Kishi, and T. Miki, "All-optical wavelength conversion with large wavelength hopping by utilizing multistage cascaded SOA-based wavelength converters," *Photonics Technology Letters, IEEE,* vol. 18, pp. 926-928, 2006.

[43]   T. Kise, K. N. Nguyen, J. M. Garcia, H. N. Poulsen, and D. J. Blumenthal, "Demonstration of cascadability and phase regeneration of SOA-based all-optical DPSK wavelength converters," in *Optical Fiber Communication Conference and Exposition (OFC/NFOEC), 2011 and the National Fiber Optic Engineers Conference*, pp. 1-3, 2011.

[44]   L. Pei-Li, H. De-Xiu, and Z. Xin-Liang, "SOA-Based Ultrafast Multifunctional All-Optical Logic Gates With PolSK Modulated Signals," *Quantum Electronics, IEEE Journal of,* vol. 45, pp. 1542-1550, 2009.

[45]   W. Jing, G. Meloni, G. Berrettini, Poti, x, L., and A. Bogoni, "All-Optical Clocked Flip-Flops and Binary Counting Operation Using SOA-Based SR Latch and Logic Gates," *Selected Topics in Quantum Electronics, IEEE Journal of,* vol. 16, pp. 1486-1494, 2010.

[46]   M. Suzuki and H. Uenohara, "Investigation of all-optical error detection circuit using SOA-MZI-based XOR gates at 10 Gbit/s," *Electronics Letters,* vol. 45, pp. 224-225, 2009.

[47]   K. Joo-Youp, K. Jeung-Mo, K. Tae-Young, and H. Sang-Kook, "All-optical multiple logic gates with XOR, NOR, OR, and NAND functions using parallel SOA-MZI structures: theory and experiment," *Lightwave Technology, Journal of,* vol. 24, pp. 3392-3399, 2006.

[48]   T. Hung Nguyen, M. Matsuura, and N. Kishi, "Parallel WDM regenerative waveform conversion for mixed NRZ and RZ transmission networks using a SOA-based multiple switching-window optical gate," in *Optical Fiber Communication Conference and Exposition (OFC/NFOEC), and the National Fiber Optic Engineers Conference*, pp. 1-3, 2011.

[49]   A. V. Tran, C. J. Chae, and R. S. Tucker, "Optical packet power equalization with large dynamic range using controlled gain-clamped SOA," in *Optical Fiber Communication Conference, 2005. Technical Digest. OFC/NFOEC*, Vol. 1, p. 3, 2005.

[50] K. Obermann, I. Koltchanov, K. Petermann, S. Diez, R. Ludwig, and H. G. Weber, "Noise analysis of frequency converters utilizing semiconductor-laser amplifiers," *Quantum Electronics, IEEE Journal of,* vol. 33, pp. 81-88, 1997.

[51] H. Soto Ortiz and D. Erasme, "Modelling and experimental measurements of the switching behaviour of semiconductor optical amplifiers " *Optical and Quantum Electronics,* vol. 28, pp. 669-682, 1996.

[52] S. Philippe, A. L. Bradley, B. Kennedy, F. Surre, and P. Landais, "Experimental Investigation of Polarization Effects in Semiconductor Optical Amplifiers and Implications for All-Optical Switching," *Lightwave Technology, Journal of,* vol. 26, pp. 2977-2985, 2008.

[53] M. Premaratne, D. Nesic, and G. P. Agrawal, "Pulse Amplification and Gain Recovery in Semiconductor Optical Amplifiers: A Systematic Analytical Approach," *Lightwave Technology, Journal of,* vol. 26, pp. 1653-1660, 2008.

[54] T. Silveira, A. Teixeira, A. Ferreira, G. T. Beleffi, D. Forin, S. Stevan, and P. Monteiro, "All-Optical Signal Processing Using Gain Clamped Semiconductor Optical Amplifiers," in *Transparent Optical Networks, 2007. ICTON '07. 9th International Conference on*, pp. 307-310, 2007.

[55] A. Borghesani, "Semiconductor Optical Amplifiers for Advanced Optical Applications," in *Transparent Optical Networks, 2006 International Conference on*, pp. 119-122, 2006.

[56] J. van der Tang and D. Kasperkovitz, "Fast phase noise analysis method for noise optimisation of oscillators," in *Solid-State Circuits Conference, 1998. ESSCIRC '98. Proceedings of the 24th European*, pp. 504-507, 1998.

[57] M. J. Connelly and G. Li-Qiang, "Mueller matrix based modeling of nonlinear polarization rotation in a tensile-strained bulk SOA," in *Numerical*

Simulation of Optoelectronic Devices, 2008. NUSOD '08. International Conference on, pp. 63-64, 2008.

[58] X. Jing, Z. Xinliang, and J. Mrk, "Investigation of Patterning Effects in Ultrafast SOA-Based Optical Switches," *Quantum Electronics, IEEE Journal of,* vol. 46, pp. 87-94, 2010.

[59] J. Xu, X. Zhang, and J. Mork, "Investigation of patterning effect in ultrafast SOA-based optical switches," in *Lasers and Electro-Optics 2009 and the European Quantum Electronics Conference. CLEO Europe - EQEC 2009. European Conference on*, pp. 1, 2009.

[60] P. Zhong, Y. Haijun, Z. Zuqing, C. Jing, V. Akella, S. Butt, and S. J. B. Yoo, "Demonstration of variable-length packet contention resolution and packet forwarding in an optical-label switching router," *Photonics Technology Letters, IEEE,* vol. 16, pp. 1772-1774, 2004.

[61] J. L. Pleumeekers, M. Kauer, K. Dreyer, C. Burrus, A. G. Dentai, S. Shunk, J. Leuthold, and C. H. Joyner, "Acceleration of gain recovery in semiconductor optical amplifiers by optical injection near transparency wavelength," *Photonics Technology Letters, IEEE,* vol. 14, pp. 12-14, 2002.

[62] A. Matsumoto, K. Nishimura, K. Utaka, and M. Usami, "Operational design on high-speed semiconductor optical amplifier with assist light for application to wavelength converters using cross-phase modulation," *Quantum Electronics, IEEE Journal of,* vol. 42, pp. 313-323, 2006.

[63] M. A. Dupertuis, J. L. Pleumeekers, T. P. Hessler, P. E. Selbmann, B. Deveaud, B. Dagens, and J. Y. Emery, "Extremely fast, high-gain and low-current semiconductor optical amplifier by optical speed-up at transparency," in *Lasers and Electro-Optics,. (CLEO 2000). Conference on*, p. 470, 2000.

[64] T. P. Hessler, M. A. Dupertuis, B. Deveaud, J. Y. Emery, and B. Dagens, "Experimental demonstration of optical speed-up at transparency in semiconductor optical amplifiers," in *All-Optical Networking: Existing and Emerging Architecture and Applications/Dynamic Enablers of Next-Generation Optical Communications Systems/Fast Optical Processing in Optical Transmission/VCSEL and Microcavity Lasers. IEEE/LEOS Summer Topi*, pp. TuK2-23-TuK2-24, 2002.

[65] O. R. Qasaimeh, "Ultra-Fast Gain Recovery and Compression Due to Auger-Assisted Relaxation in Quantum Dot Semiconductor Optical Amplifiers," *Lightwave Technology, Journal of,* vol. 27, pp. 2530-2536, 2009.

[66] L. Xiaoxu and L. Guifang, "Comments on "Theoretical Analysis of Gain-Recovery Time and Chirp in QD-SOA"," *Photonics Technology Letters, IEEE,* vol. 18, pp. 2434-2435, 2006.

[67] C. M. Gallep and E. Conforti, "Reduction of semiconductor optical amplifier switching times by preimpulse step-injected current technique," *Photonics Technology Letters, IEEE,* vol. 14, pp. 902-904, 2002.

[68] M. H. Lee, S. M. Shin, and S. K. Han, "Wavelength-converting optical space switch using a semiconductor-optical-amplifier-based Mach-Zehnder interferometer," *Optical Engineering.,* vol. 39, pp. 3255-3259, 2000.

[69] E. Desurvire, *Erbium Doped Fiber Amplifier*. New Jersey: John Wiley, 2002.

[70] R. J. Mears, "The EDFA: past, present and future," in *Communications, 1999. APCC/OECC '99. Fifth Asia-Pacific Conference on ... and Fourth Optoelectronics and Communications Conference*, vol.2, p. 1332, 1999.

[71] M. Connelly, *Semiconductor optical amplifiers*. New York: Springer-Verlag, 2002.

[72] R. Boerner and M. Goeken, "Service identification in SOA Governance literature review and implications for a new method," in *Digital Ecosystems and Technologies, 2009. DEST '09. 3rd IEEE International Conference on*, pp. 588-593, 2009.

[73] W. Yaping, W. Chongqing, W. Yongjun, W. Zhi, and S. Xinzhi, "Optical Packet Replicator Using Cascaded SOA-Based Active Fiber Ring," *Photonics Technology Letters, IEEE,* vol. 21, pp. 1320-1322, 2009.

[74] S. Jun-Hyuk, C. Chang-Soon, C. Woo-Young, K. Young-Shik, C. Yong-Duck, and K. Jeha, "Bi-directional 60 GHz radio-on-fiber systems using cascaded SOA-EAM frequency up/down-converters," in *Microwave Symposium Digest, 2005 IEEE MTT-S International*, p. 4, 2005.

[75] L. Gong-Ru, Y. Kun-Chieh, P. Ci-Ling, and L. Yu-Sheng, "All-Optical Decision-Gating of 10-Gb/s RZ Data in a Semiconductor Optical Amplifier Temporally Gain-Shaped With Dark-Optical-Comb," *Lightwave Technology, Journal of,* vol. 25, pp. 1651-1658, 2007.

[76] K. E. Stubkjaer, "Semiconductor optical amplifier-based all-optical gates for high-speed optical processing," *Selected Topics in Quantum Electronics, IEEE Journal of,* vol. 6, pp. 1428-1435, Dec 2000.

[77] J. Yu, Y. Yeo, O. Akanbi, and G. Chang, "Bi-directional transmission of 8 X 10Gb/s DPSK signals over 80 km of SMF-28 fiber using in-line semiconductor optical amplifier," *Optics Express,* vol. 12, pp. 6215-6218, 2005.

[78] S. Iezekiel, S. Bennett, and C. M. Snowden, "Chaos in Fabry-Perot and multiple quantum well laser diodes: a review," in *High Performance Electron Devices for Microwave and Optoelectronic Applications, 1997. EDMO. 1997 Workshop on*, pp. 80-85, 1997.

[79]   H. Young-Geun, F. Fresi, L. Poti, A. Bogoni, L. Ju Han, and L. Sang Bae, "Continuously FSR tunable all fiber Fabry-Perot filter and its application to tunable multiwavelength SOA ring laser," in *Optical Fiber Communication and the National Fiber Optic Engineers Conference, 2007. OFC/NFOEC 2007. Conference on*, pp. 1-3, 2007.

[80]   M. J. Connelly, "Wideband semiconductor optical amplifier steady-state numerical model," *IEEE JOURNAL OF QUANTUM ELECTRONICS,* vol. 37, pp. 439-447, 2001.

[81]   K. Djordjev, C. Sang-Jun, C. Won-Jin, C. Seung-June, K. In, and P. D. Dapkus, "Two-segment spectrally inhomogeneous traveling wave semiconductor optical amplifiers applied to spectral equalization," *Photonics Technology Letters, IEEE,* vol. 14, pp. 603-605, 2002.

[82]   T. Saitoh and T. Mukai, "Traveling-wave semiconductor laser amplifiers for optical communications systems," in *Global Telecommunications Conference, 1990, and Exhibition. 'Communications: Connecting the Future', GLOBECOM '90., IEEE*, vol.2, pp. 1274-1280, 1990.

[83]   G. P. Agrawal and N. A. Olsson, "Self-phase modulation and spectral broadening of optical pulses in semiconductor laser amplifiers," *Quantum Electronics, IEEE Journal of,* vol. 25, pp. 2297-2306, 1989.

[84]   M. Eiselt, W. Pieper, and H. G. Weber, "SLALOM: semiconductor laser amplifier in a loop mirror," *Lightwave Technology, Journal of,* vol. 13, pp. 2099-2112, 1995.

[85]   L. Guo and M. Connelly, "All-optical AND gate with improved extinction ratio using signal induced nonlinearities in a bulk semiconductor optical amplifier," *optics Express,* vol. 14, pp. 2938-2943, 2006.

[86]   P. Borri, W. Langein, J. Hvam, F. Heinrichsdorff, M. Mao, and D. Bimberg, "Spectral hole-burning and carrier-heating dynamics in quantum-dot

amplifiers: comparison with bulk amplifiers," *physica status solidi,* vol. 224, pp. 419-423, 2001.

[87]   B. S. Ryvkin and E. A. Avrutin, "Spatial hole burning in high-power edge-emitting lasers: A simple analytical model and the effect on laser performance," *Journal of Applied Physics,* vol. 109, pp. 043101-043101-5, 2011.

[88]   H. Ju, A. Uskov, R. Notzel, Z. Li, J. Vazquez, D. Lenstra, G. Khoe, and H. Dorren, "Effects of two-photon absorption on carrier dynamics in Quantum-dot optical amplifiers," *applied physics B. lasers and optics,* vol. 82, pp. 615-620, 2006.

[89]   K. Tajima, S. Nakamura, and Y. Ueno, "semiconductor nonlinearities for ultrafast all-optical gating," *measurement science and technology,* vol. 13, pp. 1692-1697, 2002.

[90]   R. Soma Venugopal, K. Moutzouris, M. Ebrahimzadeh, A. De Rossi, G. Gintz, M. Calligaro, V. Ortiz, and V. Berger, "Influence of scattering and two-photon absorption on the optical loss in GaAs-Al$_2$O$_3$ nonlinear waveguides measured using femtosecond pulses," *Quantum Electronics, IEEE Journal of,* vol. 39, pp. 478-486, 2003.

[91]   G. Agrawal, *Nonlinear fiber optics*, 2 ed. San Diego, USA: Academic Press, 1995.

[92]   J. G. Mendoza-Alvarez, L. A. Coldren, A. Alping, R. H. Yan, T. Hausken, K. Lee, and K. Pedrotti, "Analysis of depletion edge translation lightwave modulators," *Lightwave Technology, Journal of,* vol. 6, pp. 793-808, 1988.

[93]   I. H. White, R. V. Penty, and R. E. Epworth, "Demonstration of the optical Kerr effect in an all-fibre Mach-Zehnder interferometer at laser diode powers," *Electronics Letters,* vol. 24, pp. 340-341, 1988.

[94] S. Lam and N. Papageorgis, "Quasi-equilibrium vibrational population distributions for anharmonic molecular lasers," *Quantum Electronics, IEEE Journal of,* vol. 11, pp. 715-716, 1975.

[95] C. Cheng, X. Zhang, Y. Zhang, L. Liu, and D. Huang, "Measurement of the carrier recovery time in SOA based on dual pump FWM," in *Communications and Photonics Conference and Exhibition (ACP), Asia*, pp. 1-2, 2009.

[96] G. Contestabile, A. Maruta, S. Sekiguchi, K. Morito, M. Sugawara, and K. Kitayama, "80 Gb/s multicast wavelength conversion by XGM in a QD-SOA," in *Optical Communication (ECOC), 2010 36th European Conference and Exhibition on*, pp. 1-3, 2010.

[97] T. Hung Nguyen, M. Matsuura, and N. Kishi, "Reduction of FWM and XGM for dynamic range improvement in SOA-based multiwavelength amplification using holding beam," in *OptoeElectronics and Communications Conference (OECC), 15th*, pp. 192-193, 2010.

[98] T. T. Ng, A. Perez, S. Sales, D. J. Richardson, and P. Petropoulos, "Characterization of XGM and XPM in a SOA-MZI using a Linear Frequency Resolved Gating Technique," in *Lasers and Electro-Optics Society, 2007. LEOS. The 20th Annual Meeting of the IEEE*, pp. 656-657, 2007,.

[99] M. V. Drummond, L. N. Costa, R. N. Nogueira, P. Monteiro, and A. Teixeira, "GVD and PMD monitoring by means of SPM and XPM effects in a SOA," in *Transparent Optical Networks, 2008. ICTON 2008. 10th Anniversary International Conference on*, pp. 106-108, 2008.

[100] H. Zhaoyang, M. Davanco, and D. J. Blumenthal, "Extinction ratio improvement by strong external light injection and SPM in an SOA for OTDM pulse source using a DBR laser diode," *Photonics Technology Letters, IEEE,* vol. 15, pp. 1419-1421, 2003.

[101] M. Jabbari, M. K. Moravvej-Farshi, R. Ghayour, and A. Zarifkar, "XPM Response of a Chirped DFB-SOA All-Optical Flip-Flop Injected With an Assist Light at Transparency," *Lightwave Technology, Journal of,* vol. 27, pp. 2199-2207, 2009.

[102] L. K. Oxenlowe, D. Zibar, M. Galili, A. T. Clausen, L. J. Christiansen, and P. Jeppesen, "Clock recovery for 320 Gb/s OTDM data using filtering-assisted XPM in an SOA," in *Lasers and Electro-Optics Europe, 2005. CLEO/Europe. Conference on*, p. 486, 2005.

[103] A. M. Clarke, G. Girault, P. Anandarajah, C. Guignard, L. Bramerie, L. P. Barry, J. C. Simon, and J. Harvey, "FROG characterisation of SOA-based wavelength conversion using XPM in conjunction with shifted filtering up to line rates of 80 GHz," in *Lasers and Electro-Optics Society. LEOS 2006. 19th Annual Meeting of the IEEE*, pp. 152-153, 2006.

[104] D. Jianji, Z. Xinliang, X. Jing, H. Dexiu, F. Songnian, P. Shum, Z. Liren, and Y. D. Gong, "40 Gb/s both inverted and non-inverted wavelength conversion based on transient XPM of SOA," in *Optical Fiber Communication and the National Fiber Optic Engineers Conference, 2007. OFC/NFOEC 2007. Conference on*, pp. 1-3, 2007.

[105] H. Bingchen, Y. Jinlong, W. Wenrui, Y. Enze, and Y. Chengquan, "Simultaneously Wavelength Conversion of Two Data Signals Based on FWM in a Single SOA," in *Control, Automation and Systems Engineering (CASE), 2011 International Conference on*, pp. 1-4, 2011.

[106] G. Contestabile, M. Presi, and E. Ciaramella, "Multiple wavelength conversion for WDM multicasting by FWM in an SOA," *Photonics Technology Letters, IEEE,* vol. 16, pp. 1775-1777, 2004.

[107] M. Matsuura and N. Kishi, "High-Speed Wavelength Conversion of RZ-DPSK Signal Using FWM in a Quantum-Dot SOA," *Photonics Technology Letters, IEEE,* vol. 23, pp. 615-617, 2011.

[108] D. Ning, C. Kit, C. Chun-Kit, and C. Lian-Kuan, "An all-optical XOR logic gate for high-speed RZ-DPSK signals by FWM in semiconductor optical amplifier," *Selected Topics in Quantum Electronics, IEEE Journal of,* vol. 12, pp. 702-707, 2006.

[109] R. Sabella, E. Iannone, and G. Alcini, "Effect of phase noise in the chromatic dispersion compensation by FWM in semiconductor optical amplifiers," in *Lasers and Electro-Optics Society Annual Meeting, 1994. LEOS '94 Conference Proceedings. IEEE*, vol.1, pp. 190-191, 1994.

[110] R. P. Schreieck, M. H. Kwakernaak, H. Jackel, and H. Melchior, "All-optical switching at multi-100-Gb/s data rates with Mach-Zehnder interferometer switches," *Quantum Electronics, IEEE Journal of,* vol. 38, pp. 1053-1061, 2002.

[111] R. Ngah and Z. Ghassemlooy, "Self-synchronization scheme for OTDM packet signal using a symmetric Mach Zehnder switch," in *Networks, 2005. Jointly held with the IEEE 7th Malaysia International Conference on Communication., 13th IEEE International Conference on*, p. 4, 2005.

[112] P. Runge, C. A. Bunge, and K. Petermann, "All-Optical Wavelength Conversion With Extinction Ratio Improvement of 100 Gb/s RZ-Signals in Ultralong Bulk Semiconductor Optical Amplifiers," *Quantum Electronics, IEEE Journal of,* vol. 46, pp. 937-944, 2010.

[113] L. Pei-Li and S. Wei-Hua, "Ultrahigh-speed all-optical wavelength conversion and format conversion for polarisation-shift-keying signal based on four-wave mixing in light-holding semiconductor optical amplifier," *Optoelectronics, IET,* vol. 5, pp. 72-76, 2010.

[114] C. Y. Li and P. K. A. Wai, "External wavelength contention resolution for optical crossconnects," in *OptoElectronics and Communications Conference, 2009. OECC 2009. 14th*, pp. 1-2, 2009.

[115] Z. Mian and J. Siwei, "Performance Evaluation of OPS Contention Resolution Scheme Based on SPC Wavelength Conversion," in *Computational and Information Sciences (ICCIS), 2010 International Conference on*, pp. 917-919, 2010.

[116] C. Ming, H. Weisheng, S. Weiqiang, Y. Fangfang, and H. Hao, "Wavelength Converted Broadcast-Selective Buffering Contention Resolution in Synchronous WDM OPS Networks," *Lightwave Technology, Journal of,* vol. 28, pp. 1356-1362, 2010.

[117] T. Durhuus, C. Joergensen, B. Mikkelsen, R. J. S. Pedersen, and K. E. Stubkjaer, "All optical wavelength conversion by SOA's in a Mach-Zehnder configuration," *Photonics Technology Letters, IEEE,* vol. 6, pp. 53-55, 1994.

[118] G. Contestabile, N. Calabretta, R. Proietti, and E. Ciaramella, "Simultaneous multi-wavelength conversion by double stage XGM in SOAs," in *Lasers and Electro-Optics Society, 2005. LEOS 2005. The 18th Annual Meeting of the IEEE*, pp. 155-156, 2005.

[119] H. Wei, L. Minghao, Z. Xinliang, S. Junqiang, and H. Dexiu, "Dynamic Analysis of All-Optical Wavelength Conversion of Differential Phase-Shift Keyed Signals Based on Semiconductor Optical Amplifier Mach–Zehnder Interferometer," *Lightwave Technology, Journal of,* vol. 27, pp. 5580-5589, 2009.

[120] D. M. Patrick and R. J. Manning, "20 Gbit/s wavelength conversion using semiconductor nonlinearity," *Electronics Letters,* vol. 30, pp. 252-253, 1994.

[121] C. Politi, D. Klonidis, and M. J. O'Mahony, "Dynamic behavior of wavelength converters based on FWM in SOAs," *Quantum Electronics, IEEE Journal of,* vol. 42, pp. 108-125, 2006.

[122] J. Herrera, F. Ramos, and J. Marti, "Compensation for dispersion-induced carrier suppression effect in microwave/millimetre-wave optical links using

optical phase conjugation in semiconductor optical amplifiers," *Electronics Letters,* vol. 42, pp. 238-239, 2006.

[123] M. F. C. Stephens, D. Nesset, K. A. Williams, R. V. Penty, I. H. White, and M. J. Fice, "Dispersion compensation at 40 Gbit/s over 100 km of standard fibre via mid-span spectral inversion in semiconductor optical amplifier with integrated pump laser," *Electronics Letters,* vol. 35, pp. 1359-1361, 1999.

[124] T. Sakamoto, S. Koji, K. Taira, M. Nam Su, and K. Kikuchi, "Polarization-insensitive all-optical time-division demultiplexing using a fiber four-wave mixer with a peak-holding optical phase-locked loop," *Photonics Technology Letters, IEEE,* vol. 16, pp. 563-565, 2004.

[125] M. A. Ali, A. F. Elrefaie, H. Issa, and S. A. Ahmed, "High-speed optical time-division demultiplexer using semiconductor optical amplifiers," *Lightwave Technology, Journal of,* vol. 10, pp. 1735-1742, 1992.

[126] M. Schilling, K. Daub, W. Idler, D. Baums, U. Koerner, E. Lach, G. Laube, and K. Wunstel, "Wavelength converter based on integrated all-active three-port Mach-Zehnder interferometer," *Electronics Letters,* vol. 30, pp. 2128-2130, 1994.

[127] K. Magari, "Semiconductor optical amplifier gate array integrated with spot-size converters," in *Lasers and Electro-Optics, 1999. CLEO/Pacific Rim '99. The Pacific Rim Conference on*, vol.4, pp. 1153-1154, 1999.

[128] H. Wang, J. Wu, and J. Lin, "Studies on the material transparent light in semiconductor optical amplifiers," *Journal of Optics A:Pure and Applied Optics,* vol. 7, pp. 479-492, 2005.

[129] VPIsystems, *VPI transmission maker and VPI component maker: photonic modules reference manual*, 2001.

[130] F. Girardin, G. Guekos, and A. Houbavlis, "Gain recovery of bulk semiconductor optical amplifiers," *Photonics Technology Letters, IEEE,* vol. 10, pp. 784-786, 1998.

[131] J. L. Pleumeekers, M. A. Dupertuis, T. Hessler, P. E. Selbmann, S. Haacke, and B. Deveaud, "Longitudinal spatial hole burning and associated nonlinear gain in gain-clamped semiconductor optical amplifiers," *Quantum Electronics, IEEE Journal of,* vol. 34, pp. 879-886, 1998.

[132] A. E. Willner and W. Shieh, "Optimal spectral and power parameters for all-optical wavelength shifting: single stage, fanout, and cascadability," *Journal of Lightwave Technology,* vol. 13, pp. 771-781, 1995.

[133] N. S. Ribeiro, A. L. R. Cavalcante, C. M. Gallep, and E. Conforti, "Data rewriting after carrier erasing by ultra-long SOA," in *Optical Fiber Communication Conference and Exposition (OFC/NFOEC), and the National Fiber Optic Engineers Conference*, pp. 1-3, 2011.

[134] G. Bramann, H. J. Wunsche, U. Busolt, C. Schmidt, M. Schlak, B. Sartorius, and H. P. Nolting, "Two-wave competition in ultralong semiconductor optical amplifiers," *Quantum Electronics, IEEE Journal of,* vol. 41, pp. 1260-1267, 2005.

[135] P. Runge, R. Elschner, and K. Petermann, "Time-Domain Modeling of Ultralong Semiconductor Optical Amplifiers," *Quantum Electronics, IEEE Journal of,* vol. 46, pp. 484-491, 2010.

[136] M. F. Chiang, Z. Ghassemlooy, N. Wai Pang, H. Le Minh, and A. A. El Aziz, "Multiple-Hop Routing in Ultrafast All-Optical Packet Switching Network Using Multiple PPM Routing Tables," in *Communications, 2008. ICC '08. IEEE International Conference on*, pp. 5321-5325, 2008.

[137] K. Nishimura, R. Inohara, M. Tsurusawa, and M. Usami, "Patterning effect at 40 Gbit/s of wavelength converter utilizing cross-phase modulation in

InGaAsP/InP electroabsorption modulator," in *Indium Phosphide and Related Materials, 2003. International Conference on*, pp. 198-201, 2003.

[138] A. Shafarenko, A. Skidin, and S. K. Turitsyn, "Weakly-Constrained Codes for Suppression of Patterning Effects in Digital Communications," *Communications, IEEE Transactions on,* vol. 58, pp. 2845-2854, 2010.

[139] K. E. Zoiros, C. O'Riordan, and M. J. Connelly, "Semiconductor Optical Amplifier Pattern Effect Suppression Using a Birefringent Fiber Loop," *Photonics Technology Letters, IEEE,* vol. 22, pp. 221-223, 2010.

[140] M. J. O'Mahony, "An overview of WDM research in Europe," in *Multiwavelength Optical Networks: Devices, Systems and Network Implementations (Ref. No. 1998/296), IEE Colloquium on*, pp. 1-3, 1998.

[141] P. J. Urban, H. De Waardt, E. Ciaramella, and A. M. J. Koonen, "Reduction of the influence of optical interferometric crosstalk noise in a WDM-PON system with a reflective semiconductor optical amplifier: An overview," in *Transparent Optical Networks (ICTON), 12th International Conference on*, pp. 1-4, 2010.

[142] Y. Kobayashi, K. Kinjo, K. Ishida, T. Sugihara, S. Kajiya, N. Suzuki, and K. Shimizu, "A comparison among pure-RZ, CS-RZ and SSB-RZ format, in a 1 Tbit/s (50X20 Gb/s, 0.4 nm spacing)cWDM transmission over 4,000 km," *Proceeding of the 26th European Conference on Optical Communication (ECOC 2000),* vol. PDP 1.7, 2000.

[143] G. P. Agrawal, *Fiber-Optic Communication Systems*, 3rd ed. New York, USA: Wiley-Interscience, 2002.

[144] J. Dakin and R. G. W. Brown, *Handbook of Optoelectronics.* London, UK: Taylor & Francis Group, 2006.

[145] B. Mukherjee, *Optical WDM Networks*. New York, USA: Springer-Verlag New York Inc., 2006.

[146] R. Calvani, R. Caponi, F. Delpiano, and G. Marone, "An experiment of optical heterodyne transmission with polarization modulation at 140 Mbit/s bitrate and 1550 nm wavelength," in *Global Telecommunications Conference. GLOBECOM '91. 'Countdown to the New Millennium. Featuring a Mini-Theme on: Personal Communications Services*, vol.3, pp. 1587-1591, 1991.

[147] Z. Xinhui, Y. Yong, S. Yunxu, and L. Chao, "Circle Polarization Shift Keying With Direct Detection for Free-Space Optical Communication," *Optical Communications and Networking, IEEE/OSA Journal of,* vol. 1, pp. 307-312, 2009.

[148] F. Songnian, W. Minxue, Z. Wen-De, P. Shum, W. Yang Jing, W. Jian, and L. Jintong, "SOA Nonlinear Polarization Rotation With Linear Polarization Maintenance: Characterization and Applications," *Selected Topics in Quantum Electronics, IEEE Journal of,* vol. 14, pp. 816-825, 2008.

[149] I. Fazal, S. Kumar, L. Yunchu, L. Christen, P. Saghari, C. Langrock, M. M. Fejer, and A. E. Willner, "SOA-Assisted Data-Polarization-Insensitive Wavelength Conversion in a PPLN Waveguide," *Lightwave Technology, Journal of,* vol. 26, pp. 1690-1695, 2008.

[150] W. Ying, W. Lutang, F. Nian, and H. Zhaoming, "Modeling of a Dual-Channel Polarization Optical Transmission System with SOA-Based All-Optical Polarization Modulations," in *Microwave Conference, 2008 China-Japan Joint*, pp. 784-787, 2008.

[151] CIP Technologies, "Quad 40 Gb/s 2R Optical Regenerator: Premilinary datasheet''. Available at http://www.amstechnologies.com/fileadmin/amsmedia/downloads/3722_40 G-2R4-ORP_(G).pdf (Accessed 16 October 2011)"

192